SPIRAL AND SCROLL WAVE DYNAMICS IN AN EXCITABLE MEDIUM AND THEIR BEHAVIOUR AROUND EXCITATION PATTERNS AND HETEROGENEITIES

A thesis submitted to Indian Institute of Technology Guwahati

for the degree of

Doctor of Philosophy

Dhriti Mahanta

Roll No. 136122011

Supervisor: Dr. Sumana Dutta

Department of Chemistry

Indian Institute of Technology Guwahati

Guwahati-781039, Assam, India

Dedicated to My Loving Family

DECLARATION

I do hereby declare that the research work embodied in this thesis entitled "SPIRAL AND SCROLL WAVE DYNAMICS IN AN EXCITABLE MEDIUM AND THEIR BEHAVIOUR AROUND EXCITATION PATTERNS AND HETEROGENEITIES" has been carried out by me under the supervision of Dr. Sumana Dutta, Associate Professor, Department of Chemistry, Indian Institute of Technology Guwahati, Assam - 781039, India. The research works have been carried out in the period of August, 2013 to July, 2018.

In keeping with general practice of reporting scientific observations, due acknowledgments have been made wherever the work described is based on the findings of other investigations.

Place: IIT Guwahati
Date:

Dhriti Mahanta
Roll No. 136122011

INDIAN INSTITUTE OF TECHNOLOGY GUWAHATI

Dr. Sumana Dutta

Associate Professor

Department of Chemistry

Indian Institute of Technology Guwahati

Guwahati, 781039, Assam, India

Phone no. +91-361-258-2322(O)

Fax no. +91-361-258-2349

Email: sumana@iitg.ac.in

To whom it may concern

This is to certify that the research work presented in this thesis entitled "SPIRAL AND SCROLL WAVE DYNAMICS IN AN EXCITABLE MEDIUM AND THEIR BEHAVIOUR AROUND EXCITATION PATTERNS AND HETEROGENEITIES" is an authentic record of the results obtained from the research work carried out by Dhriti Mahanta (Roll No. 136122011) under my supervision in the Department of Chemistry, Indian Institute of Technology Guwahati, India. This work is original and has not been submitted elsewhere for a degree or award.

Place: IIT Guwahati
Date:

Dr. Sumana Dutta
(Thesis Supervisor)

Acknowledgments

With the grace of the almighty, as I proceed to present my PhD work, I would like to offer my sincere sense of gratitude to all the wonderful people around me who have offered their valuable ideas, guidance, support and assistance throughout this beautiful venture of mine into the world of research.

I will forever be grateful to my supervisor Dr. Sumana Dutta for introducing me to this interesting field of research. No word is sufficient to thank for your constant support, valuable guidance and scholarly inputs, throughout my PhD career. You have always been a source of inspiration for me Ma'am. As mentor, a guide, a counselor and at times even like an elder sister, you have constantly offered your continuous support to me throughout my stay at IIT Guwahati as a researcher. I have very often felt quite lucky to have a supervisor like you. I really thank you from the bottom of my heart.

I extend my sincere gratitude to my doctoral committee members, Prof. Ashish Kr. Gupta, Prof. Saurabh Basu, and Dr. Kalyanasis Sahu for their invaluable comments, suggestions and feedback that have enabled me to improve and present my work in the shape that it is today.

No amount of acknowledgment will ever be enough to do justice to the kind of support, love, guidance and encouragement I have received from my parents Ramesh Mahanta and Beenapani Mahanta, as well as my elder sister Dr. Purabi Mahanta. My family has always been the wall for me on which I could lean on at the most challenging times of my life and career.

I am grateful to IIT Guwahati and the Department of Chemistry for the facilities, access to laboratories, equipments and financial support without which this research work could never have been carried out successfully.

I express my gratitude to my past and present group members, especially Dr. Nirmali Prabha Das for her initial help, friendly working atmosphere and her nice company. I would also like to thank my friends Mahmuda, Gaurangi, Aparajita, Hiranya, Nimisha, Chandana, Satyapriya and Bedika Ba for being there beside me right from my M. Sc days. A few of my old friends have always been an integral part of my life and I can never ignore their innumerable contributions that have helped me reach the stage I am in today. Thank you Dwijasish, Momi, Parimita, Swatahsiddha, and Pranita.

Lastly, I thank all the people who have been in direct or indirect association with me for my research work and have helped me in even the slightest possible manner.

Abstract

Self organizing spatiotemporal patterns in excitable chemical media have been extensively studied in recent decades due to their close link with some complex biological phenomena. Formation and propagation of excitation waves in the heart give rise to arrhythmias that are characterized by the disruption of the normal cardiac rhythm. Complicated situations may arise when these unwanted waves interact with one another leading to their reconnection or break-up. Spiral break up or turbulence is related to a medical condition known as fibrillation, which when occurs in the ventricles, can cause sudden cardiac arrest and death of the patient within minutes. Another scenario may arise when the excitation wave encounters an unexcitable anatomic obstacle in the heart and gets attached to it. Such anchoring is known as pinning, which significantly stabilizes the waves and may even prevent the collapse of a vortex that otherwise would have a finite lifetime.

The effective treatment of arrhythmias is a challenging task that requires the complete knowledge about the reentrant waveforms and their necessary control. However, direct experimental study with a live heart on a regular basis is not feasible. Therefore chemical excitable medium is frequently used as a basis to predict the reentrant wave behavior in cardiac muscle. The Belousov Zhabotinsky reaction is one such system. This simple chemical reaction can be easily performed in a test tube or Petri dish that facilitates direct experimental observation of spiral and scroll waves under appropriate conditions. The behavioral similarities of the BZ-system with the cardiac tissue makes it one of the simplest and most widely used laboratory models for the study of excitation waves.

Our experiments with the BZ reaction and numerical simulations of reaction-diffusion models primarily focus on the detailed dynamics of pinned and reconnected scrolls of complex geometries as well as the unpinning of some anchored vortices in response to external fields. In another numerical study we explore how the spiral wave dynamics depend on an excitability parameter.

Plan of the thesis

Chapter 1 is a brief introduction to our research area. In addition to a short history of the field, this chapter elaborates the two and three dimensional chemical waves with special emphasis on their biological relevance, motivation of our work and objectives of the thesis.

Chapter 2 describes all the experimental techniques, simulation models, and theoretical tools used to carry out this research work. Most of the methods have been discussed with proper pictorial examples and schematic diagrams that explain the basic features of spiral and scroll waves.

Chapter 3 of the thesis illustrates the dynamics of three-dimensional excitation vortices pinned to inert sheets with circular holes arranged on a hexagonal lattice. The pinning object is highly branched and much larger than the anchors reported in earlier studies.

Experiments with the Belousov-Zhabotinsky reaction and numerical simulations of an excitable reaction-diffusion model have revealed scroll wave pinning that prevents the rapid collapse of free vortex rings. The pinned scroll waves are affected by the topological mismatch between the original shape of the filaments and branched structure of the pinning obstacle. Depending on the initial condition, a multitude of stable vortex states have been observed having wave periods considerably different from a free scroll.

Chapter 4 is based on the behaviour of scroll waves in the presence of multiple unexcitable heterogeneities and external gradients. Scroll waves in reaction diffusion systems have been pinned to several inert obstacles that gives rise to highly enhanced lifetimes of the pinned filaments. An external gradient can be applied to unpin the scroll waves sequentially from the anchoring sites. As the number of pinning sites are increased, the strength of the field required to unpin the filament also increases. The time required for unpinning changes with the change in the number of anchors, the geometry in which they are arranged, and their placement relative to the external field direction. Experiments with the Belousov Zhabotinsky reaction are supported by numerical simulations of the simple two variable Barkley model.

Chapter 5 elaborates a study on the reconnection dynamics of several scroll waves. Reconnection of three to six scrolls, placed in close vicinity of one another and arranged in different possible geometries, have been investigated. The reconnected waves have substantially large filaments of different irregular shapes in the initial stage. The complex shapes of the huge vortices smoothen with time and gradually approach a regular geometry. This work focuses mainly on the curvature dependent shrinkage of the filaments and alteration of their lifetimes depending on the initial arrangement of the reconnecting scrolls.

Chapter 6 contains the results of a detailed study to explore the effect of excitability on the properties of two dimensional waves in the BZ-system. Numerical simulations using the Oregonator model reveals various regimes of wave activity, from sustained oscillations to wave damping, as the system undergoes a Hopf bifurcation, with changing values of the excitability parameter, ε. We also discover a short range of parameter values where random oscillations are observed. With an increase in the value of ε, the frequency of the wave decreases exponentially, as the dimension of the spiral core expands. These numerical results are confirmed by carrying out experiments in thin layers of the BZ system, where the excitability is changed by varying the concentrations of the reactant species. This study acts as a quantitative evidence of the relationship between the excitability parameter, ε, and the substrate concentrations.

List of Publications

1. Pinning of scroll waves to flat and highly branched unexcitable heterogeneities, D. Mahanta, S. Dutta, and O. Steinbock, Phys. Rev. E **95**, 032204 (2017).

2. Spirals in a reaction-diffusion system: Dependence of wave dynamics on excitability, D. Mahanta, N. P. Das, and S. Dutta, Phys. Rev. E **97**, 022206 (2018). [Experimental results reported in this paper had been included in the PhD thesis of N. P. Das]

3. Unpinning of scroll waves under the influence of a thermal gradient, N. P. Das, D. Mahanta, and S. Dutta, Physical Review E **90**, 022916 (2014). [not included in the thesis]

4. Unpinning of scroll waves attached to multiple heterogeneities, D. Mahanta and S. Dutta, *under review*.

5. Dynamics and Control of Spiral and Scroll Waves, S. Dutta, N. P. Das, and D. Mahanta, *in the book "Complexity and Synergetics"*, Springer Publishers, Heidelberg, 2018. (book chapter)

6. Nonlinearity in the Realm of Chemistry, S. Dutta and D. Mahanta, Physics News **47**, 52 (2018). (magazine article)

7. Reconnection of multiple scroll waves, D. Mahanta and S. Dutta, *communicated.*

List of Conferences/ Workshops/ Schools participated in:

1. Gordon Research Conference on Oscillations and Dynamic Instabilities in Chemical Systems, Les Diablerets, Switzerland, July 08-13, 2018.
2. Asia-Pacific Conference of Theoretical and Computational Chemistry (APCTCC 8), IIT Bombay, Dec 15-17, 2017.
3. 5th International Conference on Complex Dynamical Systems and Applications, IIT Guwahati, Dec 04-06, 2017.
4. Dynamics Days Europe International Conference, University of Szeged, Hungary, June 05-09, 2017.
5. Hands-on Research in Complex Systems School, International Centre for Theoretical Physics, Italy, July 17-29, 2016. [Distinguished Poster Award]
6. International Conference on Nonlinear Dynamics and its Applications in Physical and Biological Sciences (ICNDAPBS), Darjeeling Govt. College, Darjeeling, Nov 01-03, 2014.
7. "ACS on Campus" conducted by American Chemical Society, IIT Guwahati, Jan 16, 2017
8. Frontiers in Chemical Sciences (FICS 2016), IIT Guwahati, Dec 08-10, 2016.
9. National Seminar on Emerging Trends in Chemical Sciences, Gauhati University, Nov 05-06, 2015.
10. Contemporary Developments in Chemical Sciences (CDCS 2015), Tezpur University, Nov 23-24, 2015. [Best Oral Presentation Award]
11. Research Scholars' Congress 2015 (Workshop on Advanced Microsoft Excel, Latex and Lyx), IIT Guwahati, May 23-24, 2015.
12. ChemConvene 2015, IIT Guwahati, April 08, 2015.
13. ChemConvene 2017, IIT Guwahati, July 25, 2017.
14. Technical Communication and Writing Workshop, IIT Guwahati, April 13-17, 2015.
15. 8th Mid-year CRSI (Chemical Research Society of India) National Symposium in Chemistry, CSIR-NEIST, Jorhat, July 10-12, 2014.
16. National Symposium on Nonlinear Statistical Physics and Nonlinear Dynamics, Indian Association for the Cultivation of Science (IACS), Kolkata, January 02-04, 2014.

Contents

List of Tables

List of Figures

Chapter 1

INTRODUCTION

1. INTRODUCTION

1.1 Self organizing patterns in biology and chemistry

Self organized patterns are abundant in nature. Starting from the spots and stripes on animal coats, butterfly wings, fishes, reptiles, or sea shells to the wind blown ripples of the sand dunes, ordered structures are profusely observed in our surrounding. The fascinating fact about these patterns is their spontaneous emergence without the intervention of any external agent. Apart from the natural world, a large variety of such patterns are found in diverse fields including physics, chemistry, biology, ecology, sociology, economics, medicine, technology etc [3].

The spiral is a frequently observed structural element of many natural patterns and its three dimensional counterpart is known as a scroll [2, 3]. These structures, both static and dynamic, are widely encountered in numerous systems starting from tiny living organisms to large galaxies [4] [Fig. 1.1].

Fig. 1.1: Spirals in nature (a) a snail shell (b) arrangement of sunflower seeds (c) spiral like arrangement of leaves in plant (d) a beautiful spiral galaxy NGC 1566 [5].

Rotating spirals have been the subject for extensive theoretical and experimental research in recent decades due to their close link with some intriguing biological phenomena. An interesting example at the cellular level is the complex dynamics of calcium concentrations in the intracellular medium of the cell. Nonlinearities in the calcium cycling process give rise to spatial patterns of Ca^{2+} waves that often look like spirals [Fig. 1.2(a)]. Such intracellular Ca^{2+} waves are observed in Xenopus oocytes [6]. Another classic example of spiral pattern in the biological world is found during the aggregation of soil living social amoeba *Dictyostelium discoideum* [7], as seen in Fig. 1.2(b). When there is extreme scarcity of nutrients, these amoeba aggregate to form colonies by communicating with other cells even over large distances. Some individual amoeba cells release a pulse of $3', 5'$-cyclic adenosine monophosphate (cAMP) molecules. The communication is thus initiated, other amoeba respond to which by releasing more cAMP molecules. Finally these pulses orga-

nize into large spiral waves of cAMP concentration. Depending on the population density, the large-scale pattern formed in this manner may sometimes be concentric circles, known as target waves. Experiments have shown that target patterns are obtained when the population density is low, whereas higher density favors the formation of spirals [8].

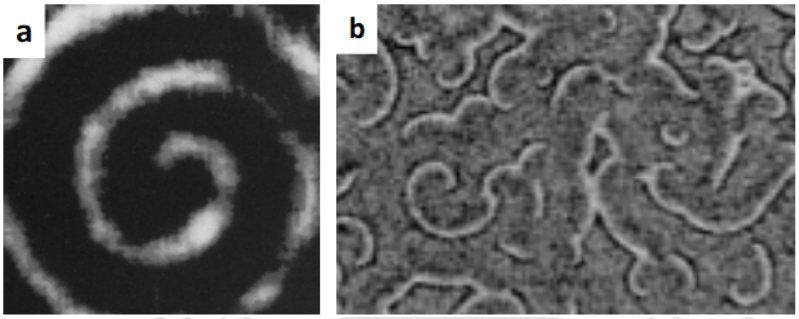

Fig. 1.2: (a) Intracellular Ca^{2+} release in Xenopus oocyte leading to the formation of a spiral of wavelength $\sim$ 150 μm and period $\sim$ 6 s. (b) Spirals evolved in laboratory experiments using slime mold *dictyostelium discoidium*, 6 hours 16 minutes after the point of food deprivation. The bright bands and the accompanying dark shadows indicate the cells in an active state, while the gray background corresponds to inactive cells. Reprinted with permission [8, 9].

Spiral wave activity is also found in vital organs like brain, retina and heart. Formation and propagation of these waves in the heart gives rise to arrhythmias, which are characterized by the disruption of the normal cardiac rhythm [10]. Diffusive waves of depolarization, known as spreading depression (SD), propagating in the retina and neocortex of the brain have been suggested to be associated with migraine and stroke [14]. SD waves have been shown to evolve into different kinds of spatial patterns in rats [11] and spiral waves in isolated chicken retina [12]. It has also been suggested that spontaneous uterine contraction in women during delivery of the fetus may involve some reentrant waves [15]. Different hypotheses involving gap junctions and pacemaker cells have been proposed to explain the transition from a quiescent state to a state of rhythmic contraction that begins at the onset of labor, although nothing has been clearly established yet. However, direct experimental studies on these biological systems are quite challenging as they usually require sophisticated techniques in addition to high level of expertise. Moreover, regular studies with living biological systems are generally not cost effective. Hence simpler prototypes of these systems, if available, are often opted for by researchers. An interesting class of chemical reactions, which are relatively much easier and straightforward to investigate, have been widely used as model systems for studying spiral and scroll wave activities in biological systems. The prototypical behaviour of these simple reactions lies in their oscillatory nature and capability of sustaining spatiotemporal patterns.

The oscillatory chemical reactions have been the subjects for extensive theoretical and experimental research in recent decades. The history of this field is relatively brief, although the description of the first homogeneous chemical reaction exhibiting an oscillatory

clockwork was published by Bray in 1921 [16]. He reported oscillations in the catalytic decomposition of hydrogen peroxide under the influence of iodate ion. Unfortunately his idea was rejected by most chemists as they assumed the oscillations to arise from the presence of dust particles in the reaction system. Research in the area progressed significantly only after the landmark publication of Turing on morphogenesis, accidental discovery of the Belousov Zhabotinsky reaction, and the pioneering work of Prigogine on dissipative structures in the mid 1900s.

1.2 A brief history of oscillating reactions and nonlinear chemical dynamics

In 1952, the British mathematician Alan Turing first proposed a chemical mechanism for biological pattern formation in his masterpiece "The Chemical Basis of Morphogenesis" [5]. He suggested that suitable chemical reactions coupled appropriately with diffusion could give rise to stationary patterns. These patterns arise from a homogeneous initial state and thus can be regarded as symmetry breaking structures. Turing's model involves two types of morphogens or chemicals that act as shape formers, a slowly diffusing activator and a fast diffusing inhibitor. The model can generate spots and stripes, two specific kinds of patterns similar to those encountered on animal coats. Turing's work had profound influence on theoretical studies in the area of pattern formation in the following years. Apart from biological morphogenesis, his mechanism inspired studies describing patterns in semiconductor physics [18], star formation in galaxies [7], spiral like arrangement of sunflower seeds [20], formation of hair fibers [21], tissue regeneration in hydra [22], and patterns formed in chemical reactions [6]. However, identifying the morphogens responsible for pattern formation in a biological system is extremely difficult and demonstrating the initially stable homogeneous state was not an easy task either. Thus in spite of extensive theoretical work, Turing patterns remained experimentally elusive until 1990 when the first experimental evidence was reported using a chemical reaction [24].

Meanwhile in Russia, biochemist Boris Pavlovich Belousov (1893-1970) accidentally discovered an oscillating chemical reaction while looking for an inorganic analog of Krebs cycle, a key metabolic process of all aerobic organisms. The series of chemical reactions constituting the Krebs cycle involve citric acid as an intermediate. Belousov's investigation was based on a solution of bromate, citric acid, and cerium ions (Ce^{4+}), where he expected a monotonic conversion of yellow Ce^{4+} into colorless Ce^{3+}. However, to his astonishment, the solution exhibited a periodic color change between colorless and yellow even when the initial conditions and temperature were varied. Again, yellow traveling waves were observed in an unstirred system. He tried to publish his work several times between 1951 to 1958, but did not not succeed since his observations were believed to contradict the second law of thermodynamics. Later another Russian young scholar, Anatol Zhabotinsky, working with an aqueous solution of $KBrO_3$, $[Ce(SO_4)]_2$, citric acid, H_2SO_4, and water made a similar observation in 1961 [25]. His formulation, where he replaced citric acid

by malonic acid, was better in the sense that it did not produce precipitate. Zhabotinsky and coworkers also found that ferroin, a redox indicator that Belousov used in some of his experiments to enhance the color change, could catalyze the reaction and cerium catalyst is redundant in the reaction [26]. Ferroin is red in reduced state ($[Fe(o\text{-}phen)_3]^{2+}$) and blue when oxidised ($[Fe(o\text{-}phen)_3]^{3+}$) and therefore the color change of the oscillations during the reaction are more sharp as compared to the pale yellow to colorless change of $Ce^{4+}|Ce^{3+}$ system. He successfully published his work and his recipe is the most widely used version of the reaction today. The reaction is known as Belousov-Zhabotinsky reaction after the names of both the Soviet scientists. The overall reaction is,

$$2BrO_3^- + 3CH_2(COOH)_2 + 2H^+ \rightarrow 2BrCH(COOH)_2 + 3CO_2 + 4H_2O \tag{1.1}$$

Belousov's report of an oscillatory reaction was primarily rejected on the basis of a wrong notion regarding the Second Law of Thermodynamics, which states that the entropy (S) of the universe must increase during a spontaneous process. This is mathematically expressed as,

$$\Delta S_{total} > 0 \tag{1.2}$$

the Second Law of thermodynamics predicts the direction of spontaneous change in terms of entropy and another state function, Gibbs free energy, which is defined as,

$$G = H - TS \tag{1.3}$$

where, H is the enthalpy function and T is the temperature. Since it is not easy to keep track of entropy of the universe in a chemical reaction, generally spontaneity of the reaction is predicted by measuring the change in Gibb's free energy. Under constant temperature and pressure conditions, equation 1.2 implies that change in the Gibb's free energy ΔG should be negative for a reaction to be spontaneous [3]. The concept of oscillatory chemical reactions was rejected mainly because of the wrong assumption that during the course of the reaction reactants get converted to products and then products are again converted to reactants, similar to the motion of an oscillating pendulum. Under such circumstances, Gibb's free energy was thought to be decreasing and then again increasing, which would violate the Second Law of Thermodynamics. But the dynamics of these reactions completely differ from that of a pendulum since they do not pass through the equilibrium point during each cycle of oscillation unlike the latter. The difference is clearly understood from Fig. 1.3.

As Fig. 1.3 indicates, a chemical oscillatory reaction can occur only under far-from-equilibrium conditions. Ilya Prigogine and his coworkers suggested that a system could organize, which implies a decrease in the entropy of the system, so long as the net entropy change in the universe was positive [27]. If the reaction involves intermediates, their concentrations may increase and decrease with time, the only condition to be satisfied being a

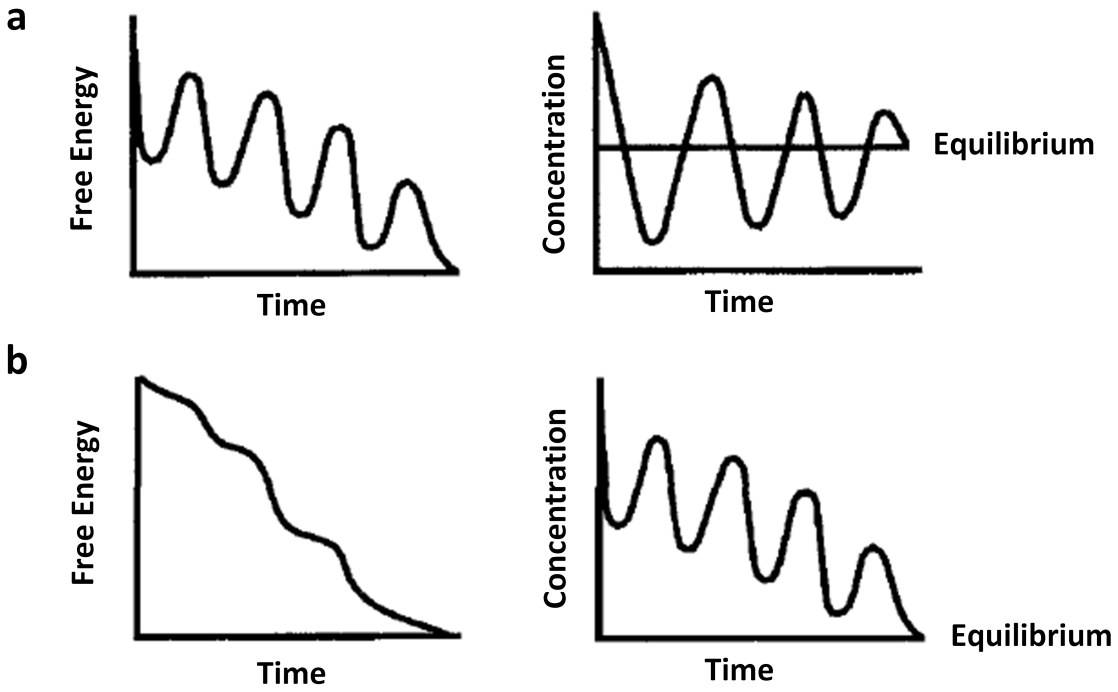

Fig. 1.3: Two types of conceivable oscillations in closed systems, (a) Oscillations around equilibrium; this is not consistent with the Second Law because the free energy must monotonically decrease to the equilibrium value, (b) Oscillations on the way to equilibrium, consistent with the Second Law. [3]

monotonic decrease in the free energy during the process. Prigogine suggested that open systems that are kept far from equilibrium could exhibit spontaneous self-organization by dissipating energy to the surroundings, thereby compensating for the entropy decrease in the system. The temporal or spatial structures arising in such a fashion were termed "dissipative structures" by Prigogine. On the other hand, a closed system can exhibit only transitory oscillations while eventually approaching equilibrium. Prigogine was awarded the Nobel prize in Chemistry in 1977, for his theory on dissipative structures. This new theory could successfully explain the idea of oscillatory BZ-reaction where periodic changes in colors are observed due to the changing concentrations of intermediates like bromide and bromous acid, and not the concentrations of reactants and products.

Zhabotinsky's experimental evidence of oscillating chemical reaction and the path-breaking work of Prigogine in non-equilibrium thermodynamics paved the way for more detailed exploration of such systems. Later Zhabotinsky and coworkers discovered chemical waves in an unstirred BZ medium. They demonstrated the propagation of concentric rings, called target waves, and two dimensional spiral waves in thin layers of BZ-solutions [26, 28]. The three dimensional analogues of spirals, known as scrolls, were reported by Winfree using thick BZ-layers in 1973 [29]. Their work established that in addition to the temporal patterns, a homogeneous system can exhibit spatial selforganization. In the year 1972, in addition to the first ever pictorial demonstration of spiral waves by

Winfree [30], a detailed mechanism of the Belousov Zhabotinsky reaction was described by R. Field, E. Körös, and R. Noyes [13]. Both these pioneering works inspired and helped chemists, by giving a sense of complete understanding of the reaction, to carry out systematic studies on the Belousov Zhabotinsky system. The design and implementation of continuous-flow, stirred tank reactor (CSTR) was another breakthrough that set the stage for discovering new chemical oscillators. The use of this device in experimental practices facilitated a means of maintaining a far from equilibrium condition by a continuous supply of fresh reactants and outflow of reacted material so as to maintain a constant volume [32]. The following decades witnessed an explosion of interest that led to the design as well as development of a large number of new chemical oscillators, and extensive work on spatiotemporal patterns formed in those systems.

1.3 New chemical oscillators

The Briggs-Rauscher reaction is another chemical oscillator discovered by two high school teachers Thomas S. Briggs and Warren C. Rauscher. They combined some of the reactants of already known BZ and Bray reactions to design an oscillator that exhibits cyclic colour changes from colorless to gold to blue [33]. The reaction comprises of hydrogen peroxide, iodate, manganese(II), and malonic acid. This reaction helped to discuss the Bray reaction, mechanistic details of which is only partially understood despite several studies over the years.

The catalytic surface oxidation of carbon monoxide (CO) on platinum surface [Pt (110)] is a reaction that shows oscillatory behavior and formation of spatio-temporal structures. The reaction involves the heating of a mixture of CO and O_2, both at extremely low partial pressures, in a chamber containing a single-crystal wafer of platinum. It results in the adsorption of the gases onto the crystal surface, where they react to form carbon dioxide (CO_2) that again goes back into the gas phase. If the flow is continuously maintained, this reaction continues without the depletion of the catalyst. The system can display target patterns, traveling pulses and spirals as seen in Fig. 1.4. This process is significant from an environmental perspective, as it can be employed in designing car exhaust catalysts with an aim to reduce CO pollution. Gerhard Ertl and his coworkers discovered these patterns and also figured out how to control them [34]. Gerhard Ertl won the Nobel Prize in Chemistry in 2007 for his very imaginative studies in this area.

In contrast to most of the oscillating chemical reactions, which were discovered accidentally, the arsenite-iodate-chlorite system was the first homogeneous oscillator to be designed by a systematic approach [35]. The development of many oscillating systems by varying the oxyhalogen species viz. chlorite, bromate or iodate soon followed this discovery. An important solution phase oscillating system exhibiting temporal oscillations as well as spatial patterns in both open and closed (batch) systems is the chlorite-iodide-malonic acid (CIMA) reaction [36]. Using this reaction De Kepper's group reported the first exper-

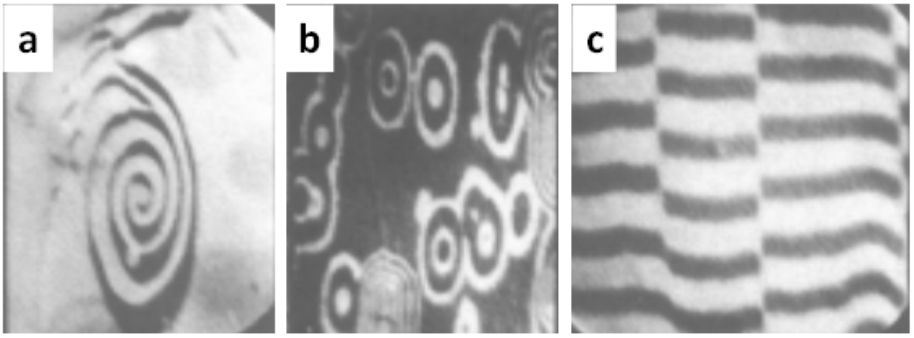

Fig. 1.4: (a) Spirals, (b) target patterns and (c) standing waves in the oscillatory oxidation of carbon monoxide (CO) on a Pt(110) surface. Reprinted from ref [34] with permission.

imental evidence of the occurence of Turing patterns in experimental systems, nearly forty years after the publication of Turing's visionary paper [24]. As the name suggests, the initial reactants used in the CIMA reaction are chlorite (ClO_2^-), iodide (I^-), and malonic acid ($CH_2(COOH)_2$). The overall reaction mechanism is a complex one due to the presence of the organic species malonic acid. Starch is typically used as color indicator in the reaction. The starch, widely used as the indicator for reactions involving iodine, shows a color change from dark blue in the reduced state to pale yellow or colorless in the oxidized state. It plays another important role by binding iodine and iodide, thereby slowing down their effective diffusivity compared to that of chlorite and chlorine dioxide. It has been shown that high starch concentrations lead to the formation of Turing patterns, while only waves are obtained for its lower concentrations [3]. Later variants of the CIMA reaction and some newly developed systems such as the thiourea-iodate-sulfite (TuIS) reaction also successfully produced beautiful spots and stripes in chemical systems, similar to those observed in the biological kingdom [37].

These reactions have emerged as powerful tools for studying the dynamics of a large variety of systems outside chemistry, especially in the biological world. They, apparently, have no link with the complex biological systems such as the heart, brain, frog oocytes or a colony of social amoeba. But all these systems share a common feature known as excitability, which can make a simple table-top chemical experiment an ideal model of a complex phenomenon. All excitable systems have a few key characteristics. When a small perturbation is applied to such a system, it quickly returns to the steady state, but if a sufficiently large stimulation is applied, the perturbation amplifies before the system returns to the original state [3, 11]. Thus there exists a threshold of perturbation, below which no excitation can occur. Besides, all excitable media are characterized by a refractory period. It is the time duration following an excitation, during which the system cannot be re-excited even by applying a stimulus much greater than the threshold value [7]. The systems possessing these properties are referred to as excitable media and are governed by similar mathematical description. The heart is an excellent example of excitable media.

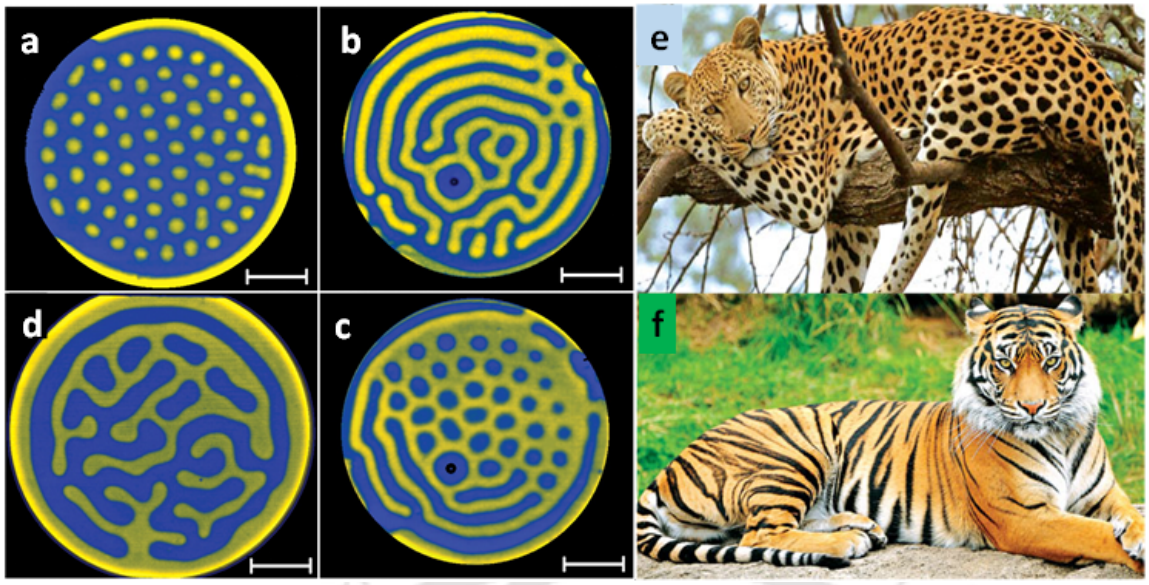

Fig. 1.5: (a-d) Turing patterns observed in the in the thiourea-iodate-sulfite system. (a)hexagonal array of spots (b) stripe pattern (c) coexistence of spots and stripes (d) irregular branch pattern. (e-f) Turing pattern on the skin of tiger. Figure is used from ref [37] with permission.

1.4 The heart

The heart is a complex biological organ and its primary function is blood circulation through the body by means of a coordinated contraction. It acts as a mechanical pump to send oxygen-rich blood to all the organs of the body. The heart is composed of four chambers - two upper chambers called the atria, and two lower chambers known as the ventricles, as shown in Figure 1.6. During a cardiac cycle, deoxygenated blood coming from the body through the vena cava first enters the right atrium and then flows into the right ventricle, from where it is sent to the lungs. The blood releases waste gases in the lungs, and picks up oxygen. This oxygen-rich blood returning from the lungs through the left atrium flows into the left ventricle, which finally pumps it to all the organs. The mechanical contraction during such a cycle is triggered by an electrical impulse. A small region of specialized muscle cells called the sinoatrial (SA) node acts as the spontaneous pacemaker of the heart and sets the cardiac rhythm, also known as the sinus rhythm. Action potentials generated by SA nodal cells propagate through all the chambers of the heart in a coordinated manner [40]. Since the SA node lies in the right atrium, near the entrance of the superior vena cava, an electrical excitation first leaves the atria, reaches the atrioventricular (AV) node and from there it is channeled through specialized conducting bundles, called the His-Purkinje system, to the ventricles. The AV node, being the only conductive link between the atria and the ventricles, is responsible for the relay of the wave of excitation to the ventricles. Its slow conduction allows sufficient time for atrial contraction and ventricular filling. On the other hand, the His-Purkinje system permits rapid conduction of action potentials and ensures effective contraction of ventricular cardiomyocytes

to displace blood out of the ventricles. This entire process is repeated approximately 70 to 100 times per minute under normal conditions, thereby pumping 5 liters of blood each minute [41].

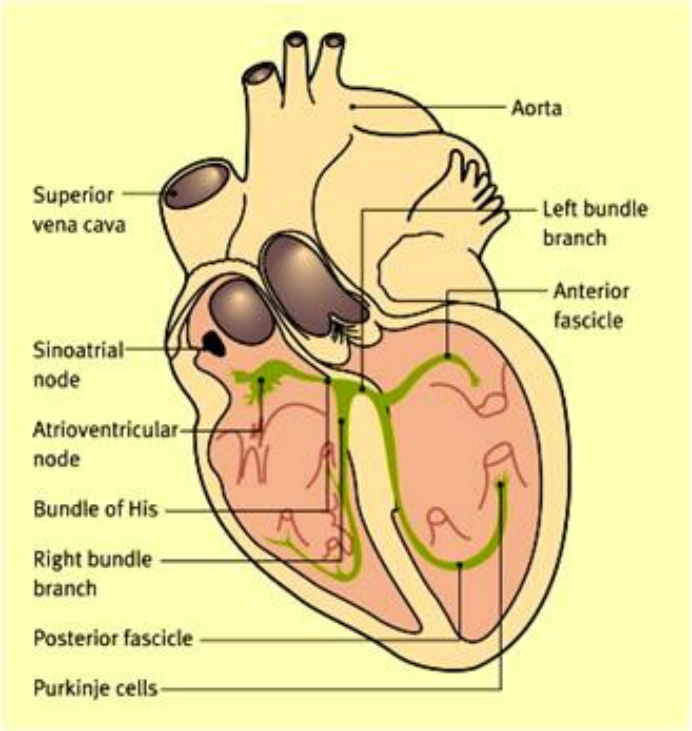

Fig. 1.6: Structure of the heart: its impulse generating and impulse conducting systems. Figure reprinted from [42] with permission.

The electrical and muscular functions of the heart are typically monitored by electrocardiography. It is a simple noninvasive diagnostic tool which measures heart's electrical activity using electrodes placed on the surface of the torso. The graphic trace obtained from the electrocardiograph is referred to as an electrocardiogram, often abbreviated as ECG. It is a plot of voltage changes over time and gives information about the rate, rhythm as well as electrical conduction patterns of the heart. Figure 1.7 shows the normal cardiac rhythm on an ECG. It comprises three major components: the P wave, QRS-complex, and the T wave. The P wave accounts for the depolarization of the atrial myocardium, the QRS complex is related to the ventricular excitation, and the T wave is associated with the recovery state of the ventricles while they are being refilled with blood. The PR interval is a measure of the time taken by the electrical impulse to travel from the SA node to the AV node. The QRS interval indicates the duration of travel time through the ventricles, and QT shows the time required for the ventricles to recover and prepare for another beat [41].

1.4.1 Cardiac arrhythmia

Abnormalities in the cardiac excitation waves leads to cardiac arrhythmias,a clinical condition characterized by abnormal heart rhythms. Some of them are fatal and may cause death

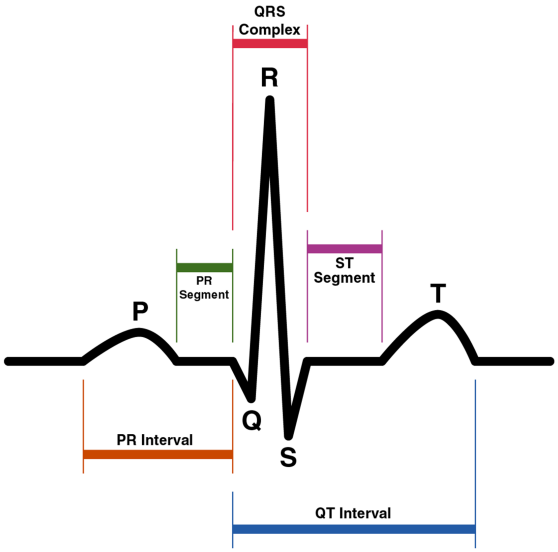

Fig. 1.7: Normal cardiac rhythm

of the patient within a very short period [41]. Cardiac arrhythmias have been one of the leading causes of death in developed nations. They arise basically from abnormal initiation of cardiac impulse, irregularity in its propagation, or some combination of both. Cardiac arrhythmias have been classified in several ways based on their origin, nature etc. Generally, a heart rate of 60-100 beats per minute is considered to be normal in adults. Thus an accelerated heart rate, usually greater than 100 beats per minute, is termed as Tachyarrhythmia in the language of cardiophysiology. The faster rhythm results in reduced blood flow to the organs, which may subsequently lead to decreased ability to exercise, faintness or even death. These arrhythmias can be further classified on the basis of the specific region from where they originate. For example, they may originate from a point within the ventricles and be termed ventricular tachycardia. Similarly if the abnormality arises anywhere above the ventricles, including the SA node, the atria, and the AV node, then they are said to be supraventricular. On the other hand when the rate falls below 100 beats per minute,the rhythm is referred to as bradycardia [41].

Arrhythmias can also be classified based on whether they arise by a reentrant or non-reentrant pathway. In cardiology, reentry is the phenomenon of repetitive excitation of the heart by a single impulse. The mechanisms of some of the complex arrhythmias like atrial fibrillation, polymorphic VT, and ventricular fibrillation have been suggested to involve a reentry [11]. Initially, in the early 1900s, it was believed that an obstacle, around which the electrical wave would rotate, is the primary requirement for reentry to occur. This type of reentry is now called anatomical reentry, where conduction velocity of the medium as well as the size of the obstacle play critical roles [11]. The minimum critical size of the obstacle, that can support such repeated excitation, is decided by the refractory period of the medium. The circumference of the obstacle must be greater than this critical size, so that the excitation front does not hit the recovering medium behind the preced-

ing wave [7]. Anatomical reentry can arise when the cardiac tissue contains some anatomic heterogeneities like scar tissues, coronary vessels, etc. They can act as the anchors for electrical waves if the perimeter of the geometric entity is longer than the wavelength. Thus anatomic reentry is frequently observed in atria, since heterogeneities including large blood vessels are abundant there [43]. Another kind of reentrant phenomenon was demonstrated later, in the 1960s, by a group of Russian scientists led by Valentin Krinsky. They showed that an inexcitable anchor is not always required for reentry to occur and such activity can be sustained even in a completely homogeneous medium. This kind of reentry is referred to as functional reentry [7]. Many tachyarrhythmias originating in the atrial or ventricular myocardium have been suggested to involve such reentrant activity. However, both forms of reentry may have the same underlying mechanism and functional reentry can be converted to anatomical reentry if a drifting excitation wave comes into contact with an obstacle and anchors to it. Reentrant arrhythmias may be associated with either of these two types of reentry.

A number of models have been proposed to explain the mechanistic details of reentrant arrhythmias. The spiral wave hypothesis is one among them. This comparatively new model is more widely accepted now due to its solid theoretical background. The theory has been used widely to explain the mechanisms of monomorphic and polymorphic ventricular tachycardia and fibrillation.

The electrocardiographic patterns observed during monomorphic and polymorphic cardiac arrhythmias can be properly explained by spiral wave activity [44]. It has also been successfully used to describe the ECG patterns during fibrillation [45]. Monomorphic ventricular tachycardia (VT) has been suggested to occur due to the presence of an anchored spiral wave that is unable to drift within the ventricular myocardium. On the other hand, a polymorphic VT is related to a meandering or drifting spiral wave. Ventricular fibrillation (VF) is somewhat more complex in nature, which corresponds to multiple spiral waves. It is often preceded by VT [Fig. 1.8]. It is because, the single spiral giving rise to VT may break up to produce multiple spirals, which may eventually lead to VF. A large number of mechanisms have been proposed by various groups to explain the onset of spiral wave break-up [46, 47] in cardiac tissues. However, the precise mechanisms of both spiral wave breakup and fibrillation are yet to be clearly understood, which may further differ depending on the species, conditions and the different regions of the heart [43].

Elucidation of the mechanisms that lead to reentrant arrhythmias require detailed knowledge about the propagation of electric waves in the thick myocardial tissue, which is essentially three dimensional. Mathematical models and computational techniques prove quite useful in this regard. However, the experimental studies on the reentrant waves in a living heart is still very challenging in spite of the advances in experimental techniques in recent decades. It is not easy to carry out experiments to directly observe what happens in the thick atrial or ventricular wall owing to the complicated electrophysiology and anatomy of the heart. This type of experimental studies will require recording of the propagating waves

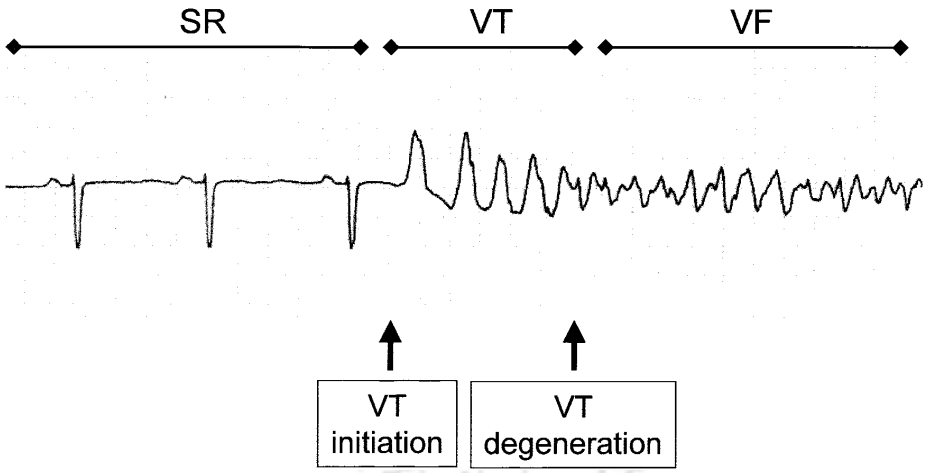

Fig. 1.8: Surface ECG showing the transition from normal sinus rhythm (SR) to ventricular tachycardia that finally ended up in ventricular fibrillation in human heart. Reprinted from [45] with permission.

with sufficient temporal and spatial resolution [11]. Two techniques, known as electrode arrays and optical mapping, are often used for data acquisition. Electrode arrays can be used to acquire information not only from the surface, but also from the depth of tissue. Despite that, the method cannot be always used as it suffers from serious disadvantage of coarse spatial resolution and may result in damage of the heart [48]. On the contrary, data obtained from optical mapping is of much higher spatial resolution, but limited to surface only [49]. Besides, interpretation of the data collected is often difficult in both these methods.

The knowledge about the behaviour of spiral and scroll waves in the cardiac tissue often comes from some much simpler homogeneous systems. The Belousov-Zhabotinsky (BZ) reaction is such a medium facilitating detailed studies on the dynamics of spiral and scroll waves. It is the cleanest, simplest and one of the best understood models of cardiac wave propagation that allows direct experimental observation of the waves in a petri dish or test tube. Even though this homogeneous chemical medium is much less complex than the heart, which is highly heterogenous and anisotropic, they share some crucial properties. Both these nonlinear systems are excitable. Thus both are characterized by an excitation threshold, a refractory period and can undergo self-sustaining oscillations under suitable conditions. Moreover, their dynamics are governed by similar mathematical description. These behavioural similarities make the BZ reaction a basis for understanding and predicting the dynamics of wave propagation in two and three dimensional cardiac muscle.

1.5 The Belousov Zhabotisky reaction

The Belousov-Zhabotinsky (BZ) reaction is one of the best understood and most familiar examples of oscillatory chemical reaction occurring under far from equilibrium conditions [25]. The reaction is basically a catalytic oxidation of various, usually organic, reductants by an acidified bromate solution at low pH. The catalyst of the reaction is a transition metal

ion, the most widely used metal ion couples being $Fe^{2+}|Fe^{3+}$ and $Ce^{3+}|Ce^{4+}$. There is an interesting variant of the BZ reaction that uses ruthenium catalyst and exhibits light sensitivity [50, 51].

As mentioned in the earlier section, a group of three scientists reported the detailed and complete mechanism of the Belousov Zhabotinsky reaction in 1972. Field, Körös, and Noyes, then working in the university of Oregon, used the basic principles of chemical kinetics and thermodynamics governing ordinary chemical reactions to explain the qualitative behavior of the reaction. The mechanism, known as Field-Körös-Noyes (FKN) mechanism, after their names, consists of the following ten steps that involve many chemical species and cerous-ceric system as the metal ion catalyst [13].

$$HOBr + Br^- + H^+ \rightleftharpoons Br_2 + H_2O \tag{1.4}$$
$$HBrO_2 + Br^- + H^+ \rightarrow 2HOBr \tag{1.5}$$
$$BrO_3^- + Br^- + 2H^+ \rightarrow HBrO_2 + HOBr \tag{1.6}$$
$$2HBrO_2 \rightarrow BrO_3^- + HOBr + H^+ \tag{1.7}$$
$$BrO_3^- + HBrO_2 + H^+ \rightleftharpoons 2BrO_2 + H_2O \tag{1.8}$$
$$BrO_2 + Ce^{3+} + H^+ \rightleftharpoons HBrO_2 + Ce^{4+} \tag{1.9}$$
$$BrO_2 + Ce^{4+} + H_2O \rightarrow BrO_3^- + Ce^{3+} + 2H^+ \tag{1.10}$$
$$Br_2 + CH_2(COOH)_2 \rightarrow BrCH(COOH)_2 + Br^- + H^+ \tag{1.11}$$
$$6Ce^{4+} + CH_2(COOH)_2 + 2H_2O \rightarrow 6Ce^{3+} + HCOOH + 2CO_2 + 6H^+ \tag{1.12}$$
$$4Ce^{4+} + BrCH(COOH)_2 + 2H_2O \rightarrow Br^- + 4Ce^{3+} + HCOOH + 2CO_2 + 5H^+ \tag{1.13}$$

The above mechanism can be divided into three main processes: process A, process B, and process C [52].

Process A:

BrO_3^- is reduced to Br_2 by a series of oxygen atom transfers and subsequent bromination of malonic acid occurs by Br_2

$$BrO_3^- + Br^- + 2H^+ \rightarrow HBrO_2 + HOBr \tag{1.14}$$
$$HBrO_2 + Br^- + H^+ \rightarrow 2HOBr \tag{1.15}$$
$$HOBr + Br^- + H^+ \rightarrow Br_2 + H_2O \tag{1.16}$$
$$Br_2 + CH_2(COOH)_2 \rightarrow BrCH(COOH)_2 + Br^- + H^+ \tag{1.17}$$

The overall reaction of process A thus becomes,

$$BrO_3^- + 2Br^- + 3CH_2(COOH)_2 + 3H^+ \rightarrow 3BrCH(COOH)_2 + 3H_2O \tag{1.18}$$

Process B:

Process B is an autocatalytic one involving free radical oxybromine intermediates that results in the reduction of BrO_3^- to Br_2. The transition metal ion acting as the catalyst (Ce^{3+} or Fe^{3+}) undergoes oxidation (to Ce^{4+} or Fe^{4+}) thereby supplying an electron to the free radical for the one electron transfer step:

$$BrO_3^- + HBrO_2 + H^+ \rightarrow Br_2O_4 + H_2O \quad (1.19)$$

$$Br_2O_4 \rightarrow 2BrO_2^{\cdot} \quad (1.20)$$

$$BrO_2^{\cdot} + Ce^{3+} + H^+ \rightarrow HBrO_2 + Ce^{4+} \quad (1.21)$$

$$BrO_3^- + HBrO_2 + 2Ce^{3+} + 3H^+ \rightarrow 2HBrO_2 + 2Ce^{4+} + H_2O \quad (1.22)$$

The autocatalytic growth of $HBrO_2$ is limited by the its self-disproportionation:

$$2HBrO_2 \rightarrow BrO_3^- + HOBr + H^+ \quad (1.23)$$

Process C:

This process involves the organic species malonic acid. According to the FKN mechanism, HOBr can brominate malonic acid to yield bromomalonic acid. Ce^{4+} oxidises both malonic acid and bromomalonic acid to regenerate the reduced form of the catalyst and and Br^- ion:

$$CH_2(COOH)_2 + 6Ce^{4+} + 2H_2O \rightarrow 6Ce^{3+} + HCOOH + 2CO_2 + 6H^+ \quad (1.24)$$

$$BrCH(COOH)_2 + 4Ce^{4+} + 2H_2O \rightarrow 4Ce^{3+} + Br^- + HCOOH + 2CO_2 + 5H^+ \quad (1.25)$$

$$Br_2 + HCOOH \rightarrow 2Br^- + CO_2 + 2H^+ \quad (1.26)$$

1.5.1 Patterns formed in the BZ-reaction

The BZ-system can support kinematic and phase waves, pulses or wavetrains, as well as both two and three dimensional waves depending on the composition and thickness of the bulk mixture. Kinematic waves have very little involvement of diffusion. A kinematic wave is obtained when there is a spatial gradient of some properties such as temperature or pH [15]. Phase waves also have very little to do with diffusion and can play a role in the formation of patterns in the BZ-reaction only when coupled with trigger waves. On the other hand, one dimensional trigger waves or pulses are observed, when the concentrations of the reactants are adjusted to make the system spontaneously oscillatory or spontaneously excitable. In the latter case, the reaction remains in steady state if left unperturbed. If a small perturbation is applied, it can quickly come back to the steady state. However, on applying perturbations exceeding a threshold critical value, the system can return to the steady state only after undergoing a large excursion [3]. Thus a sufficiently large disturbance can give rise to a single wave pulse in an excitable BZ-system. The front of the pulse is a wave of oxidation and the reaction mixture is in the reduced state ahead of the

front. The front causes a sharp increase in [$HBrO_2$] and the oxidized form of the transition metal catalyst ([M_{ox}]), while causing a decrease in [Br^-]. A waveback, which is wave of reduction, follows after a certain interval, consumes $HBrO_2$ and M_{ox}. It also results in the production of Br^- and thus the pre-front concentrations are restored [15]. The speed at which the wave propagates is constant and is dependent on the diffusion of $HBrO_2$. The following equation, often used to determine the speed of similar reaction-diffusion fronts, can be employed to approximate the speed of a BZ-wavefront:

$$c = 2(Dk)^{1/2} \tag{1.27}$$

here, c is the speed, D the diffusion coefficient and k is the rate constant for the autocatalytic reaction producing bromous acid. The autocatalytic step is given by,

$$BrO_3^- + HBrO_2 + 2M_{red} + 3H^+ \rightarrow 2HBrO_2 + 2M_{ox} + H_2O \tag{1.28}$$

The rate equation for this step is,

$$rate = \frac{d[HBrO_2]}{dt} = k[H^+][BrO_3^-][HBrO_2] \tag{1.29}$$

Thus, the expression for speed becomes,

$$c = 2(Dk[H^+][BrO_3^-])^{1/2} \tag{1.30}$$

The dependence of the magnitude of wave velocity on $[H^+]^{1/2}$ and $[BrO_3^-]^{1/2}$ have been demonstrated experimentally [21]. However, due to difficulties in making the measurements in this experimental system and the approximation inherent in Eq. 1.30, make the results less precise. It is possible to obtain more accurate results for velocity using the complete mechanism rather than a single step.

1.5.2 Waves in two dimensions

Two dimensional waves can be initiated and propagated in thin layers of BZ-reaction mixture, usually taken in a petri dish. As mentioned in the earlier section, a point source initiation results in an expanding circular wave pulse provided the system is excitable. In the presence of stimulation, either continuous or periodic, a series of concentric blue rings appear on a red background. These concentric circles are known as target patterns [Fig. 1.9(a)]. The presence of heterogeneities such as dust particles or defects in the surface of the reaction chamber is crucial for the spontaneous initiation of target patterns.

The collision of target patterns leads to their annihilation. In a thin BZ reaction mixture containing both high and low frequency target patterns, high frequency patterns gradually grow at the expense of low frequency ones, and occupies the entire volume if allowed to propagate for a sufficiently long time [15].

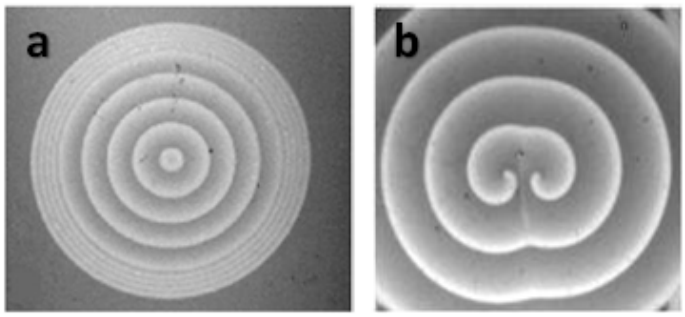

Fig. 1.9: Two dimensional patterns in a homogeneous BZ reaction. (a) Target patterns and (b) spiral wave formed in the ferroin catalyzed BZ-system.

The other kind of two dimensional pattern observed in thin BZ-system are the spiral waves [Fig. 1.9(b)]. These are formed by cleavage of an excitation wave, which when cleaved gives rise to two wavefronts. The broken wavefronts have two velocity components. The longitudinal component acts along the direction of motion of the plane wavefront while there is a transverse component in the perpendicular direction. The magnitudes of these two components being unequal, make the open ends curl in to form a pair of counter rotating spirals. In contrast to the target patterns, spiral waves in a homogeneous reaction system rotate with same frequency and hence equal wavelength. Also the speed at which they propagate is uniform, unlike target patterns. Properties and dynamics of spiral waves have been extensively studied in recent decades.

The geometry and properties of the spiral waves differ significantly from planar or circular excitation waves. Generally the wavefront in a linear or circular wave is always followed by a finite refractory zone. Also the wavefront moves with a velocity that is relatively constant at all its points [11]. Therefore there is always a finite distance, equal to the wavelength (WL), between the wave front and repolarizing tail that prohibits their edges to meet [Fig. 1.10(a,b)]. On the other hand spiral waves have a unique geometry in the sense that their excitation front and the recovering tail actually join to form a phase singularity as shown in Fig. 1.10 [44]. This intersection of the wavefront and the waveback, or the phase singularity, is referred to as the tip of the spiral, and can be considered as the pivot point or the rotor.

In contrast to the linear [Fig. 1.10(a)] or circular [Fig. 1.10(b)] wavefront having equal curvature throughout, the curvature of a spiral wave is not constant along the wavefront. It is well known that the curvature of plane wave is zero and it moves faster [Fig. 1.11(b)] than a convex wavefront for which curvature is positive [Fig. 1.11(c)]. On the other hand the propagation velocity of a concave wave having a negative curvature is still higher than that of a plane wave [Fig. 1.11(a)]. Also, very large curvature of a convex wavefront creates a region of zero propagation [11]. The geometry of the spiral wave is so unique that its curvature varies continuously and becomes maximum at the tip. In that region curvature exceeds the maximum critical value above which the wave cannot propagate along

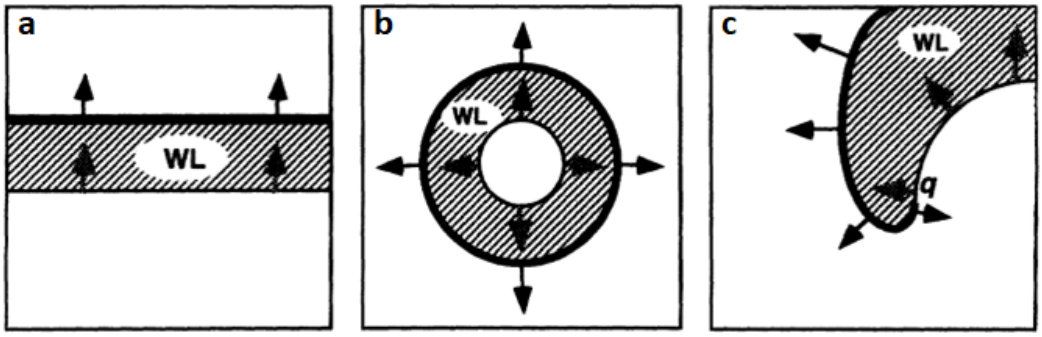

Fig. 1.10: Schematic representation of three types of waves propagating in a homogeneous isotropic medium: a) a planar wave, b) a circular wave, and c) a spiral wave. In each case, the wave front is depicted by thick black edge. The direction of propagation at different points is indicated by black arrows. The distance between the wave front and the repolarizing tail is the wavelength (WL). The wave front of the spiral in (C) has variable curvature and conduction velocity (length of arrow indicates relative conduction velocity). There is a point (q), known as the tip of the spiral, where the wave front meets its own repolarizing tail. Figure reprinted with permission.

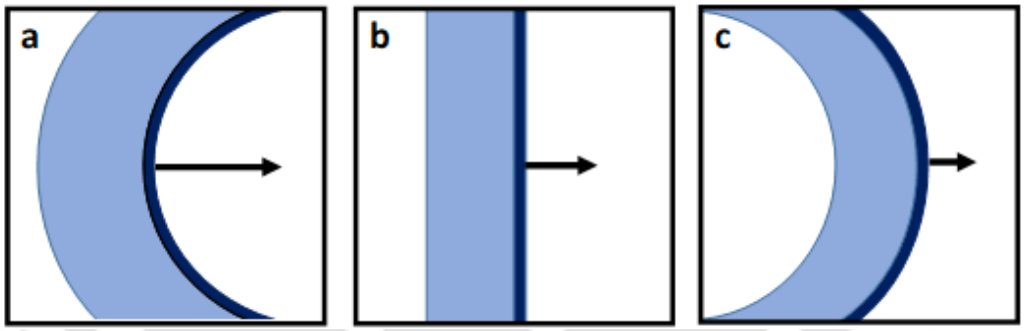

Fig. 1.11: Schematic representation showing the effects of curvature on wave propagation. a) A (concave) wave with negative curvature b) a planar wave, c) a (convex) wave with positive curvature. The length of arrows indicate the relative conduction velocities [11].

the transverse direction. As a result there exists an unexcited region of zero propagation, referred to as the core of the spiral. The rotations of the spiral tip around the core give rise to spiral wave activity. In other words a spiral core can be defined as the trajectory traced by the tip of the spiral.

Early studies on two dimensional chemical waves in the BZ system mainly involved spirals rotating steadily around the core in a circular path. Arthur Winfree suggested that these spiral waves may not always rotate rigidly about fixed centers [30]. It might be possible for the spiral tips to trace out complex trajectories, which he called “meandering”. Later it was demonstrated both experimentally and theoretically that the tip can execute either periodic rotations or a variety of complicated quasiperiodic motions depending on the conditions of the medium. For some specific range of excitability of the medium, the spiral rotations give rise to beautiful flower-like patterns of either epicycloidal [Fig. 1.12(b)] or hypocycloidal [Fig. 1.12(d)] nature. Moreover, the meandering can also occur in a linear

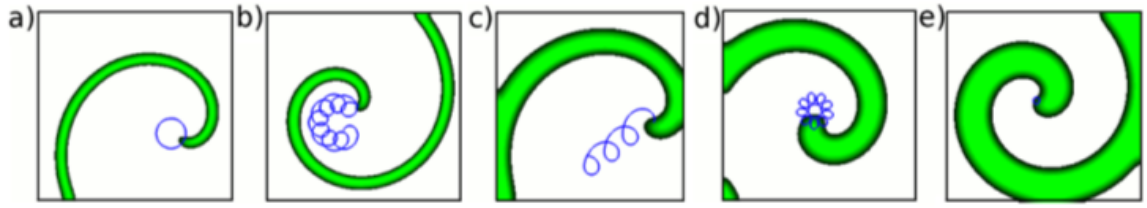

Fig. 1.12: Different types of trajectories traced by spiral wave tips in simulations (a) Rigidly rotating spiral wave with large core, (b) meandering spiral wave with inward loops, (c) drift meandering spiral, (d) meandering spiral wave with outward loops, (e) rigidly rotating spiral wave with small core. Reprinted from [54] with permission.

translational manner, as a result of which the spiral core drifts along a particular direction Fig. 1.12(c) [11]. Figure 1.12 shows different kinds of trajectories traced out by spiral tips.

1.5.3 Waves in three dimensions: scrolls

The three-dimensional counterpart of a spiral is known as a scroll wave. The existence of scroll waves in thick layers of chemical excitable media was first reported by Winfree in 1973 [29]. He also predicted their existence in cardiac tissues. Later various groups have proved their presence in a variety of biological and chemical media.

The simplest scroll wave can be visualized as a set of spirals stacked up exactly on top of one another. The imaginary line joining the tips of these spirals is crucial for the dynamics of the scroll. This one dimensional curve is known as the filament in the literature of nonlinear dynamics and the continuous rotation of the three dimensional vortex occurs around this line. In the simplest case the geometry of the filament is a straight line, but it is not always necessarily so. It can acquire any shape depending on the spatial configuration of the wave and may even be bent, curved, twisted or knotted. A scroll ring is obtained when the stack of spirals form a closed loop giving rise to a ring-shaped filament [Fig. 1.13(c)].

A filament is not rigid, rather it tends to either shrink or expand depending on the properties of the medium. It is a unique characteristic of a scroll wave and is known as the filament tension. The filament undergoes curvature dependent motion accordin to the Eq. 1.31.

$$\frac{\mathrm{d}\mathbf{s}}{\mathrm{d}t} = \alpha\kappa\hat{\mathbf{N}} + \beta\kappa\hat{\mathbf{B}}, \tag{1.31}$$

where α is the filament tension, β the translational drift coefficient, κ the local curvature, $\hat{\mathbf{N}}$ the unit normal vector, and $\hat{\mathbf{B}}$ the unit binormal vector of the curve. This model describes the expansion or shrinkage of the filament as well as its drifting. A positive filament tension $\alpha > 0$, will always result in the shrinkage of the filament, while scroll rings with negative filament tension ($\alpha < 0$) will continue to expand with time [54]. The value of β decides the drifting of the filament along the direction perpendicular the plane of the filament.

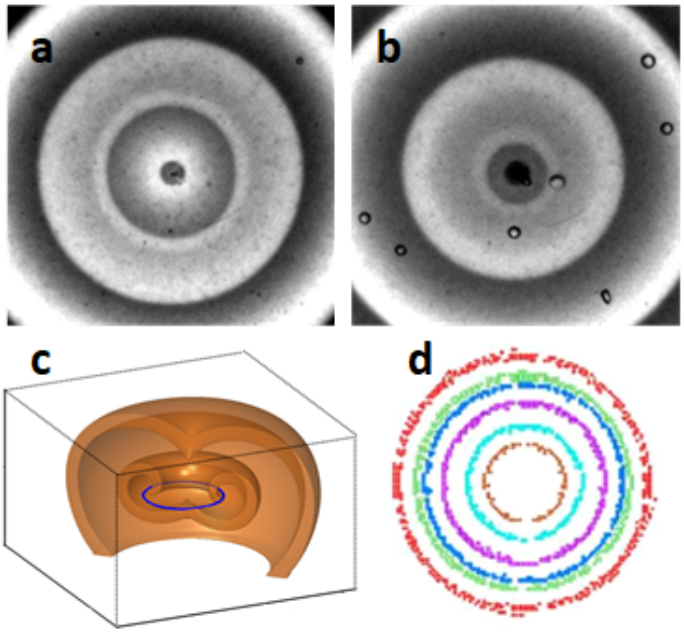

Fig. 1.13: Three dimensional chemical wave. Snapshot of a scroll ring in an experiment with the BZ reaction at time at (a)644 s (b) 4544s. (c) Three dimensional view of the scroll ring rotating around its filament (blue circular curve). (d) Time evolution of the filament showing its gradual shrinkage in simulation.

It has been demonstrated that both shrinking and drifting of the filament accelerate with decreasing size and increasing curvature of the filament [Fig. 1.14]. Eventually the filament shrinks completely and collapse, as in the case of a scroll ring [Fig. 1.13(d)], or acquires a stable shape with the minimal possible length, as in a straight scroll. In contrast, an expanding scroll ring having negative filament tension may collide with the boundaries of the medium giving rise to newer filaments, leading to interesting situations like turbulence. In the BZ system, $\beta \sim 0$ for an appreciable range of concentration, which ascertains that there is no movement in the $z-$direction in that concentration range. Under normal or high excitability regimes the scroll filaments tend to contract, whereas filament expansion occurs for lower excitability regimes [7].

1.5.4 Some interesting behaviour of spiral and scroll waves: Motivation and objectives

Chemical waves can get anchored to unexcitable heterogeneities present in the medium. This phenomenon is known as pinning in the realm of nonlinear dynamics. The exploration of such a phenomenon is of paramount importance from a biomedical perspective too. As discussed in section 1.4.1, pinning of rotors to anatomic obstacles is believed to be responsible for monomorphic ventricular tachycardia. Therefore, this topic has attracted considerable attention of researchers from diverse backgrounds. There have been some interesting reports of pinning of spiral and scroll waves in clinical as well as fundamental studies. All these investigations indicate that anchoring to unexcitable obstacles can

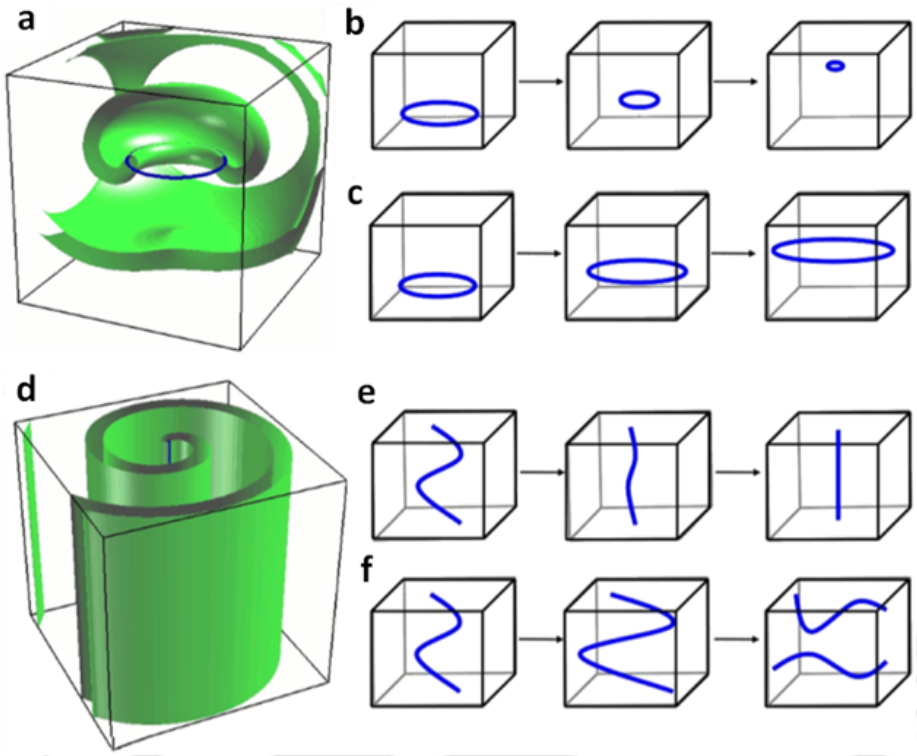

Fig. 1.14: (a) Scroll ring with a circular filament depicted in blue. (b) Shrinkage and drift of a filament ring with positive filament tension, (c) negative filament tension leading to expansion and drift of a scroll ring, (d) straight filament of a scroll wave, (e) an initially perturbed straight filament recovering the stable straight configuration under positive filament tension, and (f) increase in length of an initially perturbed filament that finally breaks into two filaments upon touching the boundary. Reprinted from [54] with permission.

give rise to local stabilization of the rotors [56, 57]. It has also been established that reentrant waves propagating in the heart can get pinned to all kind of heterogeneities such as blood vessels, ionic heterogeneities, pectinate and ventricular muscles [58–60]. Hence, it is desirable to have complete knowledge about the mechanism of pinning and dynamical behaviour of the pinned waves.

Pinning of both spiral and scroll waves have also been observed in chemical media. These studies employing the BZ reaction, the simplest prototype of the heart, show that the chemical waves can anchor to inert heterogeneities introduced into the system. Pinning increases the stability of the filament and considerably increases the lifetime of the scroll [61,62]. This stabilization has been demonstrated by Steinbock and coworkers, introducing inert obstacles of toroidal, spherical, and cylindrical shapes. Figure 1.15 shows some of the inert heterogeneities used in earlier experiments [62, 63].

In some cases the filament may form closed loops [64], whose stability increases manifold [Fig. 1.15(b)] as compared to the vortex anchored at one pinning site [Fig. 1.15(a)]. The obstacles used to arrest the motion of the waves in the earlier experimental studies with the BZ system involve small and discrete objects, with the most complex one being a

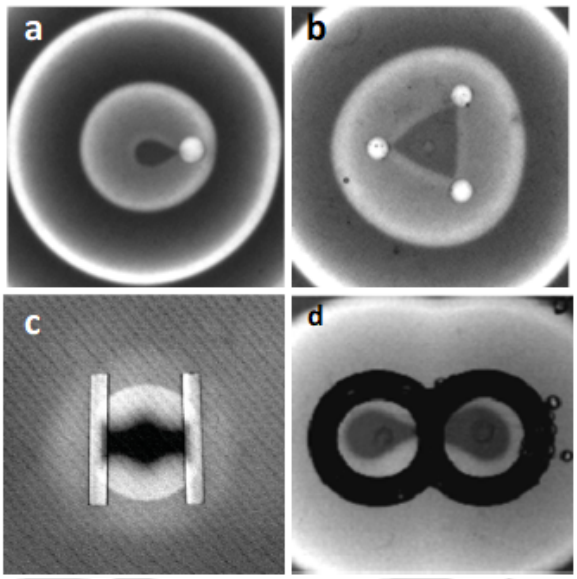

Fig. 1.15: Pinning of three dimensional chemical waves to inert obstacles of different shapes. A scroll wave pinned to (a) a spherical glass bead, (b) three spherical beads forming a triangle-shaped closed loop with the obstacles at the three vertices, (c) two rods and (d) a double torus. (c),(d) Reprinted with permission from [62] and [63] respectively.

double torus that exhibits topologically mismatched pinning [63]. We tried to explore the fate of scroll waves in presence of a much larger and complex inert heterogeneity having numerous branching points. Using a thin polymer sheet with regular arrangement of small circular holes, we have carried out a detailed experimental study with the BZ reaction, which is well supported by numerical simulations of the Barkley model. Our experimental and theoretical observations are described in Chapter 3.

The phenomenon of pinning has detrimental effects on cardiac health. The pinned vortices anchored to anatomical obstacles are usually removed by applying a single electric pulse or train of pulses. This technique is known as antitachycardia pacing (ATP), success rate of which is only about 60–90%. On the other hand, in order to cure fibrillation a strong electric shock ($\sim$5 kV or 100 V) has to be applied directly to cardiac muscle that leaves many side effects [57]. Some other techniques such as ablation are also used to remove the reentrant waves from the heart [65]. All these clinical methods are based on the interaction of the waves with external fields. This requires a detailed knowledge about how the wave behaviour changes in response to external gradients.

It has been established by earlier studies that reaction diffusion systems react to external field gradients [20, 66]. Spiral and scroll waves in the BZ system can also be controlled by external field gradients. On the application of external thermal and electric gradients, spiral waves meander away from their point of initiation [68]. On the other hand, scroll waves try to undergo reorientation to align themselves perpendicular to the direction of the applied gradient [19]. Figure 1.16 shows the effect of externally applied fields on a free scroll wave. In presence of a thermal field, the scroll moves towards the hot end [fig. 1.16(a,b)] and in

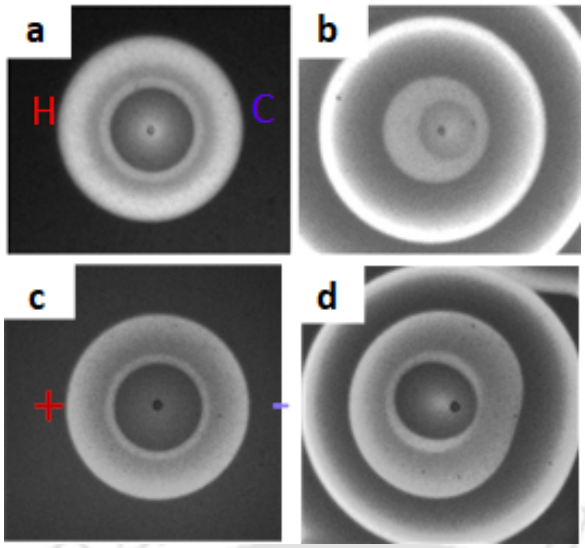

Fig. 1.16: Effect of external fields on free scroll waves. (a,b) Reorientation of a scroll under a thermal gradient ($\nabla T = 1^\circ$ C cm^{-1}). (a) Is just before and (b) 26 min after applying the gradient. (c,d) Effect of an electric field of strength 1 V cm^{-1} on a scroll ring. Time interval between the two snapshots is 10 minutes.

response to an external electric field it moves towards the positive electrode [fig. 1.16(c,d)]. These principles were later employed in experimental studies, which showed that both external thermal [70] and electric gradients [71] can unpin a stably pinned scroll ring in the BZ system. Figure 1.17 shows that the scroll wave undergoes reorientation in presence of a thermal gradient and gets detached from the anchoring sites. The unpinning studies

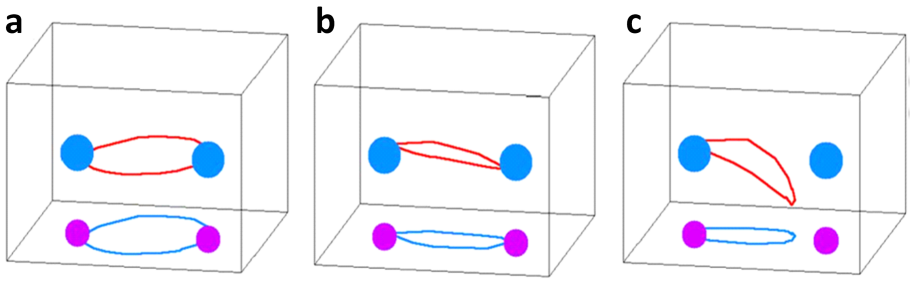

Fig. 1.17: Unpinning of a filament pinned to two spherical obstacles in presence of thermal gradients. (a,b,c) Show the gradual reorientation and unpinning of the filament (shown in red. The blue and purple spheres are the anchoring obstacles. The two dimensional projection of the filaments are seen in the bottom of the box as blue curves.)

are of therapeutic value, since they can provide crucial information about the removal of anatomically reentrant waves that in the long run, may help limiting the use of damaging defibrillating shocks. Chapter 4 contains the results of our experimental and theoretical studies on unpinning of scroll waves. Using multiple spherical obstacles in the homogeneous BZ system, we systematically explored the process of unpinning of the scroll waves. The numerical studies based on the two variable Barkley model constitute the later sections

of the chapter. Apart from externally applied fields, scroll waves can also interact with each

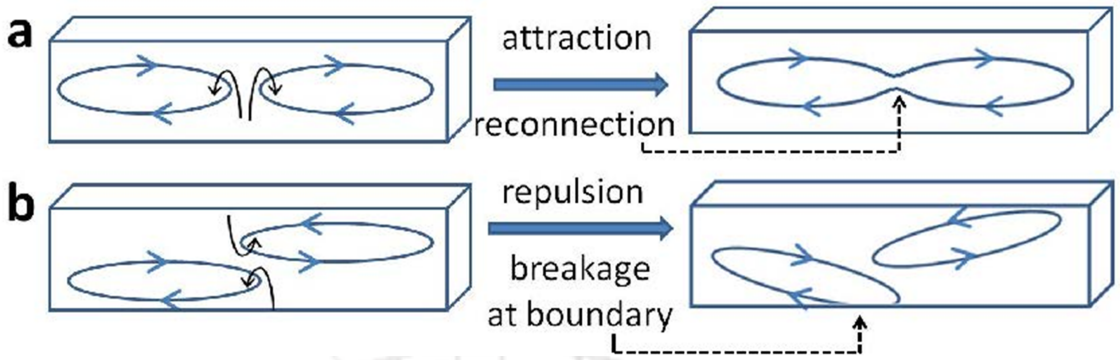

Fig. 1.18: Schematic representation of interaction of two filaments. Small black arrows denote the motion of the constituent spirals around the points of nearest approach of the filaments.(a) Reconnection of vortex filaments. The nearest approaching spirals have opposite sense of rotation. (b) Repulsion of filaments and possible rupture at the boundary. Here the nearest spirals have same sense of rotation [3].

other if they are in close proximity. The interaction of spiral waves have been studied in detail in the last few decades. However, very few experimental studies involving interaction of scroll waves with each other are available in literature. In a recent work with the BZ reaction system, reconnection of two scroll waves have been demonstrated. According to that that study, two scroll rings can either push each other away or reconnect to form a larger ring, depending on their mutual orientation [Fig. 1.18]. Further, the reconnection of filaments is possible only when they lie within close vicinity of each other [21]. The large reconnected filament then undergo curvature dependent motion [11, 17], which can have far reaching consequences in the cardiac tissue. We extended this study to more number of scrolls. In chapter 5 of this dissertation, we describe our findings on the reconnection of three to six scroll rings. The results are based on experiments with the BZ system, and simulations of the Barkley model.

Our experimental and theoretical work on chemical waves is motivated by some of the phenomena that are closely linked with the heart, especially in the context of life threatening cardiac arrhythmias. The formation and propagation of the excitations in the heart and BZ system is made possible by excitability, a common property possessed by both these systems. Excitability of the medium plays important role on the dynamics of the waves, depending on which, the waves may even display break up or chaotic behaviour [54]. In chapter 6 of the thesis, we explore how the spiral wave dynamics depend on the excitability of the medium. Numerical studies have been carried out using the Oregonator Model, since it is believed to be related more directly to the actual concentrations of the reactants of the BZ reaction.

BIBLIOGRAPHY

[1] I. R. Epstein and J. A. Pojman, *An Introduction to Nonlinear Chemical Dynamics* (Oxford University Press, Oxford 1998).

[2] S. C. Müller and T. Plesser, Spiral Wave Dynamics, *in the book "Chemical Waves and Patterns"*, Edited by R. Kapral and K. Showalter, (Springer Netherlands, 1995).

[3] S. Dutta, N. P. Das, and D. Mahanta, Dynamics and Control of Spiral and Scroll Waves, *in the book "Complexity and Synergetics"*, edited by S. C. Müller, P. J. Plath, G. Radons, and A. Fuchs (Springer International Publishing, 2018).

[4] J. P. Keener, SIAM J. Appl. Math. **39**, 528 (1980).

[5] www.nasa.gov

[6] J. Lechleiter, S. Girard, E. Peralta, and D. Clapham, Science **252**, 123 (1991).

[7] O. Steinbock, F. Siegert, S. C. Müller, and C. J. Weijer, Proc. Natl. Acad. Sci. U.S.A. **90**, 7332 (1993).

[8] K. J. Lee, E. C. Cox, and R. E. Goldstein, Phys. Rev. Lett. **76**, 1174 (1996).

[9] J. Lechleiter and D. Clapham, Cell **69**, 263 (1992).

[10] J. Jalife, M. Delmar, J. Anumonwo, O. Berenfeld, and J. Kalifa, *Basic Cardiac Electrophysiology for the Clinician* (Wiley-Blackwell, Oxford, UK, second edition 2009).

[11] M. Shibata and J. Burls, J. Neurobiol. **5**, 107 (1974).

[12] N. A. Gorelova and J. Bureš, Dev. Neurobiol. **14**, 353 (1983).

[13] Y. Yu, L. M. Santos, L. A. Mattiace, M. L. Costa, L. C. Ferreira, K. Benabou, A. H. Kim, J. Abrahams, M.V. L. Bennett, and R. Rozental, Proc. Natl. Acad. Sci. **109**, 2585 (2012).

[14] X. Huang, W. Troy, Q. Yang, H. Ma, C. Laing, S. Schiff, and J.Y. Wu, J. Neurosci. **44**, 9897 (2004).

[15] W. J. E. P. Lammers, Reprod. Sci. **20**, 182 (2012).

[16] W. C. Bray, J. Am. Chem. Soc. **43**, 1262 (1921).

[17] A. M. Turing, Philos. Trans. R. Soc. London Ser. B **237**, 37 (1952).

[18] B. Röhrich, J. Parisi, J. Peinke, and O. E. Rössler, Z. Phys. B **65**, 259 (1986).

[19] T. Nozakura and S. Ikeuchi, Astrophys. **279**, 40 (1984).

[20] C. Berding, T. Harbich, and H. Haken, J. Theor. Biol. **104**, 53 (1983).

[21] B. N. Nagorcka and J. R. Mooney, J. Theor. Biol. **98**, 575 (1982).

[22] P. M. Bode, H. R. Bode, Development **1**, 89 (1987).

[23] I. Lengyel and I. R. Epstein, The Chemistry behind the First Experimental Chemical Examples of Turing Patterns, *in the book "Chemical Waves and Patterns"*, Edited By R. Kapral and K. Showalter, (Springer Netherlands, 1995).

[24] V. Castets, E. Dulos, J. Boissonade, and P. De Kepper, Phys. Rev. Lett. **64**, 2953 (1990).

[25] A. M. Zhabotinsky , Scholarpedia **2(9)**, 1435 (2007).

[26] A. N. Zaikin and A. M. Zhabotinsky, Nature **225**, 535 (1970).

[27] I. Prigogine, I. Stengers, and A. Toffler, *Order Out of Chaos: Man's New Dialogue with Nature*, (Bantam Books, New York, 1984).

[28] A. M. Zhabotinsky, Chaos **1**, 379 (1991).

[29] A. T. Winfree, Science **181**, 937 (1973).

[30] A. T. Winfree, Science **175**, 634 (1972).

[31] R. J. Field, E. Körös, and R. M. Noyes, J. Am. Chem. Soc. **94**, 8649 (1972).

[32] I. R. Epstein, J. Chem. Educ. **66**, 191 (1989).

[33] T. S. Briggs and W. C. Rauscher, J. Chem. Educ. **50**, 496 (1973).

[34] S. Jakubith, H. H. Rotermund, W. Engel, A. von Oertzen, and G. Ertl, Phys. Rev. Lett. **65**, 3013 (1990).

[35] P. De Kepper, K. Kustin, and I. R. Epstein, J. Am. Chem. Soc. **103**, 2133 (1981).

[36] I. Lengyel, J. Li, K. Kustin, and I. R. Epstein, J. Am. Chem. Soc. **118**, 3708 (1996).

[37] J. Horváth, I. Szalai, and P. De Kepper, Science **324**, 772 (2009).

[38] J. Jalife, , M. Delmar, J. Anumonwo, O. Berenfeld, and J. Kalifa, *Basic Cardiac Electrophysiology for the Clinician*, 2nd Edn. (Wiley-Blackwell, Oxford, UK, 2009).

[39] S. Sinha and S. Sridhar, *Patterns in Excitable Media : Genesis, Dynamics, and Control*, (CRC Press, 2015)

[40] C. Antzelevitch and A. Burashnikov, Cardiac Arrhythmias: Reentry and Triggered Activity, *in the book "Heart Physiology and Patholphysiology"*, 4th Edn, edited by N. Sperelakis, Y. Kurachi, A. Terzic, and M. V. Cohen, (Academic Press, 1984).

[41] F. H. Fenton, E. M. Cherry, and L. Glass, Scholarpedia **3(7)**, 1665 (2008).

[42] D. E. L.Wilcken, Medicine **38(7)**, 336 (2010).

[43] E. M. Cherry and F. H. Fenton, New J. Phys. **10**, 125016 (2008).

[44] A. M. Pertsov, J. M. Davidenko, R. Salomonsz, W. T. Baxter, and J. Jalife, Circ. Res. **72**, 631 (1993).

[45] J. N. Weiss, A. Garfinkel, H. S. Karagueuzian, Z. Qu, and P. Chen, Circulation **99**, 2819 (1999).

[46] F. H. Fenton, E. M. Cherry, H. M. Hastings, and S. J. Evans, Chaos **12**, 852 (2002).

[47] A. V. Holden and A. V. Panfilov, Int. J. Bifurcation Chaos **1**, 219 (1991).

[48] S. G. Patel and B. J. Roth, Ann. Biomed. Eng. **29**, 1028 (2001).

[49] I. R. Efimov, V. P. Nikolski, and G. Salama, Circ. Res. **95**, 21 (2004).

[50] J. N. Demas and D. Diemente, J. Chem. Educ., **50**, 357 (1973).

[51] V. Gáspár, G. Bazsa, and M. Beck, Z. Phys. Chem. (Leipzig) **43**, 264 (1983).

[52] J. J. Tyson and P. C. Fife, J. Chem. Phys. **73**, 2224 (1980).

[53] S. K. Scott, *Oscillations, Waves, and Chaos in Chemical Kinetics*, (Oxforf University Press, 1994)

[54] S. Alonso, M. Bär, and A. V. Panfilov, Bull. Math. Biol. **75**, 1351 (2013).

[55] D. Barkley, Spiral Meandering, *in the book "Chemical Waves and Patterns"*, Edited by R. Kapral and K. Showalter, (Springer Netherlands, 1995).

[56] J. M. Davidenko, A. V. Pertsov, R. Salomonsz, W. Baxter, and J. Jalife, Nature **355**, 349 (1992).

[57] D. Pazo, L. Kramer, A. Pumir, S. Kanani, I. Efimov, and V. Krinsky, Phys. Rev. Lett. **93**, 168303 (2004).

[58] M. Valderrábano , M. H. Lee , T. Ohara , A. C. Lai , M. C. Fishbein , S. F. Lin , H. S. Karagueuzian , and P. S. Chen, Circulation **88**, 839 (2001).

[59] T. Wu, M. Yashima, F. Xie, C. A. Athill, Y, Kim, M. C. Fishbein, and Z. Qu, Circ Res **83**, 448 (1998).

[60] A. Defauw, N. Vandersickel, P. Dawyndt, and V. A. Panfilov, Am J Physiol. Heart Circ. Physiol. **307**, 1456 (2014).

[61] Z. A. Jiménez, B. Marts, and O. Steinbock, Phys. Rev. Lett. **102**, 244101 (2009).

[62] Z. A. Jiménez and O. Steinbock, Phys. Rev. E **86**, 036205 (2012).

[63] S. Dutta and O. Steinbock, J. Phys. Chem. Lett. **2**, 945 (2011).

[64] Z. A. Jiménez and O. Steinbock, Euro. Phys. Lett. **91**, 50002 (2010).

[65] S. M. Narayan, D. E. Krummen, K. Shivkumar, P. Clopton, W. Rappel, and J. M. Miller, J. Am Coll. Cardiol. **60**, 628 (2012).

[66] S. Dutta and D. S. Ray, Phys. Rev. E **75**, 066206 (2007).

[67] C. Luengviriya, S. C. Müller, and M. J. B. Hauser, Phys. Rev. E **77**, 015201(R) (2008).

[68] O. Steinbock, J. Schütze, and S. C. Müller, Phys. Rev. Lett. **68**, 248 (1992).

[69] M. Vinson, S. Mironov, S. Mulvey, and A. Pertsov, Nature **386**, 477 (1997).

[70] N. P. Das, D. Mahanta, and S. Dutta, Phys. Rev. E **90**, 022916 (2014).

[71] Z. A. Jiménez, Z. Zhang, and O. Steinbock, Phys. Rev. E **88**, 052918 (2013).

[72] N. P. Das and S. Dutta, Phys. Rev. E **91**, 030901(R) (2015).

[73] J. P. Keener and J. J. Tyson, SIAM Rev. **34**, 1(1992).

[74] S. Dutta and O. Steinbock, Phys. Rev. E **81**, 055202(R) (2010).

Chapter 2

METHODOLOGY AND BACKGROUND

2. METHODOLOGY AND BACKGROUND

2.1 Experimental methods

2.1.1 Experimental system

All the experimental studies are based on the ferroin catalyzed Belousov Zhabotinsky (BZ) reaction. Experiments are performed in agar gel layers containing the BZ reactants: malonic acid as the organic substrate, sodium bromate as the oxidizing agent, sulfuric acid as the source of hydronium ions, and ferroin as the catalyst. This BZ-system, when kept unstirred, can be used to generate two and three dimensional chemical waves due to its excitability and capability of sustaining such waves. A single thin layer of the BZ gel is used for generating 2D spiral waves, whereas two thick layers of BZ gel are required in case of 3D scroll waves. Our experimental system is closed in the sense that there is no inflow of fresh reactants and therefore, the reactants get depleted after several hours. The experiments are carried out at room temperature ($21 \pm 1^{\circ}$ Celsius). During the course of the reaction, time lapse images of the experiments are recorded at regular intervals for several hours. Subsequently, these images are analyzed using MATLAB scripts.

2.1.2 Chemicals

Malonic acid ($C_3H_4O_4$, molecular weight 104.061 g/mol) is a dicarboxylic acid with two acidic α-hydrogens facilitating bromination during the reaction. Malonic acid was purchased from Sigma Aldrich with a purity $\geq 99\%$. A 1.0 M stock solution was prepared from it.

Ferroin ($[C_{36}H_{24}FeN_6]^{2+}$) is a sulfate complex of iron with the structure shown in figure 2.1. Its active ingredient is the cation $[Fe(o\text{-}phen)_3]^{2+}$, where o-phen stands for 1,10-phenanthroline, a bidentate ligand. It is a chromophore that can be oxidized to $[Fe(o\text{-}phen)_3]^{3+}$. The redox potential ($E^{\circ}$) for this couple is 1.06 V in 1 M sulphuric acid. The reduced form is red in color and becomes blue when oxidized. This color change is reversible, rapid and sharp which makes ferroin a suitable indicator for the Belousov Zhabotinsky reaction. A 0.025 M stock ferroin solution was purchased from Merck.

Sodium bromate ($NaBrO_3$, molecular weight 150.891 g/mol) is a strong inorganic oxidant that oxidizes malonic acid to carbon dioxide in the Belousov Zhabotinsky reaction. Sodium bromate was purchased from Sigma Aldrich with a purity $\geq 99\%$, and it was used to prepare a 1.0 M stock solution.

Sulfuric acid (H_2SO_4) is a strong diprotic acid used in the BZ-reaction that facilitates

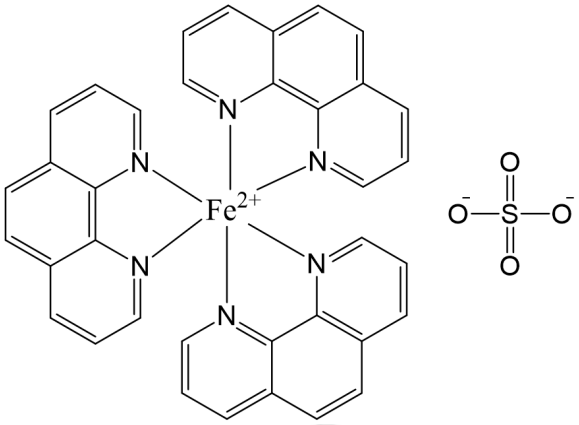

Fig. 2.1: 2D Structure of ferroin.

the low pH condition required for the system. Sulfuric acid ampoules were purchased from Thermo Fisher and used to make a 0.5 M stock solution.

Agar ($(C_{12}H_{18}O_9)_n$) is a gelling polysaccharide used in our experiments. The main purpose of embedding the reaction mixture in agar gel was to prevent hydrodynamic perturbation. Agar was purchased from Sigma-Aldrich and a fresh 0.8 % (w/v) solution was prepared in water for each experiment. The gelling temperature of Agar is $\sim 35^\circ$ C for a 1.5% solution, which is far below the temperature required for its melting ($\sim 85^\circ$ C).

A **silver wire** was used for initiating waves in the BZ-system. The silver wire, made of 99.9% silver, forms AgBr upon reacting with the Br^- ion present in the system. Thus it decreases the local concentration of the inhibitory species, Br^-, in the vicinity of the wire and gives rise to an expanding chemical wave. Silver wires of radius 0.5 mm were purchased from Sigma-Aldrich.

Ultrapure water with a resistivity of 18.2 MΩcm was used to prepare all the solutions as well as the BZ gels.

The final concentration of the different constituent chemical species in a typical BZ-reaction were as seen in Table 2.1.

Compound	Concentration (M)
H_2SO_4	0.16
Malonic acid	0.04
$NaBrO_3$	0.04
Ferroin	0.005

Tab. 2.1: Concentration of different chemicals used in the experiments.

2.1.3 Experimental setup

A schematic diagram of the experimental set up is shown in Fig. 2.2. Simple experiments that do not involve external fields were carried out in petri dishes. For applying external gradients, specially designed reaction chambers were used. The petri dish was illuminated by a cold white light (DC regulated illuminator) kept below it. A charge coupled device (CCD) camera (mvBlueFOX 220a) mounted over the reaction chamber was used to record the top view of the experiment at regular intervals. The camera was equipped with blue dichroic filter that made the color difference between the oxidized and reduced form of the catalyst more prominent, thereby facilitating better imaging.

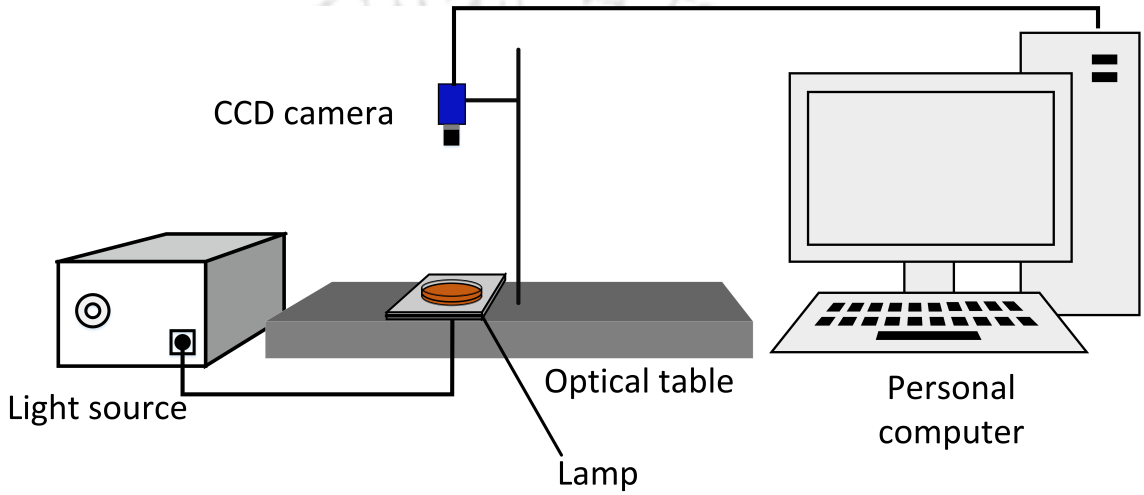

Fig. 2.2: Experimental setup.

2.1.4 Method of generating spiral and scroll waves

Spiral waves were generated using a thin layer of the BZ-solution or BZ-gel. The reaction was carried out in a Petri dish and the thickness of the reactant layer was about 2 mm. For using a gel, the reaction mixture containing all the reactants as well as the gel was poured into the Petri dish such that it was at a temperature slightly above the gelling point of the agar gel. Upon cooling further, it formed a uniform gel. A clean silver wire was dipped into the reactant layer for a few seconds until a bright circular wave emerged [Fig 2.3(a)]. The wave then expanded and when cleaved, as seen in Fig 2.3(b), the two broken ends curled in [Fig 2.3(c)] and a spiral was obtained with two tips having opposite chirality [Fig 2.3(d)].

Nucleation of the three dimensional scroll waves required two layers of reactants. The two BZ gel layers were chemically identical and thickness of each layer was 4 mm. The first pre-gel solution containing all the BZ-reactants was prepared and poured into the reaction chamber slightly above its gelling temperature.

A chemical wave, initiated by inserting the tip of a silver wire into this gel layer, was allowed to expand until it reached the desired dimension as shown in Fig. 2.4(a,d). The

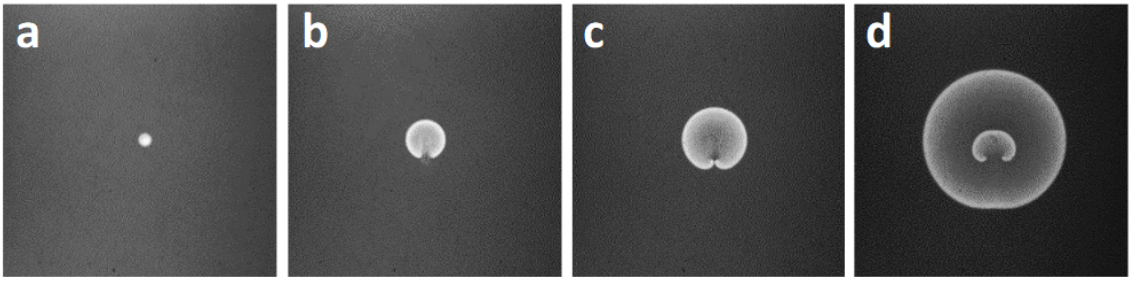

Fig. 2.3: Generation of two dimensional spiral waves in the BZ-reaction.

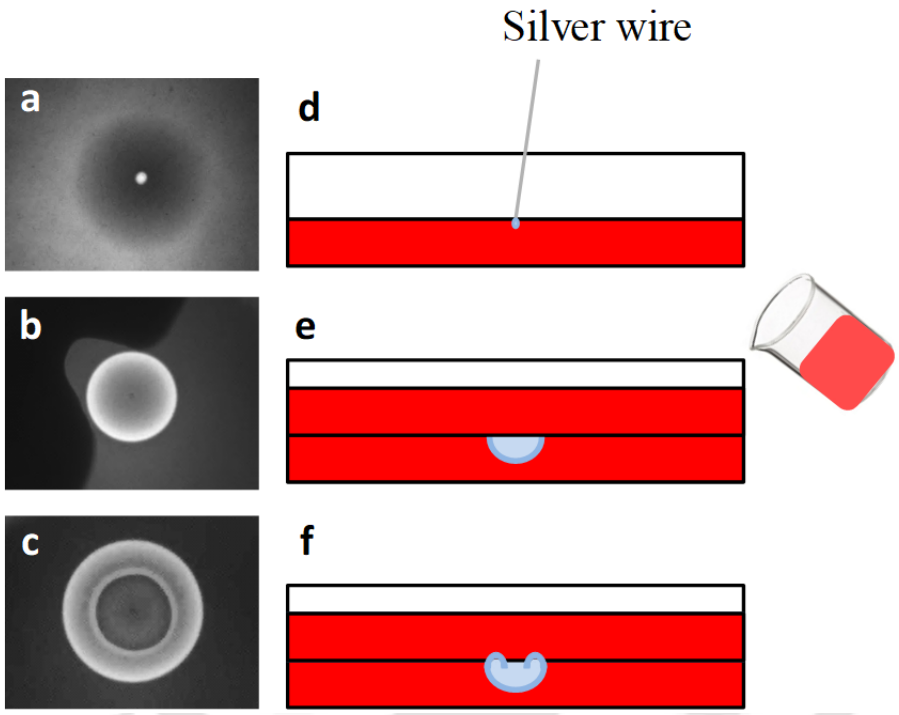

Fig. 2.4: Generation of scroll wave in experiments with BZ-system. (a-c) Snapshots of three different stages during an experiment captured from above. (d-f) Schematic representation of the side view of the experimental system during the scroll generation process

second BZ-layer was then poured over it. This led to the spontaneous curling of the the rim of the half spherical wave propagating in the bottom layer into the upper layer and nucleation of the desired scroll ring at the gel-gel interface. In case of experiments involving more than one scroll, required number of expanding waves were initiated by dipping the tips of multiple silver wires simultaneously. In these experiments, controlling the size of individual waves as well as their distance from one another at the moment of pouring the second layer were crucial factors deciding the success of the experiment.

2.1.5 **Pinning experiments**

Experiments on pinning of scroll waves to heterogeneities were carried out using different types of chemically inert obstacles based on the requirement of the experiment. Some of

these unexcitable obstacles made up of glass and polymer are shown in Fig. 2.5.

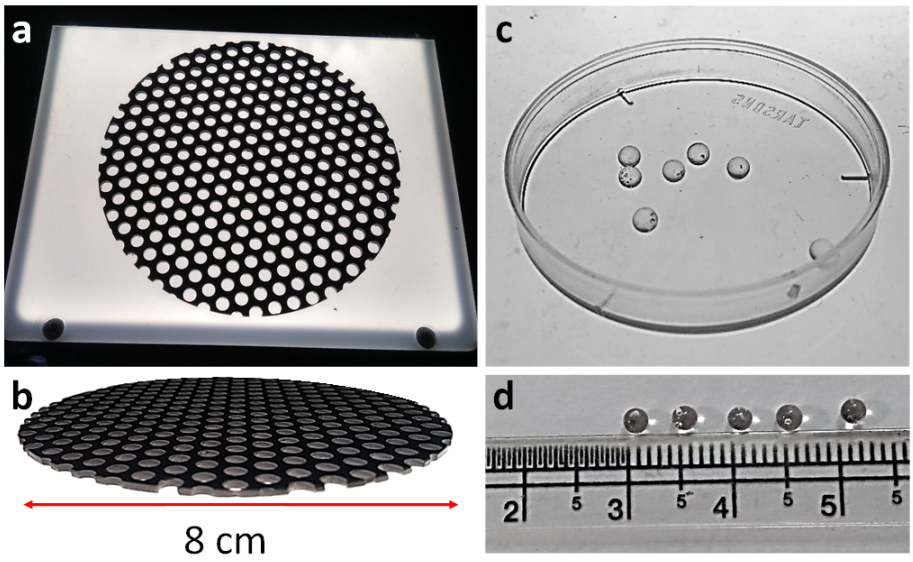

Fig. 2.5: Two kinds of obstacles used in our experimental studies. (a) A polymer sheet having regular arrangement of holes, (c) spherical glass beads. The size of the obstacles are pictorially indicated in (b) and (d)

During the gelation process, obstacles were placed onto the lower gel layer while it was still slightly soft and then gently pressed into it. When the expanding half spherical wave, initiated with a silver wire as described above [Fig 2.6(a)], grew and came into contact with the obstacles [Fig 2.6(b)], the upper gel layer was poured [Fig 2.6(c)]. It resulted in the formation of a scroll ring at the interface of the two gel layers that subsequently got anchored to the unexcitable heterogeneities at one or more positions. These two stages are seen in Fig 2.6(d) and (e) respectively.

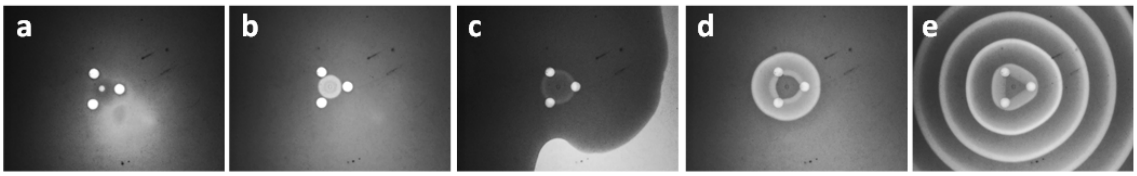

Fig. 2.6: Different stages during a pinning experiment with the BZ system in presence of three inert obstacles. The bright circular areas are glass beads of diameter 2 mm, that act as anchors. The different stages during the experiment are: (a) initiation of the chemical wave with a silver wire in the first layer almost equidistant from the obstacles, (b) sufficient expansion of the wave in the bottom layer so that it comes into contact with the three beads, (c) pouring the upper BZ-gel layer into the reaction chamber, (d) formation of the scroll ring around the spherical heterogeneities, (e) the scroll, 90 min after (c), completely pinned to the three beads.

2.1.6 Application of external fields

Specially designed reaction chambers were used to carry out experiments in presence of external gradients. A schematic diagram of the reaction vessel is shown in Fig 2.7 that has provisions for applying both thermal and electric gradients needed for our experiments.

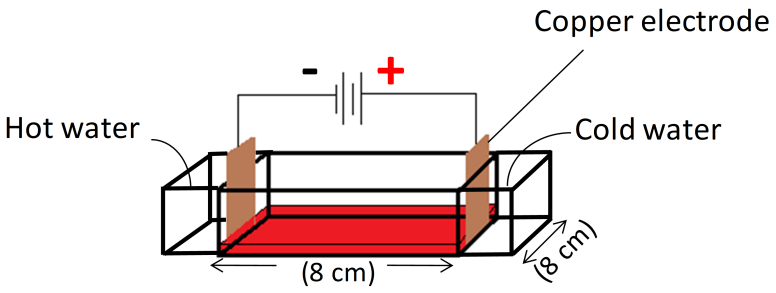

Fig. 2.7: Experimental set up for applying external gradients to the reaction system

It is basically a square shaped flat chamber made up of transparent plexiglass having two heat exchangers on its two parallel sides. Each side of the reaction vessel, excluding the space occupied by the heat exchangers, measured 8 cm. The required temperature difference for creating a thermal gradient was maintained by connecting the heat exchangers to two thermostat-controlled circulating baths kept at specific temperatures. It facilitated a horizontal temperature gradient across the reaction mixture between the two opposite walls of the vessel. On the other hand, electric fields were applied by immersing rectangular copper (Cu) plates into the BZ- mixture at parallel sides of the reaction chamber. The electrodes were connected to a DC power supply to establish the desired electric gradient across the mixture. In the latter case, the heat exchangers were used to keep the reaction chamber at a particular temperature, by passing thermostat controlled water along both sides that helped combat the Ohmic heating.

2.2 Data analysis

2.2.1 Time space plots

Time space plots are used as a tool to observe the evolution of the two and three dimensional waves over time. They provide crucial information regarding the position of the spiral tips and filaments of scroll waves. Generation of these plots is, therefore, often considered as the key method for filament detection. A time space plot is typically a set of pixel lines arranged in temporal order. Intensity profiles from each snapshot, that are recorded at definite intervals during the experiment, are extracted along a constant line as shown in yellow in Fig. 2.8(a). A plot with sequential stack of such lines from successive frames shows the time along one axis and space along the other [1]. Figure. 2.8 is the time space plot for a free scroll wave. Two representative snapshots of the scroll are seen in Fig. 2.8(a,b).

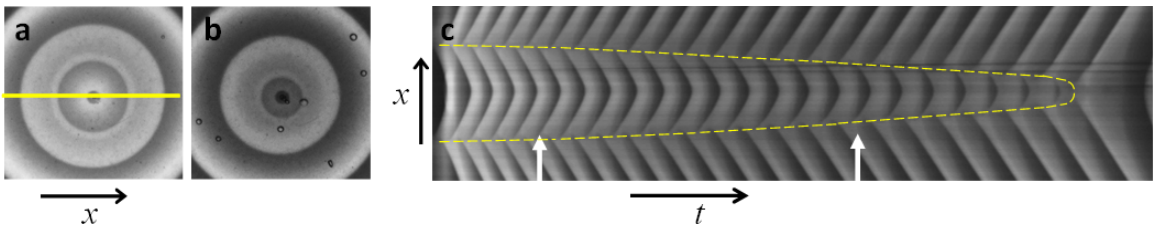

Fig. 2.8: Time space plot of a free scroll wave. Snapshots of the top view of the scroll wave at 17.5 minutes and 70 mins are seen in (a) and (b) respectively. Area of each snapshot is 1.6×1.6 cm^2. The time space plot has been constructed along the yellow line shown in (a). The total time duration of the plot is 120 mins.

Their positions in the time space plot are marked with two vertical black arrows. The time space plot Fig. 2.8(c) spans a duration of 120 minutes. In this plot time increases in the horizontal direction from left to right. The position of the filament can be located from the plot as the regions where inward and outward propagating waves emerge (shown in yellow dashes). This in turn helps to calculate the size of the scroll at a given point of time. The decreasing diameter of the filament, that finally disappears, is clearly visible from the plot. Hence, another important information obtained from the plot is the lifetime of the scroll. Fig. 2.9 depicts time space plots for four different experiments. A snapshot and the line along which the plot has been created is shown [Fig. 2.9(a-d)] on top of each time space plot Fig. 2.9(e-h). Fig. 2.9(e) is the time space plot of a two dimensional spiral wave, where the tip gives rise to a fish-bone pattern of traveling waves. How the plot helps to find out the wavelength and time period of the wave is also illustrated by the yellow arrows. Usually the time period is calculated as an average of few rotations. Fig. 2.9(b-d) are the snapshots of a scroll wave pinned to some inert obstacles. The corresponding time space plots below them show how the interesting phenomenon of pinning increases the lifetime of each of the pinned scroll waves, in contrast to the very short lifetime of the free scroll seen in Fig. 2.8. The two black strips in Fig. 2.9(f) and the bright columns in Fig. 2.9(g) arise from the obstacles used in the experiment to arrest the motion of the three dimensional waves. Fig. 2.9(c) and (d) are the snapshots of an experiment involving two glass beads as obstacles. However, the corresponding time space plots have been constructed along two perpendicular directions. Fig. 2.9(h) demonstrates how the diameter of the scroll initially decreases before getting pinned to the two anchors, and finally stabilizes after some time beyond which the scroll size does not decrease further.

2.2.2 Detection of spiral tip and filament

In-house MATLAB codes were used to detect the tips of the spiral waves and thereby trace their trajectories. Similarly filaments of the scroll waves were reconstructed from the time-lapse images of the experiments. The MATLAB-codes identified the tips and filaments on the basis of changes in image intensities during a rotation period [2]. Fig. 2.10 shows the reconstructed filaments of a free scroll wave in an experiment with the BZ-system.

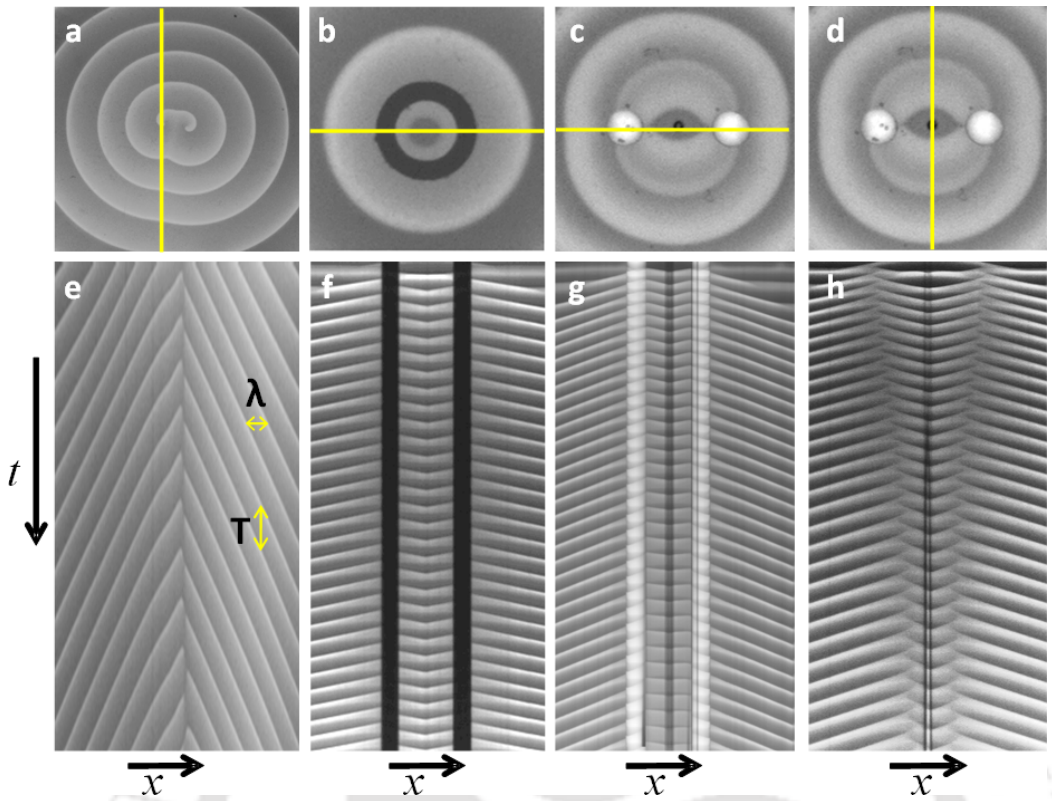

Fig. 2.9: Time space plots of four different waves. The snapshots of the waves are seen at the top panel (a-d). The time space plots of (a) a spiral wave, (b) a scroll wave pinned to a rubber ring, (c,d) scroll waves pinned to two glass beads are seen in the bottom row. In each case time increases in the vertical direction from top to bottom. The time durations for the plots are (e) 42 minutes, (f) 210 minutes, (g) 220 minutes, and (h) 180 minutes respectively. The time space plots have been constructed along the yellow lines shown in the corresponding snapshots.

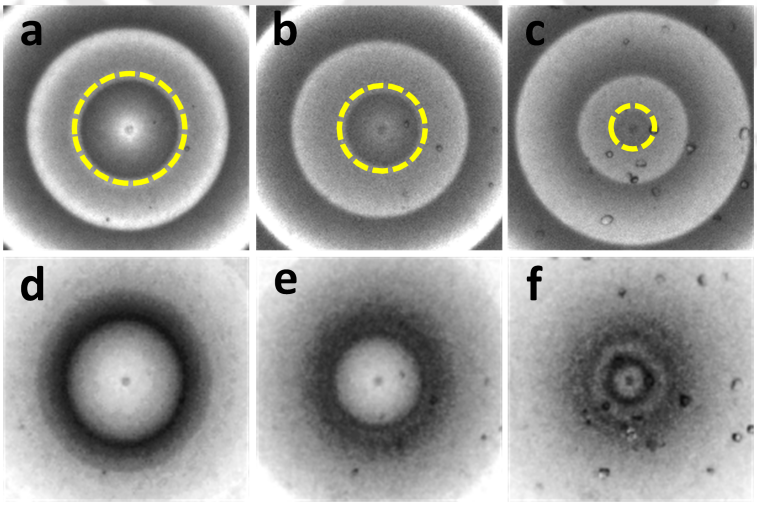

Fig. 2.10: Reconstructed filaments of a free scroll wave in the BZ system. Snapshots of experiment (a-c) and corresponding reconstructed filaments (d-f) at 12.6, 49.0 and 85.6 min after initiation. Filaments of the scroll are superimposed over the snapshots (shown as broken yellow lines) in (a-c).

2.3 Numerical tools

For numerical simulations, we considered a reaction-diffusion model that could describe the dynamics of the chemical system that we used for our experiments. Reaction diffusion models are based on the coupling of two phenomena : chemical reaction, which can lead to the production or consumption of the various chemical species; and diffusion, wherein the components can move from one point to another. These models are extensively used to study numerous spatially extended systems in physics, chemistry, biology, ecology etc [2, 3]. They can successfully explain the generation of various patterns observed in the biological world as well as exhibit different kinds of other spatiotemporal dynamical behavior [5, 6]. The simplest quantitative description of a reaction diffusion system is given by the following general equation:

$$\frac{\partial c_i}{\partial t} = f(c_i) + D_i \nabla^2 c_i. \tag{2.1}$$

Here c_i is the concentration of the i-th species. The first term in the right hand side of Eq. 2.1, $f(c_i)$, stands for the chemical reactions and hence contains details of all the local dynamical processes like rate of production and decay of the components. The reaction term is system dependent and typically nonlinear, as the rate laws are dependent on reactant concentrations and temperature [7]. The second term accounts for diffusion of the components, where D_i is the diffusion coefficient of the species i, ∇^2 is the sum of second derivatives with respect to the spatial variables (the Laplacian). Application of external fields will further modify the equations as the fluxes of the ions will change in presence of external gradients [8].

2.3.1 The Barkley model

The Barkley model is one of the simplest models widely used to study a broad range of pattern forming systems. It is a system of two coupled reaction diffusion equations that are based on the interaction of a pair of activator-inhibitor components [17]. This model facilitates rapid computations of excitable and oscillatory media. The most general form of the equations are,

$$\frac{\partial u}{\partial t} = f(u,v) + D_u \nabla^2 u, \tag{2.2}$$

$$\frac{\partial v}{\partial t} = g(u,v) + D_v \nabla^2 v. \tag{2.3}$$

where,

$$f(u,v) = \frac{1}{\varepsilon}\{u(1-u)\,(u - u_{th}(v))\}$$
$$g(u,v) = u - v.$$

The quantity u_{th} is defined as,

$$u_{th}(v) = \frac{v+b}{a}. \tag{2.4}$$

The activator variable u, and inhibitor variable v, are loosely related with the concentrations of $HBrO_2$ and the oxidized form of the catalyst respectively. D_i is the translational diffusion coefficient of the species i ($i = u$ or v).The Barkley model involves three parameters: ε, a, and b. The value of the dimensionless parameter ε is generally taken to be very small ($<< 1$), which sets the timescale separation between the fast variable u and the slow variable v. Higher value of a leads to a decrease in the activation threshold of the medium and gives longer excitation duration. The ratio $\frac{b}{a}$ determines the excitation threshold and thus smaller excitability threshold can be attained by decreasing the value of this ratio. The dynamics of the system can be altered by adjusting the values of the parameters [7, 10].

2.3.2 The Oregonator model

The Oregonator model is a realistic model describing the chemical dynamics of the Belousov-Zhabotinsky reaction and is widely used to study spatio-temporal pattern formation in that reaction medium [15]. This model originated from the FKN scheme, first derived by Field, Körös, and Noyes in 1972 [12,13]. The latter involves so many reaction steps and chemical intermediates that it becomes extremely difficult to use the complete model for analytical purposes [14]. Therefore the robust model was reduced to a much simpler one utilizing the standard methods of chemical kinetics. The model is known as the Oregonator, after the name of the place where it was first derived, as Field and Noyes were then working at the University of Oregon, USA.

The model consists of five basic irreversible elementary steps

$$A + Y \rightarrow X + P \qquad rate = k_3[A][Y] \tag{2.5}$$

$$X + Y \rightarrow 2P \qquad rate = k_2[X][Y] \tag{2.6}$$

$$A + X \rightarrow 2X + 2Z \qquad rate = k_5[A][X] \tag{2.7}$$

$$2X \rightarrow A + P \qquad rate = k_4[X]^2 \tag{2.8}$$

$$B + Z \rightarrow 1/2fY \qquad rate = k_c[B][Z] \tag{2.9}$$

The symbols used in this scheme represent the chemical species as shown in Table 2.2.

The concentrations of the reactants A and B as well as product P are usually much higher compared to that of the dynamic intermediates. Hence their concentrations are assumed to be constant. Application of the laws of chemical kinetics to the intermediates X, Y and Z gives the following rate equations:

$$\frac{dX}{dt} = k_3[A][Y] - k_2[X][Y] + k_5[A][X] - 2k_4[X]^2 \tag{2.10}$$

$$\frac{dY}{dt} = -k_3[A][Y] - k_2[X][Y] + \frac{1}{2}k_c f[B][Z] \tag{2.11}$$

Symbol	Chemical species
A	BrO_3^-
B	Organic species $CH_2(COOH)_2$
P	HOBr or $BrCH(COOH)_2$
X	$HBrO_2$
Y	Br^-
Z	$M_{ox}(eg.Ce(IV) or Fe(III))$
f	an adjustable stoichiometric factor

Tab. 2.2: Different symbols used in the Oregonator Model

$$\frac{dZ}{dt} = 2k_5[A][X] - k_c[B][Z] \tag{2.12}$$

For further simplification, the above equations are converted to dimensionless forms:

$$\frac{dx}{dt} = \frac{qy - xy + x(1-x)}{\varepsilon} \tag{2.13}$$

$$\frac{dy}{dt} = \frac{-qy - xy + fZ}{\varepsilon'} \tag{2.14}$$

$$\frac{dz}{dt} = x - z \tag{2.15}$$

where,

$$x = \frac{2k_4[X]}{k_5[A]} \tag{2.16}$$

$$y = \frac{k_2[Y]}{k_5[A]} \tag{2.17}$$

$$z = \frac{k_c k_4[B][Z]}{(k_5[A])^2} \tag{2.18}$$

$$\varepsilon = \frac{k_c[B]}{k_5[A]} \tag{2.19}$$

$$\varepsilon' = \frac{2k_c k_4[B]}{k_2 k_5[A]} \tag{2.20}$$

$$q = \frac{2k_3 k_4}{k_2 k_5} \tag{2.21}$$

Here, the parameters ε and ε' are of the order of 10^{-2} and 10^{-5} respectively. Since the value of ε' is much smaller than ε, steady state approximation can be applied for the concentration of y to get

$$y = \frac{fz}{(q+x)} \tag{2.22}$$

Substituting these values we get,

$$\frac{dx}{dt} = \frac{1}{\varepsilon}\left(x(1-x)+\frac{fz(q-x)}{(q+x)}\right) \tag{2.23}$$

$$\frac{dz}{dt} = x-z. \tag{2.24}$$

These equations are similar to typical activator-inhibitor models, with $HBrO_2$ and M_{ox} being the activator and inhibitor respectively, for the BZ system. If we denote the activator by u and the inhibitor by v, then the complete model takes the following form in presence of diffusion:

$$\frac{\partial u}{\partial t} = \frac{1}{\varepsilon}\left(u(1-u)+\frac{fu(q-u)}{(q+u)}\right)+D_u\nabla^2 u, \tag{2.25}$$

$$\frac{\partial v}{\partial t} = u-v+D_v\nabla^2 v. \tag{2.26}$$

Equation 2.25 and Eq. 2.26 are the simplest and most commonly used form of the Oregonator model.

2.3.3 Solving the differential equations

The nonlinear differential equations involved in the various reaction diffusion models are usually too complicated and have several restrictions to be solved analytically. That is why finding solutions to these models are often based on numerical techniques. To numerically integrate the equations, the system is first discretized with an appropriate step size, h. Different integration schemes can be used depending on the nature of the problem. The simplest and most widely used technique among them is the explicit Euler method. For an ordinary differential equation $\frac{dy}{dx} = f(x,y)$ with the initial condition $y(x_0) = y_0$, the forward Euler formula is given by,

$$y_{n+1} = y_n + hf(x_n, y_n) \tag{2.27}$$

Although the Euler method is really simple and easy to be implemented, it suffers from some serious disadvantages. As the method approximates the value of the function at a point by a straight line passing through it, it often fails in case of non-monotonic functions [7]. Moreover, the error in this scheme is of the order of h. For minimizing the error, the integration interval h should be very small, which consequently results in considerable increase in the computation time. Hence, many higher order methods were proposed to get more accurate results. The Runge-Kutta method, proposed in 1900s, is one such scheme that involves the following calculations:

$$y_{n+1} = y_n + \frac{1}{6}k_1 + \frac{1}{3}k_2 + \frac{1}{3}k_3 + \frac{1}{6}k_4 \tag{2.28}$$

where,

$$k_1 = hf(x_n, y_n) \tag{2.29}$$
$$k_2 = hf(x_n + \frac{1}{2}h, y_n + \frac{1}{2}k_1) \tag{2.30}$$
$$k_3 = hf(x_n + \frac{1}{2}h, y_n + \frac{1}{2}k_2) \tag{2.31}$$
$$k_4 = hf(x_n + h, y_n + k_3) \tag{2.32}$$

This scheme is often referred to as RK4 (4th order Runge-Kutta) method. The error in this method is much less than that of the Euler scheme and is of the order of h^4.

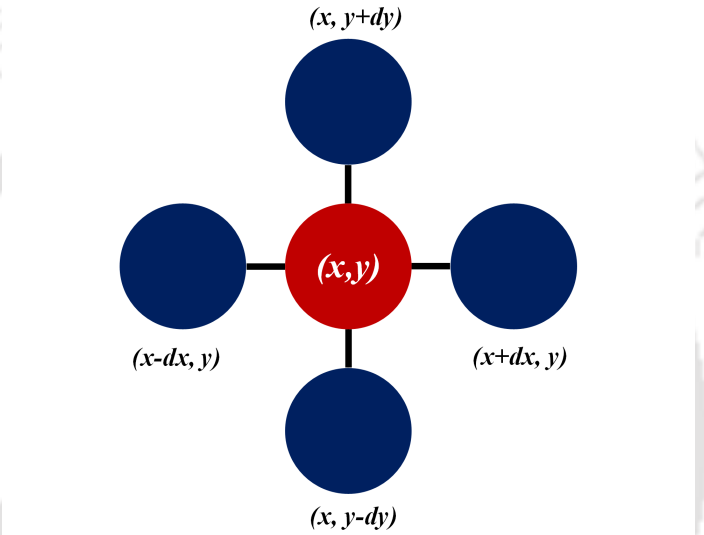

Fig. 2.11: Schematic representation of a five point Laplacian stencil.

To solve the diffusion term involving the Laplacian on the right hand side of the reaction-diffusion equation 2.1, the system is also discretized in space. To approximate the second derivative, an appropriate geometric arrangement of neighbouring points, known as a stencil, is chosen. Usually a five point stencil, as shown in Fig. 2.11, is used for two dimensional systems which considers the four neighbouring points $(x+dx, y)$, $(x-dx, y)$, $(x, y+dy)$, and $(x, y-dy)$ to determine the second derivative of a variable at the point (x, y). Here dx, dy, and dz are the grid spacing (h). Depending on the requirement of the problems, sometimes higher order stencils such as a nine point stencil can also be used.

Similarly, in three dimensional systems, a simple seven point stencil uses the nearest neighbours $(x+dx, y, z)$, $(x-dx, y, z)$, $(x, y+dy, z)$, $(x, y-dy, z)$,$(x, y, z+dz)$, and $(x, y, z-dz)$ to evaluate the derivative at (x, y, z) [Fig. 2.12]. However, 19-point or 27-point stencils are also frequently used for three dimensional lattices [16].

Another important aspect of solving the reaction diffusions equations are the boundary conditions. Appropriate boundary conditions must be defined for each system. Generally there are three types of boundary conditions: Dirichlet boundary condition, Neumann

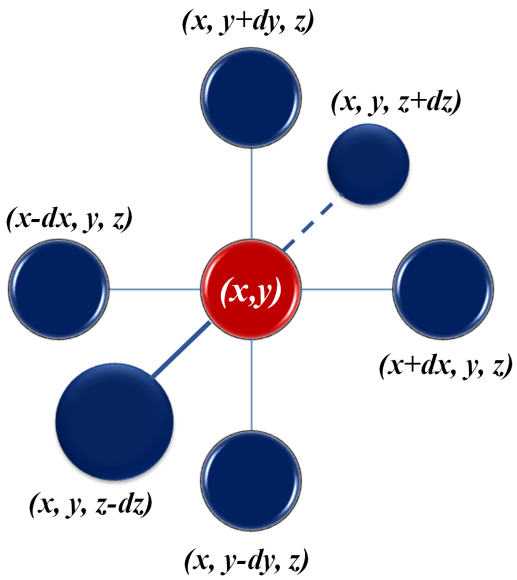

Fig. 2.12: Schematic representation of a seven point Laplacian stencil.

boundary condition and mixed boundary condition. The value of a function is specified on the boundary in case of Dirichlet boundary condition, while the normal derivative of the function is specified while using Neumann boundary conditions. On the other hand, the mixed boundary condition is a combination of the previous two types [17]. Again, zero flux boundary condition is a special case of Neumann boundary condition, which was usually applied along all the external walls and around the obstacles in our simulations.

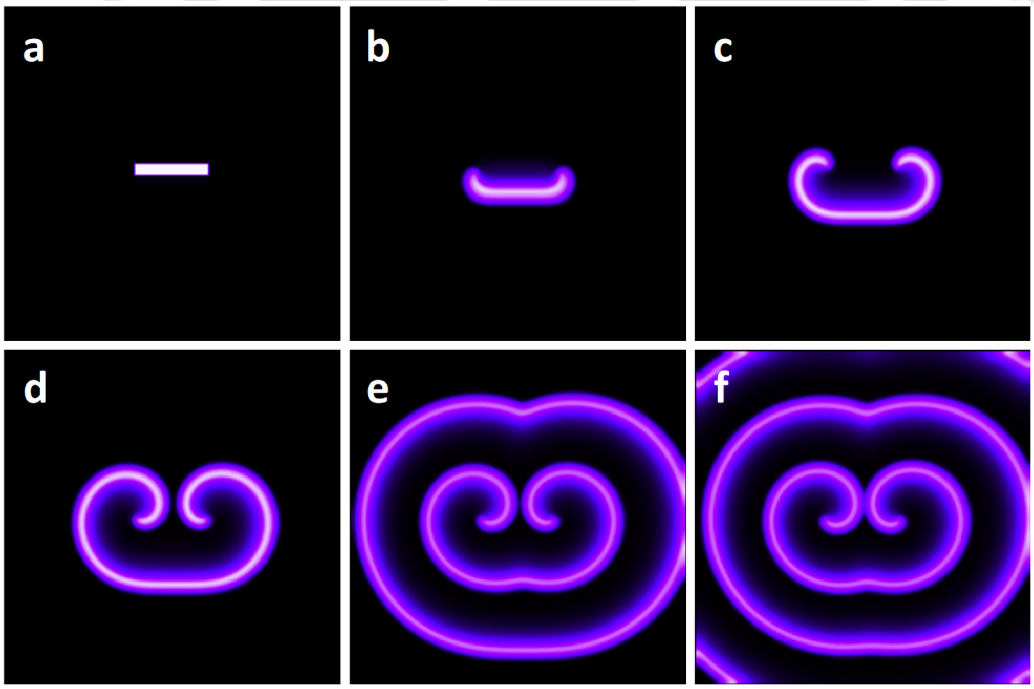

Fig. 2.13: Generation of a spiral wave employing the Barkley model in numerical simulation. Purple areas indicate high values of the activatory variable u.

The principal challenge in the simulations lies in defining the initial conditions. In order to generate the spiral waves, a bar shaped region with high values of the activator variable u was considered beside a bar shaped region of the inhibitor v. Symmetry breaking motion of the activator, due to the presence of the inhibitor, resulted in the formation of a double spiral with two counter-rotating tips as shown in Fig. 2.13. In this simulation employing the Barkley model, the values of the parameters were $a = 0.84$, $b = 0.07$, and $\varepsilon = 0.02$. An explicit Euler scheme and a nineteen point Laplacian stencil was used. Integration time step was kept constant at 0.012. A two dimensional lattice of size 300×300 grid points was chosen. The grid spacing was 0.35 and a zero flux boundary condition was applied along all the boundaries. The technique used to generate scroll waves in simulations was analogous

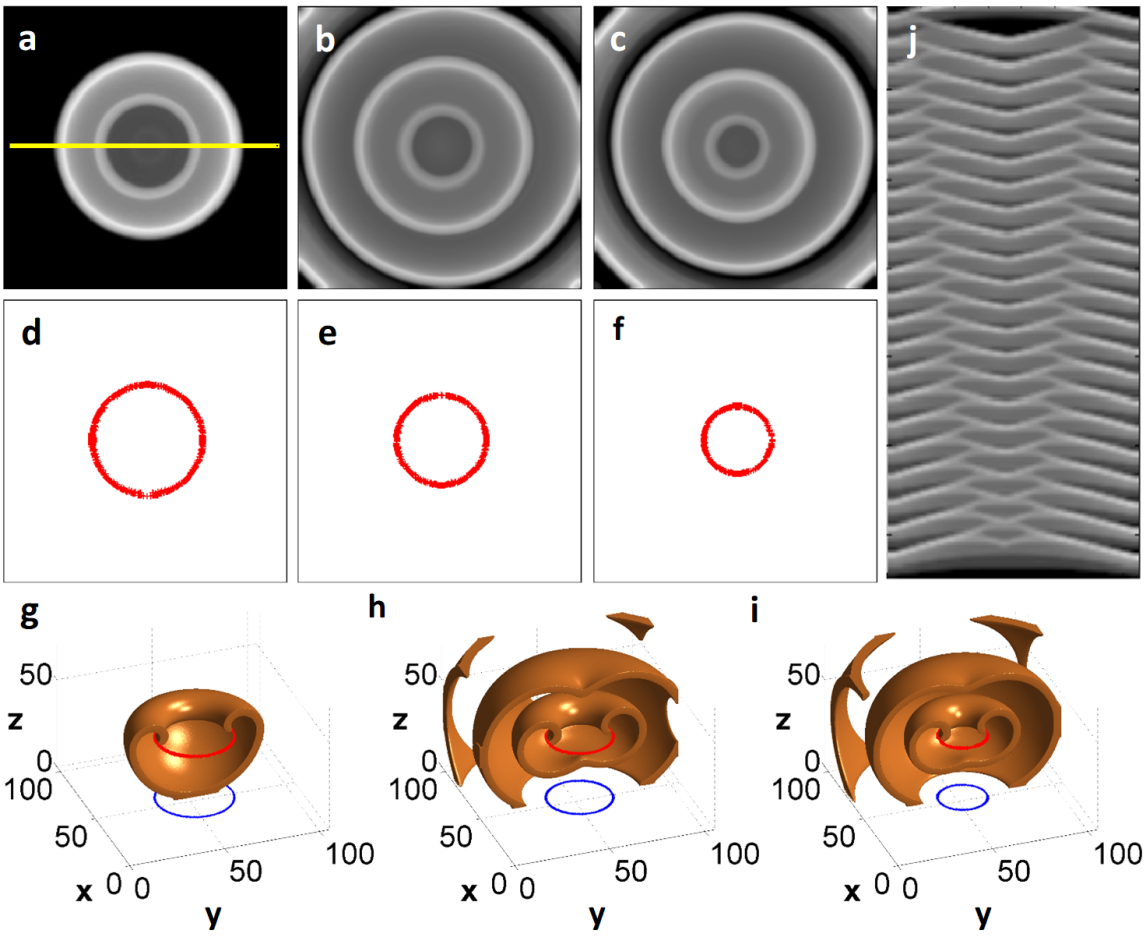

Fig. 2.14: Numerical simulation of a scroll ring in the Barkley model. Top view of the scroll at (a) 16.8 time units, (b) 49.8 time units, and (c) 82.8 time units. (d-f) Filaments corresponding to the scrolls in (a-c). (g-i) Show the evolution of the scroll wave and the filament in three dimensions. The solid brown areas represent the waves whereas the red curves depict the filaments. Only the posterior half of the wave is shown, for better visualization. The two dimensional projection of the filaments are shown at the bottom of the box in blue. (j) Time space plot of the scroll, where time increases in the downward direction.

to the experimental conditions. A sphere having high concentration of the activator was generated inside the three dimensional lattice. When it grew sufficiently, the values of both

the variables were set to zero in the upper half of the sphere. This was similar to pouring the upper gel layer in the experiments. The hemispherical wave then started curling in and eventually formed a scroll ring.

Figure 2.14 shows a scroll ring generated in a simulation using the Barkley model. Figure 2.14(a-d) depict the top view of the scroll at an interval of 33 time units. The corresponding filaments are displayed below each snapshot. The filament of the scroll wave was identified as regions where $u = 0.5$ and $v = a/2 - b$. A time space plot of the scroll spanning 120 time units is shown in (i). The values of different parameters used in this simulation were $a = 0.84$, $b = 0.07$, and $\varepsilon = 0.02$. An explicit Euler scheme and a nineteen point Laplacian stencil was used to numerically integrate the two partial differential equations. Integration time step was kept constant at 0.012. A three dimensional lattice measuring $150 \times 150 \times 150$ grid points with grid spacing 0.35 was chosen. A zero flux boundary condition was set to each diffusing species along all the boundaries.

In case of studies involving heterogeneities, the inert obstacles were modeled as regions with $(u, v) = (0, 0)$. Zero-flux boundary conditions were applied around the obstacles. The scroll initially shrank similar to the free scroll waves, and after a few rotations got anchored to the obstacles. If the simulation needed the application of external fields, the scroll was at first allowed to pin properly to the obstacles. The external fields were numerically introduced to the system only after ensuring that the shrinkage of the scroll had ceased and it got stably pinned to the anchors.

BIBLIOGRAPHY

[1] R. A. Gray, J. Jalife, A. Panfilov, W. T. Baxter, C. Cabo, J. M. Davidenko, and A. M. Pertsov, Circulation **91**, 2454 (1995).

[2] Z. A. Jiménez, PhD dissertation, Florida State University, 2012.

[3] I. R. Epstein and J. A. Pojman, *An Introduction to Nonlinear Chemical Dynamics* (Oxford University Press, Oxford 1998).

[4] S. C. Müller, P. J. Plath, G. Radons, and A. Fuchs, Complexity and Synergetics (Springer International Publishing, 2018).

[5] A. M. Turing, Philos. Trans. R. Soc. London Ser. B **237**, 37 (1952).

[6] I. Lengyel and I. R. Epstein, The Chemistry behind the First Experimental Chemical Examples of Turing Patterns, *in the book "Chemical Waves and Patterns"*, Edited By R. Kapral and K. Showalter, (Springer Netherlands, 1995).

[7] S. Sinha and S. Sridhar, *Patterns in Excitable Media : Genesis, Dynamics, and Control*, (CRC Press, 2015).

[8] N. P. Das and S. Dutta, Phys. Rev. E **96**, 022206 (2017).

[9] D. Barkley, Physica D **49**, 61 (1991).

[10] D. Barkley, Scholarpedia **3(11)**, 1877 (2008).

[11] D. Barkley, Spiral Meandering, *in the book "Chemical Waves and Patterns"*, Edited by R. Kapral and K. Showalter, (Springer Netherlands, 1995).

[12] R. J. Field, Scholarpedia **2(5)**, 1386 (2007).

[13] R. J. Field, E. Körös, and R. M. Noyes, J. Am. Chem. Soc. **94**, 8649 (1972).

[14] F. Sagúes and I. Epstein, Dalton Trans. **7**, 1201 (2003).

[15] S. K. Scott, *Oscillations, Waves, and Chaos in Chemical Kinetics*, (Oxforf University Press, 1994).

[16] M. Dowle, R. M. Mantel, And D. Barkley, Int. J. Bifurcation Chaos **7**, 2529 (1997).

[17] G. B. Arfken and H. J. Weber, *Mathematical Methods for Physicists, Sixth Edition* (ELSEVIER, 2005).

Chapter 3

PINNING OF SCROLL WAVES TO FLAT AND HIGHLY BRANCHED UNEXCITABLE HETEROGENEITIES

3. PINNING OF SCROLL WAVES TO FLAT AND HIGHLY BRANCHED UNEXCITABLE HETEROGENEITIES

3.1 Introduction

Far from the thermodynamic equilibrium, self-organized spatiotemporal patterns occur in a large number of reaction-diffusion systems. Among those patterns, nonlinear waves have attracted considerable interest as they are known to create stable wave pulses and surprising vortex states [1]. These rotating vortices are also ubiquitous in the realm of biology and often allow the relay of (desired or detrimental) information over macroscopic distances [4–6]. Important examples include the cellular slime mold *Dictyostelium discoideum* [7], which uses spiral waves to coordinate cell aggregation, and the human heart [8], in which rotating action potentials generate life-threatening arrhythmias [7, 10]. The overwhelming number of experimental and theoretical studies of these rotors focus exclusively on spatially homogeneous, two-dimensional systems [9]. However, this premise is not valid for living systems that are typically three-dimensional and intrinsically heterogeneous both at the sub- and supra-cellular level.

One of the interesting consequences of heterogeneities is the possibility of vortex pinning to inert, impermeable, or electrically insulating structures. This pinning was first studied for two-dimensional spiral waves that in homogeneous media rotate around a zero-dimensional phase-singularity at the center of the pattern [10]. The associated motion of the spiral tip occurs around this special point but the tip can also be forced to follow the boundary of appropriately chosen heterogeneities as long as the size of the defect is not much smaller than the tip orbit of the free spiral [9, 12]. Once pinned in such a manner, the slow translation of the anchoring heterogeneity relocates the rotating tip over potentially large distances [13, 14].

In three space dimensions, the situation is more complex as the vortex rotation cannot occur around a point but is organized by a one-dimensional phase singularity. This filament can move and reshapes itself according to local speeds that are essentially proportional to the local curvature [13]. Furthermore, filament loops shrink and disappear in all systems with a positive filament tension (a system-specific parameter) [16]. The vortex field itself is called a scroll wave and can be twisted if the rotation phase varies along the filament [17]. Scroll waves have been observed in experiments with the aforementioned slime mold and in the thick ventricles of the human heart [18, 19]. In addition, they have been studied systematically in the chemical Belousov-Zhabotinsky (BZ) reaction which is a convenient and highly reproducible model of excitable and oscillatory reaction-diffusion systems in

general [20].

The three-dimensional BZ system has also been used to demonstrate and study scroll wave pinning [21–23, 25]. This is usually accomplished by introducing inert and impermeable obstacles into the medium. To avoid undesired hydrodynamic effects and to reliably position the heterogeneities in the system, the reaction is often carried out in a gel. Using this approach, Jiménez et al. investigated the pinning of scroll rings to thin (complete and cut) tori [21] as well as small beads and rods [22, 23]. Most of these objects can stop the curvature-controlled decay of the filament loop and thus have a profound impact on the evolution of the system. For pinning to occur, the filament of the initial scroll wave must be at least locally in close vicinity of the anchor (less than one pattern wavelength) or reach this proximity during its free motion. Once a local contact is established, the filament tends to self-wrap around the heterogeneity [23, 24].

The pinning of scroll rings to topologically mismatched double tori and specifically also the pinning to one of the sub-tori was demonstrated by Dutta et al in 2011 [25]. Again pinning is possible and prevents vortex annihilation but the wave dynamics are more complex as the rotation around the sub-torus is periodically perturbed by the junction to the other, vortex-free sub-torus. Accompanying simulations of the dynamics showed anchoring of scroll ring pairs to double tori not only for states with equal but also opposite chirality. In this chapter, we report a continuation of the latter work and demonstrate the pinning of scroll waves to planar sheets with periodically arranged holes. These inert objects are highly branched and much larger than the vortex anchors studied earlier allowing scroll wave pinning in a multitude of discrete patterns.

3.2 Experimental Methods

We use the autocatalytic BZ reaction for our experimental study. The reaction is carried out in a Petri dish of diameter 10 cm using two BZ gel layers of thickness 4 mm each. Both layers are chemically identical and contain 0.8% (w/v) agarose. The initial concentrations of the reactants in both the layers are $[NaBrO_3]$ = 0.04 M, $[CH_2(COOH)_2]$ = 0.04 M, $[H_2SO_4]$ = 0.16 M, and $[Fe(o\text{-}phen)_3SO_4]$ = 0.5 mM. Ultra-pure water with a resistivity of 18.2 MΩ cm is used to prepare all the solutions and gels. Notice that this BZ system has positive filament tension [24] and accordingly all free scroll rings shrink and vanish in finite time. The vortex pinning heterogeneity is a rigid, hexagonal mesh made of a black, non-reactive polymer of thickness 1.1 mm. The mesh holes are circular and have a diameter of 3.1 mm. The distance between the centers of two neighboring holes is 4.5 mm. This sheet is placed onto the lower gel layer while it is still soft and then gently pressed into it, so that the forming gel covers about half of the mesh thickness. A schematic lateral view of the reaction chamber before placing the mesh over the bottom gel layer can be seen in Fig. 3.1(a). An expanding chemical wave is created by inserting the tip of a silver wire into the gel for a few seconds [Fig. 3.1(b)]. The initiation process is based on the decrease

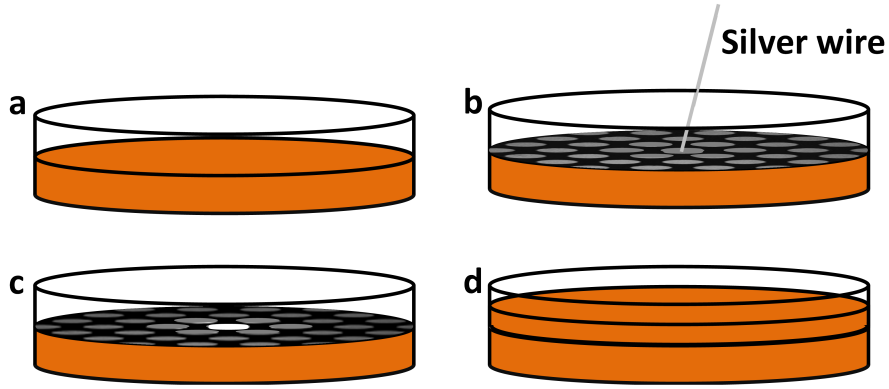

Fig. 3.1: A schematic diagram of the experimental steps. The black regions are the nonreactive polymer sheet and the bright circular areas are the holes. (a) The bottom layer of gel poured into the Petri dish before placing the polymer mesh over it. (b) Wave initiation with the help of a silver wire at the centre of a hole of the mesh. (c) Expansion of the initial wave, seen as the brightest white circle, up to the rims of the hole just before pouring the upper gel layer over the mesh in (d).

in the concentration of the inhibitor bromide via formation of solid AgBr on the wire. When the wave reaches the desired diameter Fig. 3.1(c), the second layer is poured over the mesh with the pre-gel solution being slightly above the gelling temperature Fig. 3.1(d). Subsequently, the rim of the wave spontaneously curls into the upper layer and creates the desired scroll wave. The system is illuminated from below by diffuse, white light. A charge coupled device camera equipped with a blue dichroic filter is mounted above the reaction system and records images (640×480 pixels) at 2 s intervals. The resulting image sequences are analyzed using in-house MATLAB scripts. All experiments are carried out at room temperature.

3.3 Experimental Results

Figure 3.2 shows an image of a representative wave pattern in our experimental system. The black area corresponds to the polymer mesh, while the circular areas reveal the projection of the three-dimensional wave pattern onto the image plane. In this particular experiment, we initiate a wave in the central hole of the mesh and before introduction of the second gel layer, allow the wave to propagate across the six adjacent holes. A time lapse video of the experiment suggests that the resulting scroll wave rotates around the outer rim of these six holes. More precisely, the vortex wave rises through the 12 holes that form the surrounding hexagon, moves inwards, and then descends into the lower layer through the six holes of the inner hexagon. This circulatory motion along the rings of 6 and 12 holes is illustrated in Fig. 3.2(b). Each hole-connecting line in this figure is detected by computer software that analyzes the phase relation between the excitation events in neighboring holes.

The rotation pattern of this pinned vortex is further analyzed by the time-space plots in Figs. 3.2(d)-(l). Each plot is generated by stacking consecutive, one-dimensional intensity

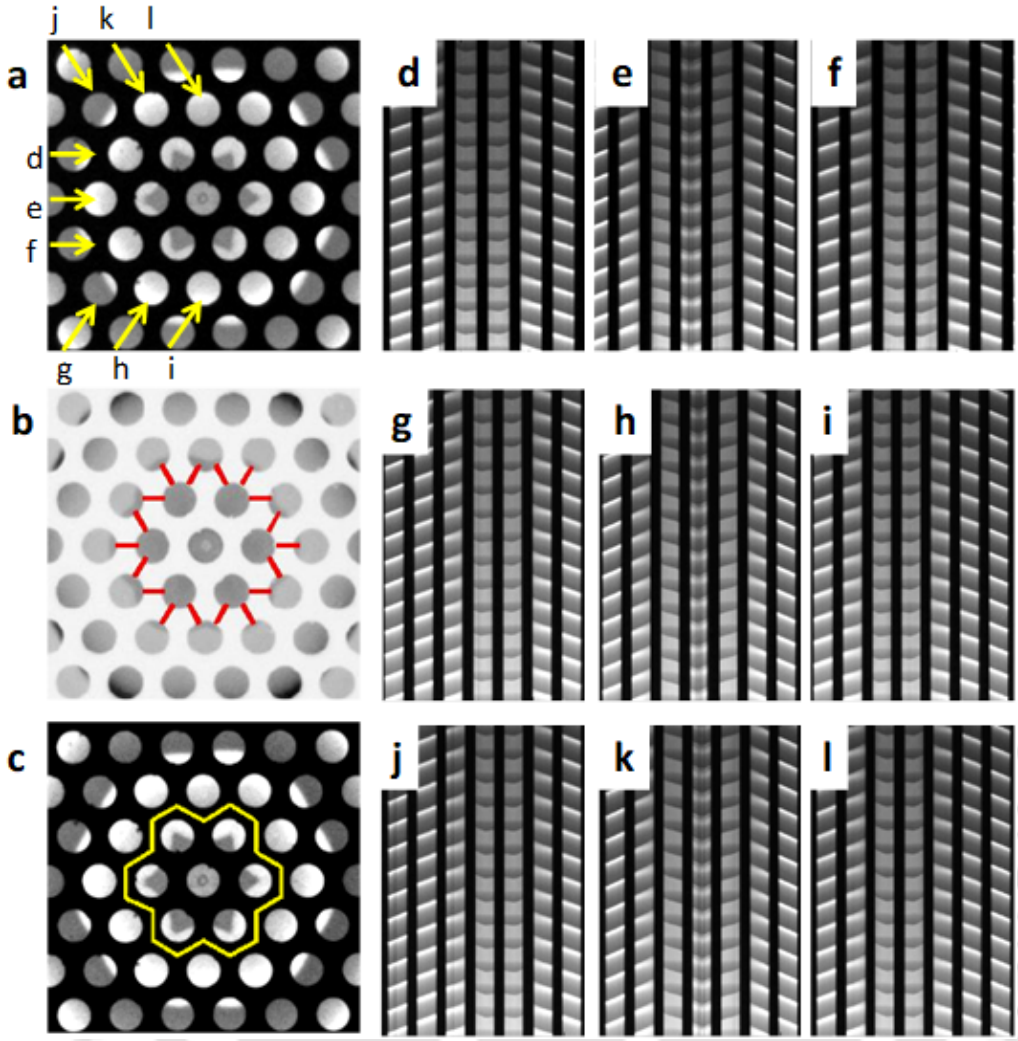

Fig. 3.2: Pinning of a three-dimensional scroll wave to an inert mesh. (a) Top view of a single scroll wave pinned to the thin rim around the seven central holes (bright circles). Field of view: 2.9 cm × 2.9 cm. (b) The same vortex rotates through next-neighbor holes that are indicated by solid (red) lines (the color of the original snapshot in (b) has been inverted). (c) The reconstructed filament. The bright yellow line can be understood as the rotation backbone or equivalent of a filament. (d)-(l) Time-space plots generated along lines marked by the yellow arrows in (b). Time increases in the downward direction spanning 100 min.

profiles so that time increases in the downward direction. Accordingly, a propagating wave pulse generates a bright, diagonal band and the stationary polymer mesh creates vertical, black lines. The different time-space plots represent the intensity dynamics along the nine lines indicated by the bright (yellow) arrows in Fig. 3.2(a). These diagrams allow us to distinguish between unidirectional wave propagation and rotating vorticity. The former manifests itself as a continuous diagonal line (interrupted by the dark stripes), whereas the latter tends to create fishbone-shaped patterns because waves are emitted in alternating directions. Lastly, wave collisions can be discerned as V-shaped patterns within a single hole. For this specific experiment, the collision feature is most prominent in the central hole and hence the corresponding time-space plots in Figs. 3.2(e,h,k). If we follow the yellow

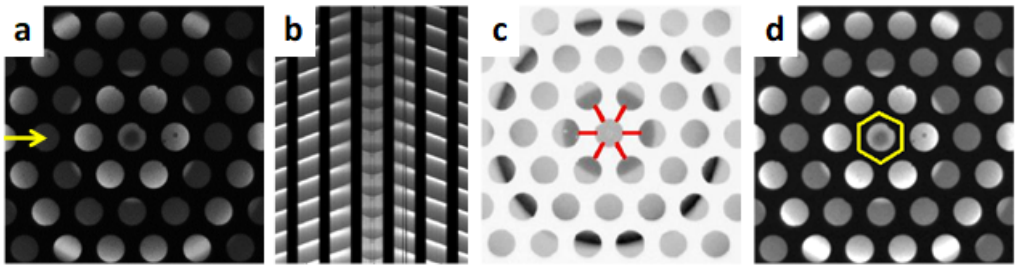

Fig. 3.3: Pinning of a three-dimensional scroll wave to a single hole of the mesh. (a) Top view of the simple wave pattern. Area of the snapshot is 2.9 cm × 2.9 cm. (b) A representative time-space plot generated along the line marked by the yellow arrow in (a). Time increases in the vertical direction from top to bottom. The time space plot spans a time interval of 100 min. (c) The position of the filament detected by a MATLAB code. (d) The reconstructed filament.

arrow "e" in Fig. 3.2(a), it cuts across seven holes separated by the dark mesh area. This is reflected in Fig. 3.2(e) as seven bright bands, interspersed by six thin black bands. The fish-bone structure that emanates from the second and fifth black bands in the latter, point to the presence of a filament section in that region of the mesh, as is evident in Fig. 3.2(c). The V-shaped pattern in the central hole of this time-space plot arises out of wave collision. The rotation feature is present in all nine plots and their locations match our earlier description.

The pinned vortex shown in Fig. 3.2 is only one of many possible states that can be selected by initiating waves in one or more holes and by controlling their expansion time. Figure 3.3 shows the simplest possible pattern observed in our experiments. The wave pattern is created from a single initiation site. Its rotation occurs downwards through the central hole and upwards through the six surrounding ones. This behavior is also illustrated in the time-space plot in Fig. 3.3(b) and has been confirmed by the solid red lines in Fig. 3.3(c).

It has been observed that similar initial conditions could give rise to different wave patterns. Fig. 3.4(a) and Fig. 3.4(d) are the initial conditions giving rise to the patterns in Fig.3.4(c) and Fig.3.4(f). In both these cases, a single hole has been excited. The extent to which the waves have been allowed to expand before introducing the top gel layer decides the final stable pattern. Our experiments show that the smaller vortex occurs only if the vortex-initiating wave is not larger than the circle defined by the centers of the six-hole hexagon, as is the case in Fig.3.4(a).

In Fig. 3.5, we show four other examples, all of which have been observed in at least three independent experiments. All the waves are created by simultaneous wave initiation in multiple, next-neighbor holes. The vortex in (a) forms after two-hole initiation and its wave front descends through this pair of holes but ascends through the surrounding eight holes. Examples of three-hole initiation are shown in Figs. 3.5(e,i). Here, the rotation involves three and six holes, respectively. Both vortex patterns result from the same initiation configuration but different expansion times. Lastly, Fig. 3.5(m) illustrates a four-hole case.

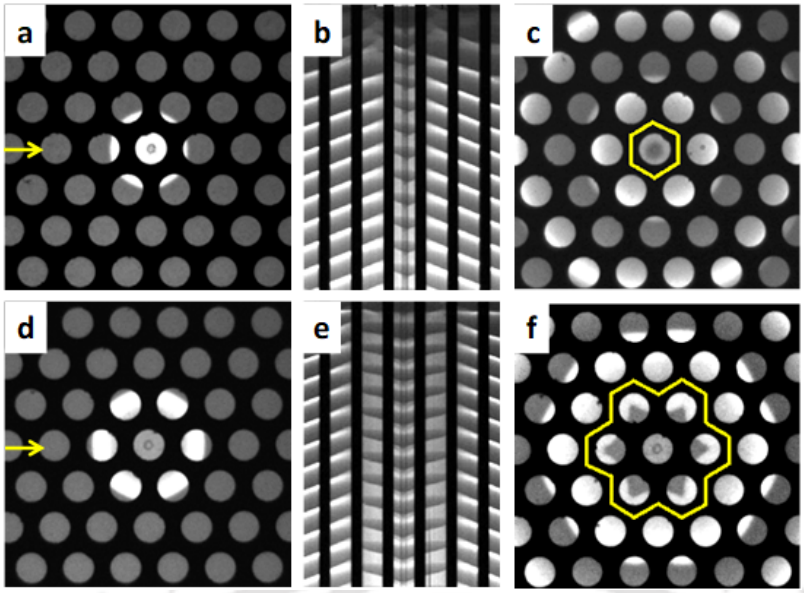

Fig. 3.4: Initial conditions for two different wave patterns. (a),(d) Snapshots of the initial waves at the moment of introducing the upper gel layer to the reaction chamber. (b),(e) Corresponding time-space plots illustrating the formation of the filament and its subsequent pinning. The time-space plots have been constructed for the first 48 min. (c),(f) The final shapes of the pinned filaments.

It has been noticed that initiation of vortices along chains of single holes has proven difficult with the exception of two holes. The resulting wave patterns are very complicated and difficult to interpret suggesting a break-up into several scroll rings.

The anchored vortices have rotation periods that differ from the system-specific period of a free scroll wave. These rotation periods are identical to the local excitation periods in the entire wave pattern. We analyze this aspect by computing the wave period from the intensity changes in the center of every hole within the field of view. From these data, we compile the distributions shown in Fig. 3.6. For instance, the orange curve (closed circles) characterizes a free, slowly collapsing scroll ring. Its average is about 360 s. All pinned vortex states have periods in the range of 430-500 s and are hence, on an average, 30% larger than the value of the free scroll ring. This increase is caused by at least two factors, namely the longer orbits enforced by the rotation around the connecting segments of the mesh and by the topological frustration created by the mismatch between a filament loop and the mesh structure.

The results in Fig. 3.6 suggest a dependence of the period on the specific vortex type. Here, the small two-hole state [Fig. 3.5(a)] is the fastest pinned rotor, with a period of 430 s. It is followed by the four-hole rotor [Fig. 3.5(m)] while all other states are close to a period of 480 s and possibly identical. Geometric parameters that could explain this ordering include the aspect ratio of the vortex line. If we consider the vortex lines to be simple polygonal curves as those shown in Fig. 3.2(c), Fig. 3.3(d), and Fig. 3.5(d,h,l,p), the width-to-height ratios (width being shorter than height) will be as shown in Table. 3.1.

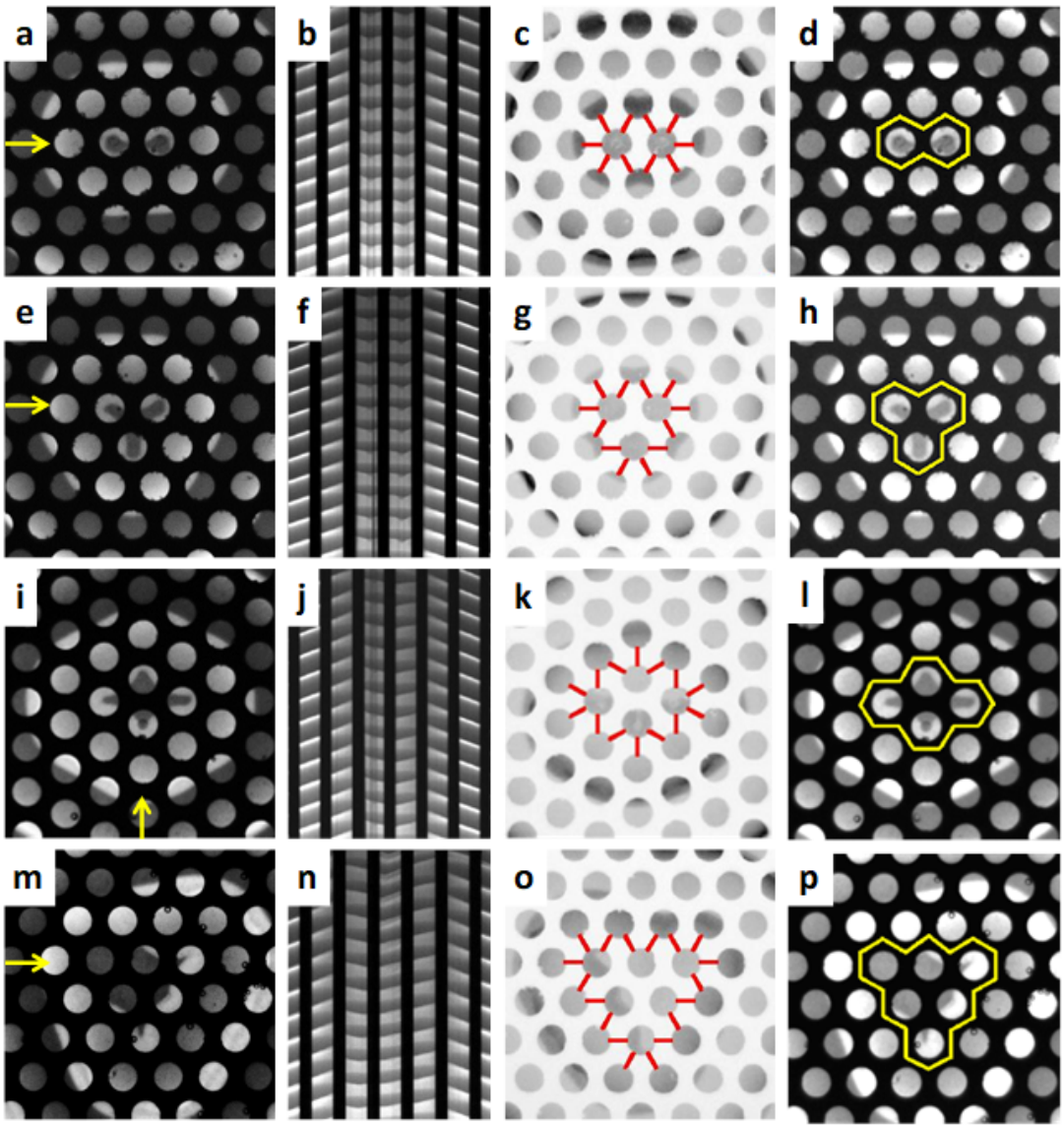

Fig. 3.5: Results of four experiments showing scroll waves with different pinning patterns. (a,e,i,m) Snapshots of the stably pinned filaments. The area of each snapshot is 2.9 cm $\times$ 2.9 cm. (b,f,j,n) Time space plots generated along the yellow arrows shown in the snapshots in the first column. In each case, time increases in downward direction. (c,g,k,o) Position of filaments detected with a MATLAB code. Whenever a filament exists in the area between two holes, the holes are linked with a solid red line (colors of snapshot have been inverted here for the sake of clarity). (d,h,l,p) The shapes of the reconstructed filaments, shown by the yellow polygons.

To evaluate the impact of the topological mismatch between the normal filament loop of a scroll ring and the branched structure of the mesh, we perform additional pinning experiments with a simple inert torus. The thickness of the torus (1.6 mm) is chosen to yield a circumference (5.0 mm) that matches the length of the shortest orbit available to the pinned scroll waves. The latter is determined by the shortest distance between neighboring holes (1.4 mm) and the thickness of the mesh (1.1 mm). This topologically matched pinning experiment yields a rotation period of about 550 s and is hence the longest period observed.

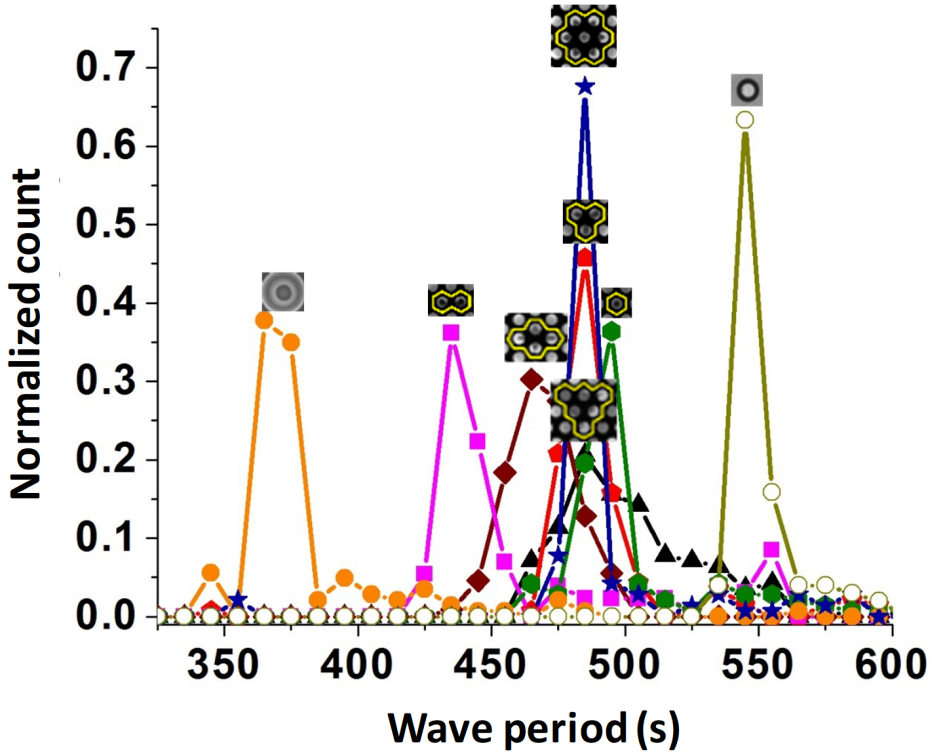

Fig. 3.6: Normalized distribution of wave periods of scroll waves having different filament geometries. The respective geometries are shown on the top of each curve. The closed circles(orange) show the frequency distribution of a free scroll wave, the open circle (olive) is for a circular scroll wave pinned to an O-ring.

This finding is very surprising as one could expect the branched structure of the mesh to hinder the rotation. A qualitatively similar result was obtained in earlier experiments on single scroll rings pinned to double tori [25]. The latter structures had a 6% shorter period than scroll waves pinned to otherwise identical single tori.

3.4 Model and Simulation Methods

To obtain further insights into the rather complex motion of the pinned scroll waves, we perform three-dimensional numerical simulations with the Barkley model [17]. This simple, two-variable model is given by the reaction-diffusion equations

$$\frac{\partial u}{\partial t} = \frac{1}{\varepsilon}\left\{u(1-u)\left(u-\frac{v+b}{a}\right)\right\}+D_u\nabla^2 u, \tag{3.1}$$

$$\frac{\partial v}{\partial t} = u-v+D_v\nabla^2 v. \tag{3.2}$$

The fast variable u and the slow variable v qualitatively describe the concentrations of $HBrO_2$ and Ferroin, respectively. Our simulations are carried out for $a = 1.1$, $b = 0.84$, $\varepsilon =$

Filament geometry	width-to-height ratio
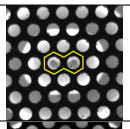	0.55
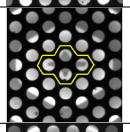	0.68
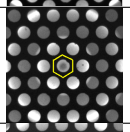	1
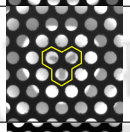	~ 1
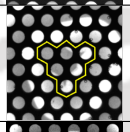	~ 1
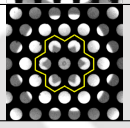	1

Tab. 3.1: Width-to-height ratios of the pinned filaments of different geometries.

0.02 and diffusion constants of $D_u = D_v = 1.0$. These parameters describe an excitable system with positive filament tension. Explicit Euler integration and a seven-point Laplacian stencil is used to numerically solve the two partial differential equations. The integration time step is kept constant at 0.012. Our simulations employ a three-dimensional lattice of $320 \times 320 \times 200$ grid points with a grid spacing of 0.35. The unexcitable mesh is modeled as a continuous domain with the approximate shape of the experimental mesh and Neumann boundaries to the surrounding excitable medium. These no-flux boundary conditions match the impermeable character of the polymer sheet in the experiments and fully block wave propagation. The hole diameter and spacing are 14 and 16.8 space units, respectively. The thickness of the mesh is 1.4 space units. A zero-flux boundary condition is also set for each diffusing species along the external boundaries. The filament of the scroll wave is identified as regions where $u = 0.5$ and $v = a/2 - b$. Following the initiation of the desired scroll wave, transients in our simulations are minor and short-lived. The reported wave patterns and filaments represent the stationary rotation patterns of the pinned vortices. Our simulations extend over time intervals during which the pinned vortex performs at least 80 rotation cycles. A free scroll ring of size comparable to the example in Fig. 3.2 would have collapsed in 24 cycles.

3.5 Simulation Results

Figure 3.7 summarizes the results of a typical simulation. The images in (b)-(f) illustrate the evolution of a three-dimensional scroll wave pinned to an unexcitable layer [Fig. 3.7(a)].

The specific case in Fig. 3.7 is analogous to the experiment shown in Fig. 3.2. The solid brown area is the excitation vortex. We omit the three-dimensional obstacle and only show the posterior half of the vortex, for better visualization. The circulatory wave activity is seen to concentrate around two hexagonal structures: an inner ring of six holes that encircles the central hole, and an outer ring of twelve holes that encircles these seven holes [Fig. 3.7(a)]. Figure 3.7(b) shows an early stage of the simulation that is similar to the initial, experimental condition, i.e. a semi-spherical wave in the lower gel layer. This bowl-shaped structure starts curling up into the top layer through the outer ring [Fig. 3.7(c,d)] and descends through the ring of inner holes [Fig. 3.7(e,f)]. Every time a wave segment emerges from a hole it collides with wave segments from the neighboring holes creating a segmented rim structure.

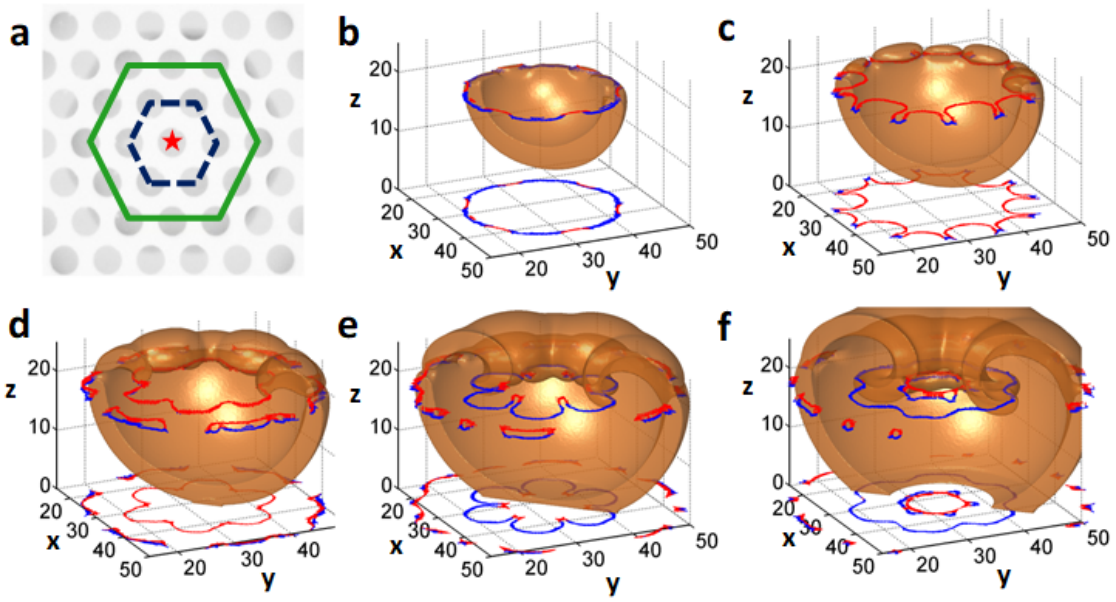

Fig. 3.7: Numerical simulation of the dynamics of a scroll wave pinned to the rim around the seven central holes. (a) A snapshot of the mesh (white) showing the hexagonal inner ring r_1 (dotted blue) and outer ring r_2 (solid green) around the central hole (red star). (b)-(f) Evolution of the wave pattern (solid brown areas) and the filament (red and blue curves). Filament sections above the central horizontal plane (z = 20) are indicated by red curves while blue curves depict those below the plane. The two-dimensional projections of the filaments are shown at the bottom of the box ($z = 0$). Time intervals between neighboring frames are 1.7, 1.2, 1.2, 1.0 time units [(b)-(f)]. The computed volume has been cropped along the boundaries.

In Fig. 3.7 filament segments above (below) the central plane are plotted in red (blue). The entire filament is also projected onto the $z = 0$ plane maintaining the aforementioned color coding. In Figs. 3.7(b,c), the filament is turning upwards and acquires twelve Ω-shaped features that correspond to the twelve holes of the outer ring. Due to the obstacles between the holes, parts of the filament stay below the mesh [blue parts in Fig. 3.7(c)]. Sub-sequently, these segments detach from the main loop and move outwards. A similar process

occurs above the mesh and sheds off additional (red) filament segments [Fig. 3.7(d)]. These red and blue parts form connected entities [Figs. 3.7(e,f)] and move outwards but are not associated with sustained wave rotation. This complicated process is the direct consequence of the topological frustration in this system, which does not allow uninterrupted rotation. Lastly, the now rather small, main loop begins to ascend between Fig. 3.7(e) and Fig. 3.7(f) to complete the rotation cycle. The shape of the filament in Fig. 3.7(d) closely resembles the suggested vortex line of the experimental result shown in Fig. 3.7(c).

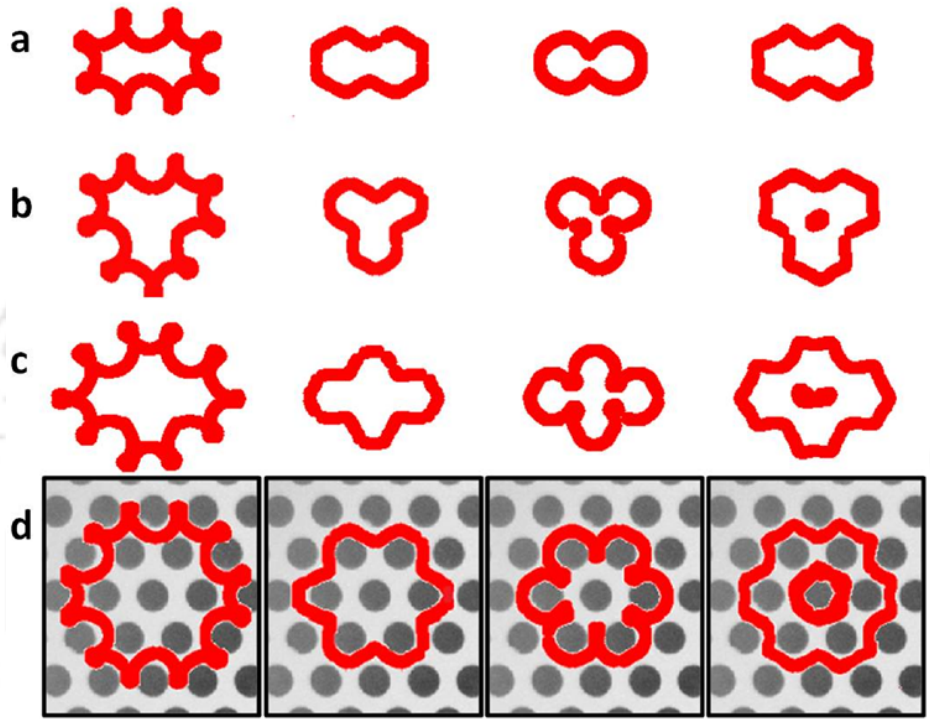

Fig. 3.8: Numerical simulations of filament shapes and dynamics for scroll waves pinned to a hexagonal mesh. (a)-(d) Each row shows the filament at four different p hases. The rows differ only in the initial conditions that have been employed during the simulations. In (d) the filament is shown as a projection over the hexagonal mesh structure. The results are similar to the experiments in Fig. 3.5(a,e,i) and Fig. 3.2.

Figure 3.8 provides additional numerical examples that are constructed from identical simulations but different initial conditions and/or expansion times. From top to bottom, the four rows correspond to scroll waves pinned to inner rings containing two, three, four, and six holes. Each row shows the filament at four different phases. Again we find good qualitative agreement with the vortex lines in Fig. 3.5. We suggest that these shapes are widely independent of the model and also the experimental system as they primarily depend on a steady spread of the wave and not subtle dynamic features.

3.6 Conclusions

We have shown that vortex structures can be readily pinned to a thin planar heterogeneity containing a periodic array of holes sufficiently large to allow the reliable passage of exci-

tation waves. The pinning prevents the collapse of the scroll waves and creates a very large number of possible vortex states.

In experiments with a three-dimensional chemical system and numerical simulation based on a simple mathematical model, we have shown that vortices of different shapes can be made to pin to a heterogenous obstacle with numerous branching points. The shape of the filament depends upon the initial size of the waveform and its proximity to the nearest heterogeneities. This study could illuminate the phenomenon of pinning of scroll waves to scar tissues and other complex unexcitable structures in the cardiac system.

Many other experiments can be envisioned for similar heterogeneities including non-uniform hole sizes. This case should be particularly interesting if some of the holes are sufficiently small to block wave passage according to firing sequences such as passage followed by blockage (1:1) or more complex sequences [28, 29]. Other more obvious variations should explore different arrangements of the holes including square patterns and nested vortices. More ambitious possibilities include three-dimensional versions of the blocking heterogeneity and even dynamic ones. For biological applications, another area of interest are random heterogeneities.

BIBLIOGRAPHY

[1] I. R. Epstein and J. A. Pojman, An Introduction to Nonlinear Chemical Dynamics: Oscillations, Waves, Patterns, and Chaos (Oxford University Press, USA, 1998).

[2] Y. Yu, L. M. Santos, L. A. Mattiace, M. L. Costa, L. C. Ferreira, K. Benabou, A. H. Kim, J. Abrahams, M.V. L. Bennett, and R. Rozental, Proc. Natl. Acad. Sci. **109**, 2585 (2012).

[3] X. Huang, W. Troy, Q. Yang, H. Ma, C. Laing, S. Schiff, and J.-Y. Wu, J. Neurosci. **24**, 9897 (2004).

[4] J. Lechleiter, S. Girard, E. Peralta, and D. Clapham, Science. **252**, 123 (1991).

[5] O. Steinbock, F. Siegert, S. C. Müller, and C. J. Weijer, Proc. Natl. Acad. Sci. **90**, 7332 (1993).

[6] E. M. Cherry and F. H. Fenton, New J. Phys. **10**, 125016 (2008).

[7] J. Jalife, M. Delmar, J. Anumonwo, O. Berenfeld, and J. Kalifa. Basic Cardiac Electrophysiology for the Clinician, 2nd ed. (Wiley-Blackwell, Oxford, UK, 2009).

[8] R. A. Gray, J. Jalife, A. V. Panfilov, W. T. Baxter, and C. Cabo, Science **270**, 1222 (1995).

[9] R. Kapral and K. Showalter, *Chemical Waves and Patterns* (Kluwer, Dordrecht, 1995).

[10] A. T. Winfree, Science **175**, 634 (1972).

[11] O. Steinbock and S. C. Müller, Phys. Rev. E **47**, 1506 (1993).

[12] Z. Y. Lim, B. Maskara, F. Aguel, R. Emokpae, and L. Tung, Circulation **114**, 2113 (2006).

[13] O. Steinbock and S. C. Müller, Physica A **188**, 61 (1992).

[14] H. Ke, Z. Zhang, and O. Steinbock, Phys. Rev. E **91**, 032930, 1 (2015).

[15] J. P. Keener and J. J. Tyson, SIAM Rev. **34**, 1 (1992).

[16] V.N. Biktashev, A.V. Holden, and H.G. Zhang, Phil. Trans. R. Soc. A **347**, 611 (1994).

[17] S. Mikhailov, A. V. Panfilov, and A. N. Rudenko, Phys. Lett. A **109**, 246 (1985).

[18] F. Siegert and C. J. Weijer, Proc. Natl. Acad. Sci. USA **89**, 6433 (1992).

[19] M. Gotoh, T. Uchida, W. J. Mandel, M. C. Fishbein, P. Chen, and H. S. Karagueuzian, Circulation **95**, 2141 (1997).

[20] W. Jahnke, C. Henze, and A. T. Winfree, Nature (London) **336**, 1222 (1988).

[21] Z. A. Jiménez, B. Marts, and O. Steinbock, Phys. Rev. Lett. **102**, 244101 (2009).

[22] Z. A. Jiménez and O. Steinbock, Phys. Rev. Lett. **109**, 098301 (2012).

[23] Z. A. Jiménez and O. Steinbock, Phys. Rev. E **86**, 036205 (2012).

[24] Z. Zhang and O. Steinbock, New J. Phys. **18**, 053018 (2016).

[25] S. Dutta and O. Steinbock, J. Phys. Chem. Lett. **2**, 945 (2011).

[26] T. Bánsági, Jr. and O. Steinbock, Phys. Rev. Lett. **97**, 198301 (2006).

[27] D. Barkley, Physica D **49**, 61 (1991).

[28] A. Toth, V. Gaspar, and K. Showalter, J. Phys. Chem. **98**, 522 (1994).

[29] B. T. Ginn and O. Steinbock, Phys. Rev. Lett **93**, 158301 (2004).

Chapter 4

UNPINNING OF SCROLL WAVES ATTACHED TO MULTIPLE HETEROGENEITIES

4. UNPINNING OF SCROLL WAVES ATTACHED TO MULTIPLE HETEROGENEITIES

4.1 Introduction

Spiral and scroll wave activities are often witnessed in nature. These are two and three dimensional excitation wave patterns, found in systems such as the Dictyostellium discoideum [7], neural cortex [2], retinal cells [3], and cardiac tissues [4]. Such structures are also observed in very diverse and unrelated environments, such as fluid flows [5], liquid crystals [6], and galactic formations [7]. A plane traveling wave may break-up and form a pair of spirals, when it encounters an unexcitable heterogeneity, or an area of low excitability in its path of motion [8]. Depending on the size and geometry of the heterogeneity, the spiral may also get attached to it [9]. This phenomenon of pinning is also displayed by the three dimensional scroll waves, when their one-dimensional filaments get anchored to obstacles of different kinds [10]. Free scroll waves can have either positive or negative filament tension, according to which they either shrink and collapse, or keep on expanding till they reach the system boundary, in accordance with curvature-dependent motion [11]. As a result of pinning, the life-time of the filaments are infinitely elongated. When this occurs in the cardiac tissues, the scroll waves responsible for disturbing the rhythm of the heart become long-lived, and threaten the very existence of the individual [8]. Unpinning of the waves from the obstacles ensure that they can subsequently undergo free curvature-dependent dynamics. So, the study of the pinning and unpinning of spiral and scroll waves, is also of importance to medical science, over and above its fundamental academic relevance.

Chemical systems, such as the Belousov Zhabotinsky (BZ) reaction, are good candidates for the table-top study of such processes. This is a system with positive filament tension, where the scroll wave filaments eventually collapse and disappear [12]. Scroll waves in the BZ have been shown to pin to spherical glass beads, cylinders, tori and extended meshes [13–15]. Depending on the nature of the heterogeneity, the collapse of the filaments can be partially or completely stopped. The dynamics of spiral and scroll waves in the otherwise homogeneous reaction diffusion systems, have been modified and controlled by employing external forces, like electric fields, concentration and thermal gradients [16, 17]. Free scroll waves drift under the influence of such fields, and their orientation is modified, depending on their position relative to the field direction. Dynamic and cross electric fields and thermal gradients have made the scroll waves trace cyclic trajectories [18]. In studies of pinned filaments, it has been demonstrated that scroll waves

pinned to two spherical beads can be unpinned by the application of such gradients [19,20]. However, it has been inferred from some recent work on the BZ system, that as the anchor size changes, the rigidity of the filament also gets modified [21]. The number of pinning sites, and the geometry in which they are arranged could also be factors influencing the stability and dynamics of the pinned filament. In this work, we carry out experiments in the homogeneous BZ system, to study the pinning of the scroll waves to multiple spherical heterogeneities, placed in different geometries. We then try to unpin them from their stably pinned configurations, using steady electric fields and thermal gradients. The influence that the bead size and bead placement has on the phenomenon of unpinning has been studied in detail. An interesting trend is found in the unpinning time as the number of pins increase. The study is complemented by numerical simulations based on the Barkley model for reaction-diffusion systems.

4.2 Experimental Methods

We used the three dimensional, Ferroin-catalyzed Belousov Zhabotinsky (BZ) reaction for our experiments. Spherical glass beads were employed to act as the heterogeneous obstacles. The reactions were performed in a specially designed reaction chamber (8 cm $\times$ 8 cm $\times$ 2.5 cm) having heat exchangers on its two sides that were connected to thermostat-controlled water baths. All reactions were carried out at room temperature. The experimental system consisted of two layers of BZ containing 0.8 wt/vol % agarose gel. Each layer was about 4 mm thick, and the initial concentrations of the reactants used were $[NaBrO_3]$ = 0.04 M, $[CH_2(COOH)_2]$ = 0.04 M, $[H_2SO_4]$ = 0.16 M, and $[Fe(o\text{-}phen)_3]SO_4$ = 0.5 mM. All solutions were prepared using Millipore water. The first layer of BZ was poured into the reaction chamber, and the required number of glass beads were embedded halfway into the forming gel. Once the gelation process was complete, the tip of a clean silver wire was slightly inserted into the gel for a few seconds, at a position equidistant from the glass beads. This initiated the formation of a chemical wave, by the local removal of the inhibitory Br^- ion, in the form of AgBr. When the expanding wave reached the glass beads, the second BZ gel layer, slightly above its gelling temperature, was poured over the system. The semi-spherical wave in the lower gel layer immediately started to curl up into the top layer, and eventually formed the scroll ring of desired dimension. For the application of electric fields, two rectangular Cu electrodes (sized 2.5 cm $\times$ 3.5 cm) were vertically placed along the walls, perpendicular to the heat exchangers such that the scroll was equidistant from the Cu plates [Fig. 4.1(i)]. The electrodes were connected to a DC power supply (Scientific Multipurpose Power Supply PSD3304). The heat exchangers along the reaction chamber could act as temperature stabilizers to compensate for Ohmic heating. Alternately, they could also be used for introducing thermal gradients into the system. The experiments were recorded as sequential snapshots with a charge coupled device (CCD) camera mounted above the reaction chamber, which was illuminated with a cold,

diffused white light source from below. A blue dichroic filter was fitted to the camera to facilitate contrast enhancement. The images were recorded onto a computer which were later analyzed using MATLAB codes.

4.3 Experimental Results

It is known that a free scroll ring in the BZ system has a positive filament tension, i.e. it shrinks with time, and finally disappears [12]. When it is attached to heterogeneous obstacles, the pinning of the wave stops the shrinkage, and stabilizes the size of the wave. In the presence of electrical and thermal gradients, scroll waves pinned to two beads were successfully unpinned and eventually removed from the system [19, 20]. In this chapter, we look at scenarios where the scroll waves are pinned to three, four or six glass beads. We carried out several experiments with different geometries for a fixed number of pinning sites, and observed that the pinning was strongest for the regular geometries, i.e. equilateral triangle for three pinning sites, square for four pinning sites, and hexagon for six pinning sites. This could be because of the competition between filament tension and rigidity [21]. For our unpinning experiments, we report only the examples with regular geometries.

Figure 4.1 shows three experiments where an electric field was applied to unpin the scroll waves attached to three beads, which were arranged in the form of an equilateral triangle. In each of these experiments, the relative position of the electric field with respect to the triangle was varied. Sequential snapshots of the experiments are shown in Fig. 4.1. In the first snapshot of each experiment [Figs. 4.1(a), 1(d), 1(g)], a bright, narrow band is seen attached to the three beads, in the form of a triangle. This is the initial position of the filament, that emits inward and outward propagating waves. The waves that propagate inward collide shortly after emission, and disappear. The outward propagating waves, on the other hand, are seen as bright bands on the dark background. The small black circles that seem to grow with time, are CO_2 bubbles, which are a product of the reaction. Once the scroll ring was stably pinned to the beads (after more than one hour of scroll wave initiation), an electric field was applied along the positive y-direction. In the first experiment [Figs. 4.1(a)-(c)], the anode lay near the base of the triangle, so that the two basal beads were equidistant from the anode. The scroll ring first unpinned from the bead nearest to the cathode [Fig. 4.1(b)], and then simultaneously from the two basal beads [Fig. 4.1(c)]. In the second experiment [Figs. 4.1(d)-(f)], the beads were placed so that the altitude of the formed triangle was at right angles to the electric field direction. In this scenario, the three beads were at different distances from the electrodes. The result was that the scroll unpinned first from the bead closest to the cathode, followed by the second bead, and finally it disappeared at the third bead which was nearest the anode. Finally, when the base of the triangle was nearer to the cathode [Fig. 4.1(g)], the application of electric field made the scroll unpin from the two basal beads simultaneously [Fig. 4.1(h)]. The scroll wave eventually shrunk and remained attached to the third bead till the end.

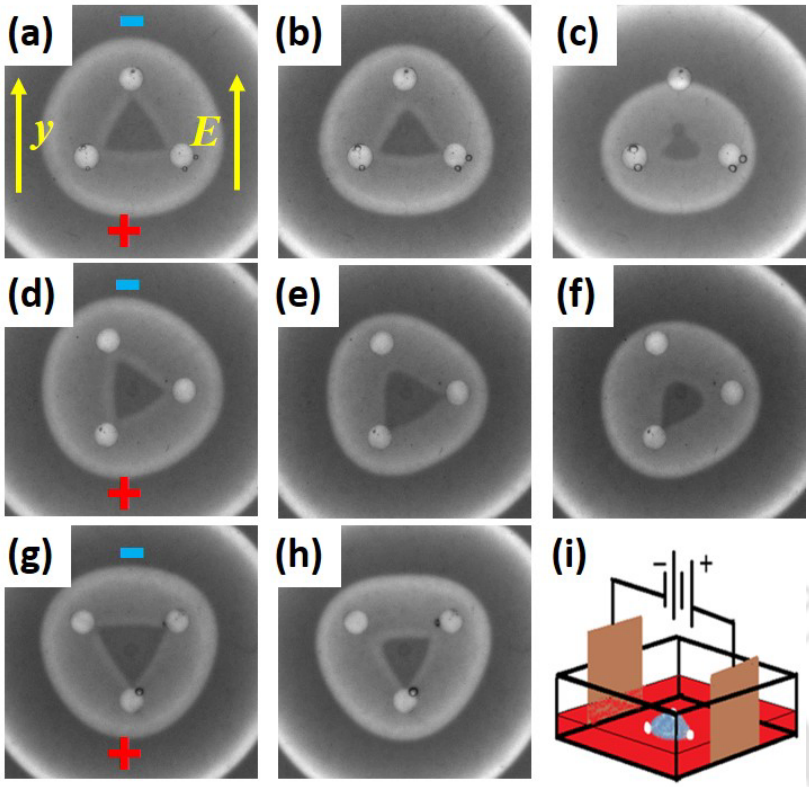

Fig. 4.1: Sequential unpinning of scroll waves from three beads in the presence of an external electric field gradient of strength 0.25 V cm^{-1}. An area of 1.91 cm $\times$ 1.91 cm is covered in each snapshot. The bright circles are obstacles of diameter 1.8 mm separated by a distance of 7.3 mm from one another. (a, d, g) are snapshots of stabilized scroll waves before the application of the electric field. The position of the anode and cathode are being designated by "+" and "-" in each experiment. Time lapsed after the application of the electric field is (b) 16.6 min and (c) 45 min in the first experiment; (e) 20 min and (f) 28 min in the second experiment; and (h) 35.6 min in the third experiment. (i) Schematic diagram of an experiment with bead positions as in (g).

It has been inferred from earlier studies [13] that the size of the obstacles change the nature of the filament pinned to it. We wanted to see if there was any effect of the size of the pinning beads to the unpinning of the filament, under the influence of electric field. We carried out three sets of experiment for each of the bead orientations (as shown in Fig. 4.1), and plotted the time required for the first and second unpinning of the scroll as a function of bead diameter. Figures 4.2(a) and 4.1(b) show the variation in the unpinning times t_1 and t_2, respectively. It is observed that the unpinning time increases with the increase in the bead diameter. For the first unpinning, the time required in the case where the scroll unpins simultaneously from two beads [like the experiment in Fig. 4.1(g)], is much higher than in the other two cases. For the latter two orientations, t_1s are similar, with a slightly larger value when the beads are placed as in Fig. 4.1(a). However, when we consider the second unpinning time t_2, we realize that there is no t_2 for the layout of the beads as shown in Fig. 4.1(g). In the other two orientations, the time required for the scroll to unpin from two beads simultaneously [like in Fig. 4.1(a)] is much larger than where it unpins from

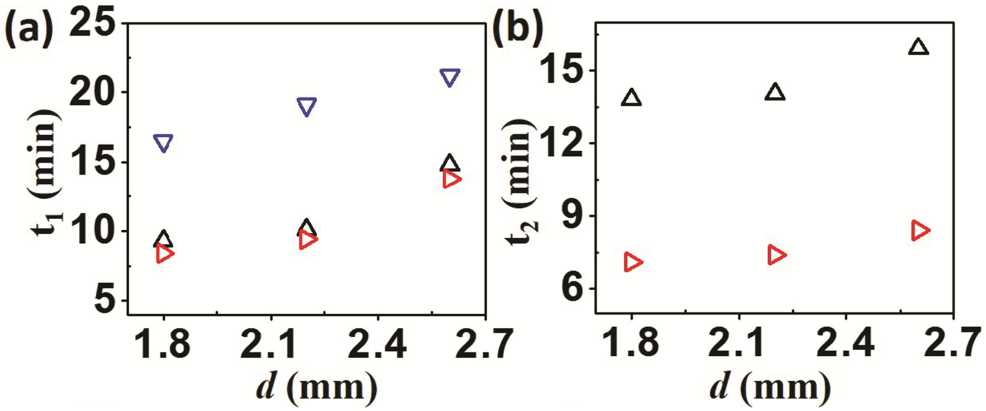

Fig. 4.2: Dependence of unpinning time t_1 and t_2 on bead diameter. The electric field strength has been maintained at 0.5 V cm^{-1} for all experiments. Black triangles, red tilted triangles and blue inverted triangles are used for three different orientations corresponding to Figs. 4.1(a), (d), and (g), respectively.

only one [Fig. 4.1(d)]. Also, interestingly, the variation in t_2 is much less as compared to t_1, with increasing bead size.

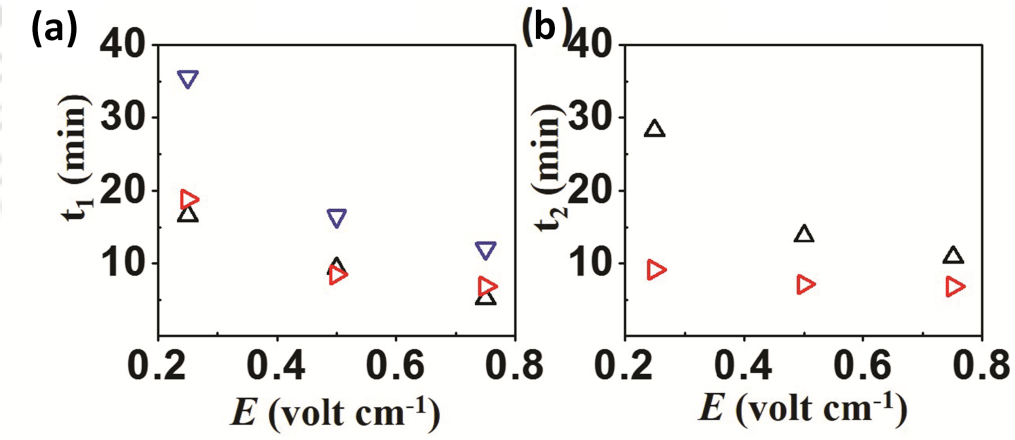

Fig. 4.3: Dependence of unpinning time t_1 and t_2 on electric field strength. For all experiments the bead diameters are 1.8 mm. Black triangles, red tilted triangles and blue inverted triangles are used for three different orientations corresponding to Figs. 4.1(a), (d), and (g), respectively.

In order to study the effect the strength of the electric field has on the unpinning of the scroll wave, we carried out several experiments, where we varied the electric field strength, while keeping the bead diameter constant. Figures 4.3 summarizes the results of nine experiments, with three different values of the field strength. It was seen that the unpinning time reduced as the electric field strength was increased, for all the different orientations of the three obstacles. As in the case of varying bead diameter, in these experiments too, unpinning time is much higher when the scroll has to detach simultaneously from two

beads. There is almost no visible difference in t_1 for the other two orientations. Similar observation was made for t_2.

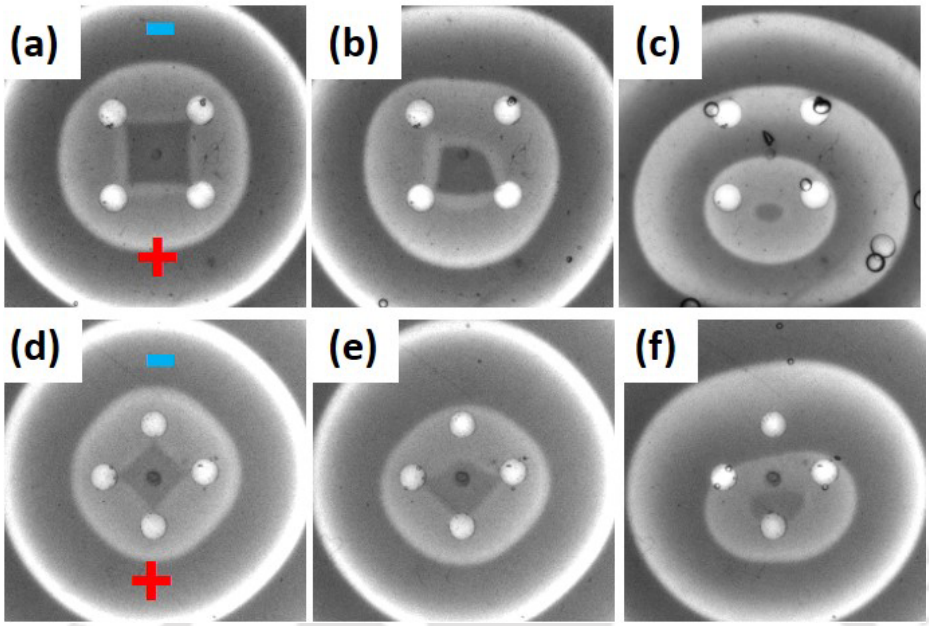

Fig. 4.4: Unpinning of scroll waves pinned to four beads. (a, d) are snapshots of stabilized scroll waves in the absence of an external field. Time-lapse after application of electric field in subsequent images in the first experiment are: (b) 21.6 min and (c) 93.6 min, respectively. In the second experiment, they are (e) 7 min and (f) 20 min, respectively. Direction of the external field is along the y-axis (from "+" to "-") in both experiments, and the electric field strength is 0.5 V cm^{-1}. The bead size and the separation between the nearest beads are 2.26 mm and 6.5 mm respectively for the first experiment; while for the second, they are 2.0 mm and 5.4 mm, respectively. An area of 2.26 cm $\times$ 2.26 cm is covered in each snapshot.

Next, we carried out experiments with four beads. Figure 4.4 shows snapshots of two such experiments, where the bead size and electric field strengths are kept constant. In the two examples, only the orientation of the beads, with respect to the electric field direction was changed. In the first experiment [Figs. 4.4(a)-4.4(c)], the beads are placed in a manner, such that there are two sets of beads, equidistant from the cathode. So, the scroll consecutively unpins from two beads at a time. This results in high unpinning times. In the second experiment [Figs. 4.4(d)-4.4(f)], the first unpinning is from a single bead, and that takes comparatively much shorter time. While, the second unpinning occurs simultaneously from two beads, and this requires a much larger time. This time of $\sim$20 minutes, is also comparable to the time required for the first unpinning in the prior experiment [Fig. 4.4(b)]. In the case of the three bead-pinning experiments, contrarily, such comparison between simultaneous two-bead unpinnings show that t_2 is always smaller than t_1. As for example, 14 min versus 16 min for d = 1.8 mm, E = 0.5 V cm^{-1}; 16 min versus 22 min for d = 2.6 mm, E = 0.5 V cm^{-1}; and 28 min versus 35 min for d = 1.8 mm, E = 0.25 V cm^{-1}; etc [Fig. 4.2, Fig. 4.3]. This suggests that there is an essential difference in the filament shape, when it is pinned to three obstacles as compared to four obstacles.

Also, as we increase the number of beads from three to four, the electric field required for successful unpinning increases. Experiments were also carried out for scroll rings pinned

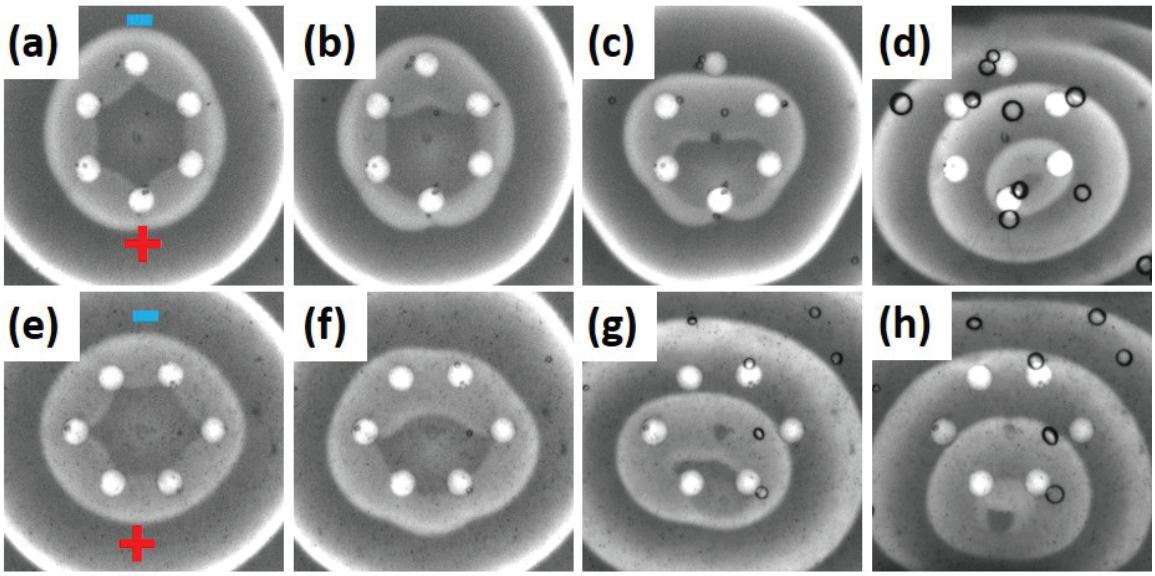

Fig. 4.5: Electric field unpinning of scroll waves attached to six beads. (a, e) are snapshots of stabilized scroll waves before the application of the field. In the first experiment (b) 5.2 min, (c) 24.7 min, and (d) 130.7 min have passed after the onset of electric field. While in the second experiment, the panels have been chosen after (f) 12.5 min, (g) 40.3 min, and (h) 98 min have passed. The electric field strength is 1.0 V cm^{-1}, the bead size is 2.26 mm, and the smallest inter-bead distance is ∼5.1 mm, in both these experiments. An area of 2.26 cm × 2.26 cm is covered in each snapshot. The electrode positions are shown by the "+" and "-" symbols in (a) and (e).

to six beads arranged in the form of a hexagon. With more number of beads, these experiments became much more complicated. There were two main challenges; one was the short time window available to place the beads, before the gelation of the first layer. This resulted in a not-so-perfect hexagonal placement of the beads. The other was that higher strengths of the electric field was required to unpin the scroll wave that was attached to six beads. This resulted in huge expansions of the scroll wave, which eventually touched the reaction chamber when it started rotating on its symmetry axis, and resulted in ring breakage. Experiments for scroll rings attached to two hexagonal orientations of six beads each, are shown in Fig. 4.5. We have successfully been able to unpin the scroll waves from their six-point anchors, using moderately high electric fields. The trends in the unpinning times are similar to the previous experiments.

Similar experiments were carried out for studying the unpinning of scroll waves attached to multiple obstacles, under the influence of a thermal gradient. Figure 4.6 shows the results of nine experiments. For low and moderate strengths of thermal gradients, the pinned scroll waves were successfully unpinned, and eventually shrunk and disappeared. However, for comparatively higher strengths of thermal gradient, the waves were seen to expand in size, and remained pinned to the obstacles. Unlike in the case of electric field,

here we were not successful in observing any exact trend in the unpinning times, with gradient strength.

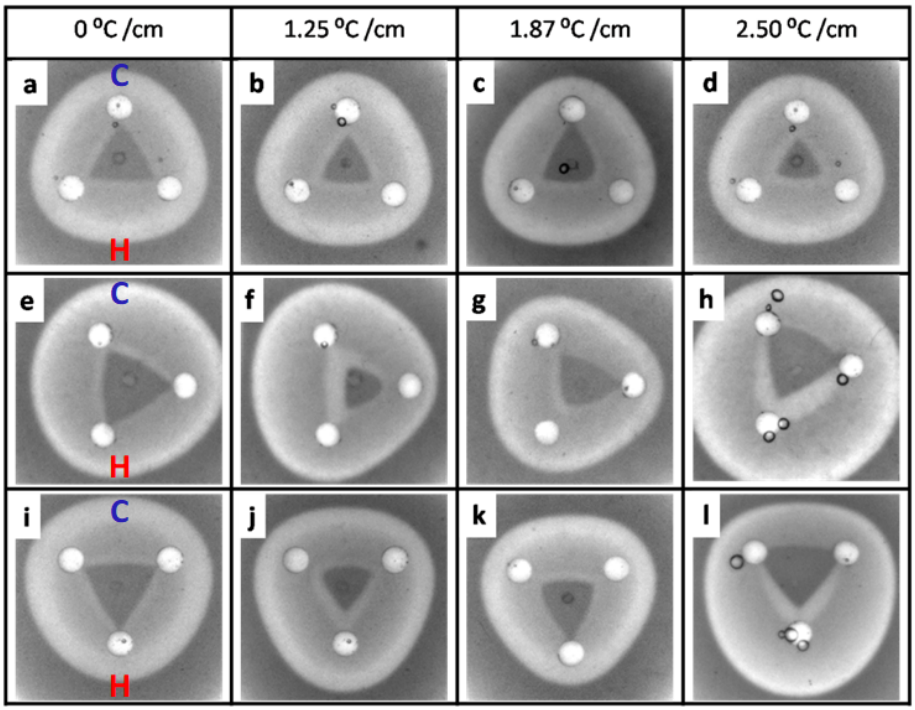

Fig. 4.6: Application of thermal gradient to a scroll wave pinned to three obstacles. (a,e,i) show the stabilized scrolls in absence of the external field. The white circular regions are glass beads of diameter 1.8 mm. In all cases except (h) and (l), the pinned wave gets unpinned from at least one bead. In these two cases however, the scroll shows expansion. Time required for unpinning corresponding to the other images are (b) 21.5 min, (c) 5.1 min, (d) 42.1 min, (f) 32.6 min, (g) 28.2 min, (j) 51 min, and (k) 11.3 min.

4.4 Numerical Simulations

In order to gain a better insight into the filament dynamics, as the scrolls unpin under the influence of the external gradients, we carried out numerical simulations of the three-dimensional Barkley model [17]. This is a two-variable activator-inhibitor model which has been widely used to study pattern forming systems like the BZ reaction and other reaction-diffusion systems [12, 14, 15, 21, 23]. In the presence of an external flux, the two coupled nonlinear differential equations take the following form [18–20],

$$\begin{aligned} \frac{\partial u}{\partial t} &= \frac{1}{\varepsilon}\left\{u(1-u)\left(u-\frac{v+b}{a}\right)\right\} - \nabla J_u, \\ \frac{\partial v}{\partial t} &= u - v - \nabla J_v. \end{aligned}$$

In the presence of diffusion alone, $J_u = -D_u \nabla u$, and $J_v = -D_v \nabla v$, where $D_u = 1.0$ and $D_v = 1.0$, are the diffusion coefficients. When an electric field is applied to the system, the fluxes modify as: $J_u = -D_u \nabla u + D_u z_u u E$, and $J_v = -D_v \nabla v + D_v z_v v E$, where E is the

strength of the applied electric field, and z_u and z_v are the charges on u and v, respectively [18]. The variables in the Barkley model, u and v, are loosely related to the concentrations of the bromous acid and the oxidized form of the indicator, ferroin, respectively. So, we consider $z_u = 0.0$ and $z_v = 3.0$. The values of the system parameters were chosen as $a = 0.84$, $b = 0.07$, and $\varepsilon = 0.02$. Under these conditions the filament of the scroll wave showed zero drift along the binormal direction.

The reaction system was modeled as a three dimensional lattice measuring $160 \times 160 \times 160$ grid points having zero flux boundaries for all diffusing species along the external boundaries. The obstacles were defined as spherical regions where the value of the variables u and v are zero. Neumann boundary conditions around these obstacles also yield identical results. The two partial differential equations were numerically integrated using explicit Euler integration scheme and a nineteen point Laplacian stencil with an integration time step of 0.012 and grid spacing of 0.35. The filament of the scroll is identified at regions having $u = 0.5$ and $v = a/2 - b$. The scroll wave is initiated similar to the experiment, by allowing a semi-spherical wave in the bottom half of the system, to curl up into the top half. The scroll is made large enough, so that its circular filament encompasses the geometry traced by the multiple obstacles. Over time, the filament shrinks and the scroll wave attaches to the obstacles. Once, it is stabilized around the obstacles, and shrinking ceases, the electric field is subsequently introduced numerically into the system.

For simulations which employ external thermal gradient, the flux of the species u (for v replace u by v) is given by, $J_u = -D_u \nabla u - D_{T_u} u(1-r_u)\nabla T$ [24]. Here, $D_{T_u} = D_u S_{T_0}/(1+k_s u)$ is the thermal diffusion coefficient of u where $S_{T_0} = -0.1$, is the Soret coefficient and $k_s = 1.0$, is a phenomenological constant. $r_u = u/c_T$, is the relative concentration of u, where $c_T = u + v$, and ∇T is the thermal gradient along the y-direction. The negative value of the Soret coefficient indicates the movement of the particles toward the hot end of the reaction chamber. The flux for v is similarly modified, with identical values of S_{T_0} and k_s.

We carried out numerical simulations for unpinning of scroll waves attached to multiple beads (two to six), arranged in regular geometries. The wave nature and filament dynamics of one such simulation is depicted in Fig. 4.7. This particular case is similar to the experiment illustrated in Figs. 4.4(a)-(c). The solid brown waves are the regions where the system is excited, or $v > 0.4$. For the purposes of better visualization, only the rear half of the wave form is shown. In Fig. 4.7(a), the semi spherical wave in the lower half of the cube is curling into the top half, while the filament is attached to all the four beads. The electric field is applied at this stage, in the direction of the y-axis. The filament starts flipping perpendicular to this direction, as is seen from the separation of the same into red and blue portions. Subsequently, the filament detaches from the two beads further away from the anode [Fig. 4.7(b)]. Since these beads are equidistant from, and nearest to the cathode, the scroll detaches from them simultaneously. The scroll ring keeps on reorienting, as it moves in the direction opposite to the electric field [Fig. 4.7(c)]. Finally it unpins from the

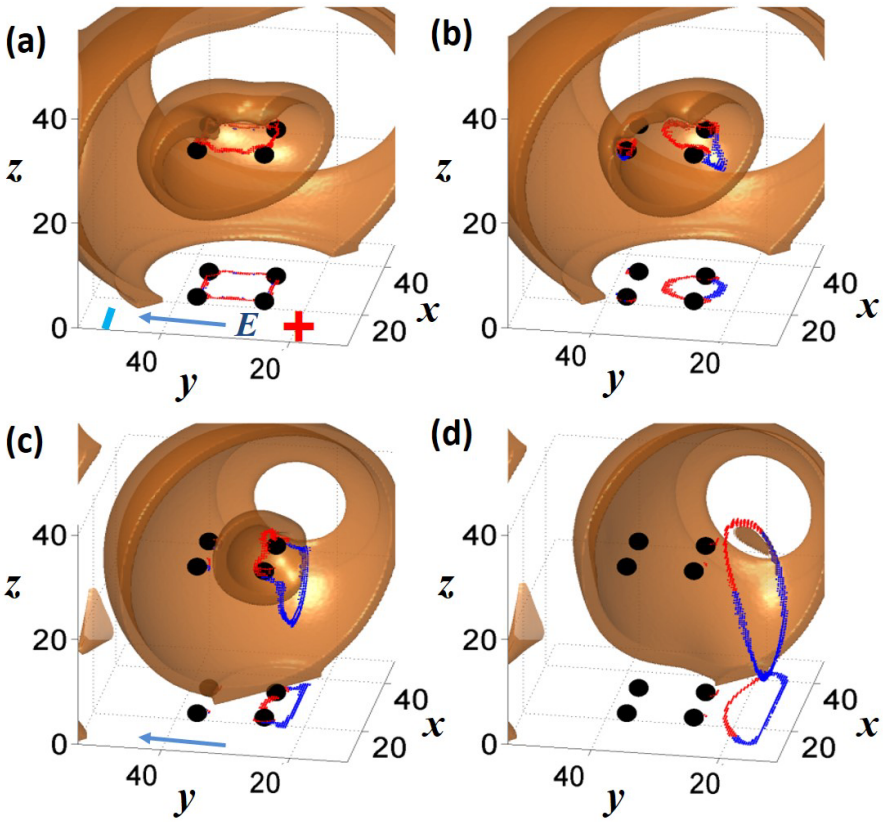

Fig. 4.7: Wave and filament dynamics of unpinning in the Barkley model. (a)-(d) The time evolution of the scroll wave (solid brown areas) and its filament (curves) which is initially pinned to four obstacles. The spherical obstacles (of diameter 2.8 space units, placed 10.5 space units apart) are designated as black balls. The sections of the filament above the plane containing the obstacles are indicated in red, while those below the plane, are drawn in blue. The curves along with the circles at the bottom of the box are the two-dimensional projections of the filament and the obstacles. (a) Shows the system before the application of electric field, $E = 0.05$ units. The time intervals between neighboring frames are 40.3, 34.1 and 40.8 time units, respectively. The computed volume has been cropped along the boundaries.

remaining two beads [Fig. 4.7(d)], and becomes almost parallel to the z-axis. After this, if the electric field is turned off, the free scroll wave will shrink due to its positive filament tension and disappear. The only difference between this simulation and the experiment in Figs. 4.4(a)-(c), is that, in the latter case there is no visible expansion of the waves after it has detached from all the beads. In the case of the simulation, the field strength can be reduced so as to achieve complete unpinning of the vortex, while avoiding any expansion of the filament. As is evident from the experiments, the bead size and inter-bead distance will also play an important role in this.

Figure 4.8 shows the results of simulation for the experimental case depicted in Figs. 4.5(e)-(h). We show only the filament dynamics in this case. Similar to the experiments, the filament detaches first from the bead furthest from the anode, i.e. the lone bead lying towards the extreme left along the y-axis. Then it unpins simultaneously from the next two

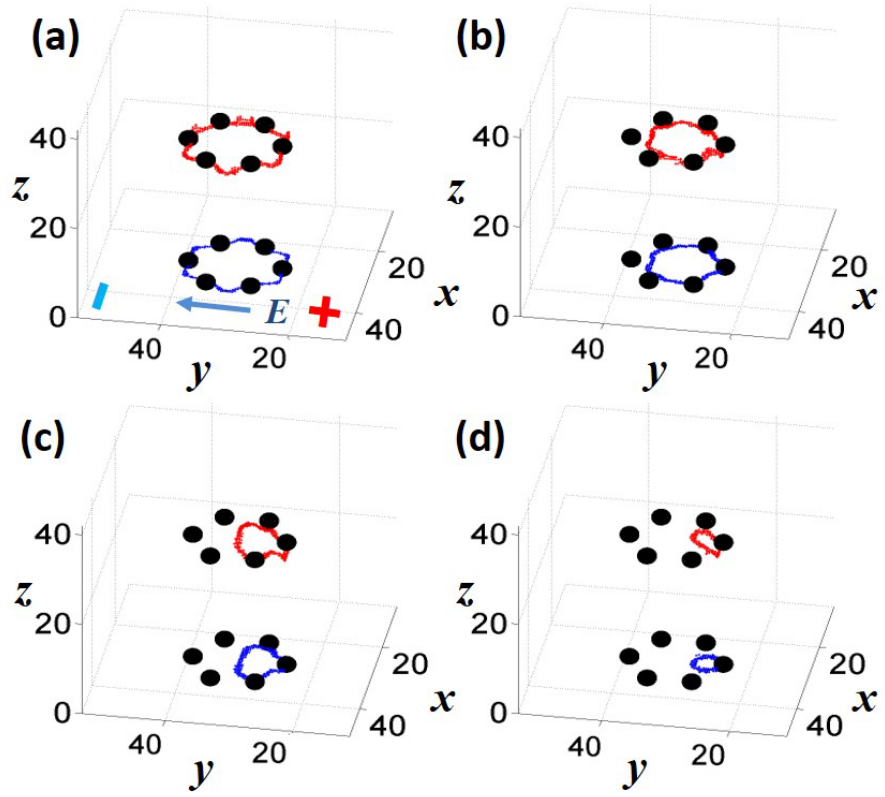

Fig. 4.8: Unpinning of a scroll wave attached to six obstacles arranged hexagonally. The (red) curves are the filaments, and the (black) spheres are the obstacles (of diameter 2.1 space units, placed 7.2 space units apart). The two-dimensional projections of the filaments are shown at the bottom of the box ($z = 0$). The electric field ($E = 0.05$ units) is applied in the y-direction. (a) Stable filament attached to the six beads, before the application of electric field. (b)-(d) sequential unpinning of the filament from the six beads. 22.6, 25.5 and 20.2 time units, respectively have elapsed between neighboring frames. The computed volume has been cropped along the boundaries.

beads, which are equidistant from the anode [Fig. 4.8(b)]. At this stage, a slight flipping of the ring in the z-direction, is visible. The filament then detaches from the next two beads, and shrinks in the vicinity of the last bead, in the extreme right along the y-axis, which is nearest the anode [Fig. 4.8(d)]. The results for the other orientation of six beads are shown in Fig. 4.9. Here the pinned wave unpins in three steps, during each of which unpinning occurs from two beads simultaneously. Considerable expansion of the filament occurs after it gets detached from all the beads.

We also carried out simulations for the case where four beads are placed identical to the experiment in Fig. 4.4(d). The simulations exactly mimicked the experiments. The results of the simulations for a scroll wave pinned to two, three and five beads, also yielded expected results.

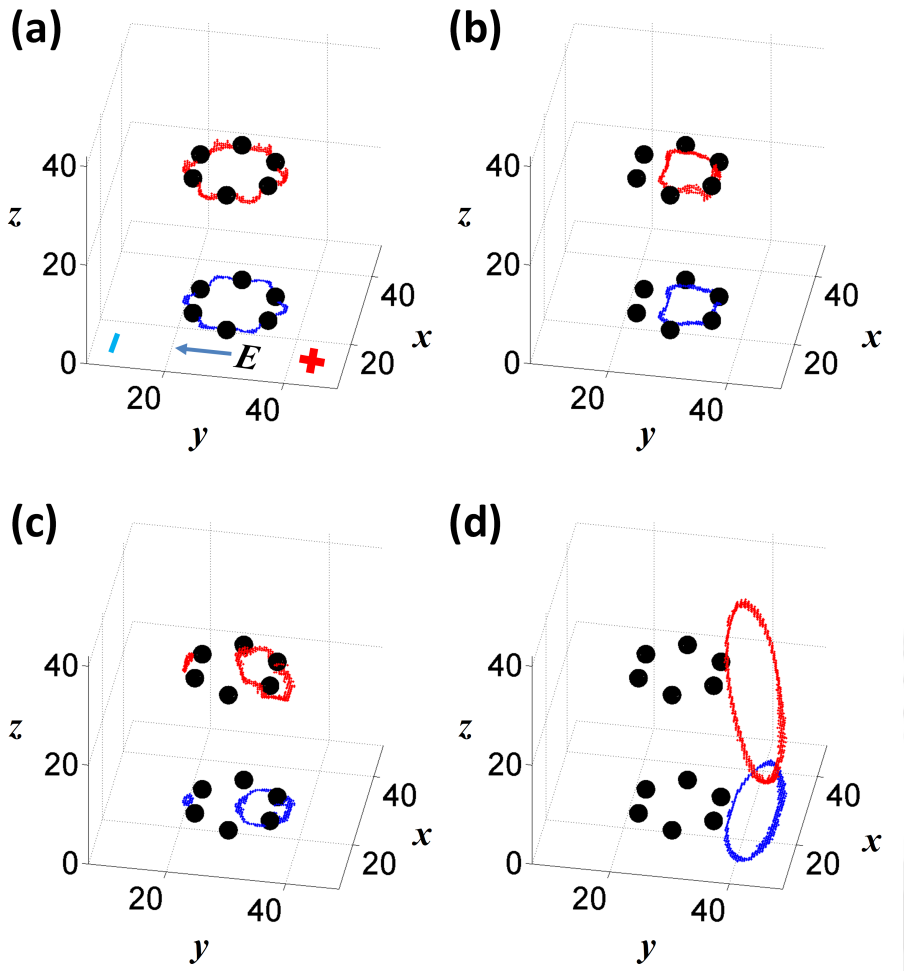

Fig. 4.9: Unpinning of a scroll wave attached to six obstacles arranged hexagonally. The (red) curves are the filaments, and the (black) spheres are the obstacles (of diameter 2.1 space units, placed 7.2 space units apart). The two-dimensional projections of the filaments are shown at the bottom of the box ($z = 0$).The electric field ($E = 0.05$ units) is applied in the y-direction. (a) Stable filament attached to the six beads, before the application of electric field. (b)-(d) sequential unpinning of the filament from the six beads. 32.6, 14.5 and 71.4 time units, respectively have elapsed between neighboring frames. The computed volume has been cropped along the boundaries.

4.5 Discussions and Conclusions

With our experiments and numerical simulations, we have shown that scroll rings can be stably pinned to multiple heterogeneities. Such pinned vortices can also be sequentially unpinned by the application of controlled external gradients. Electric field and thermal gradients have been used in our experiments for this purpose. Scroll waves pinned at three to six sites, were successfully unpinned by these methods. The experiments with electric fields can be more easily controlled, and hence give better results, and show several interesting trends. As we increased the number of pinning sites, we had to apply stronger electric fields for the successful unpinning of the waves. This also suggests that more the number of pinning sites, greater is the stability of the pinned structure. However, the rela-

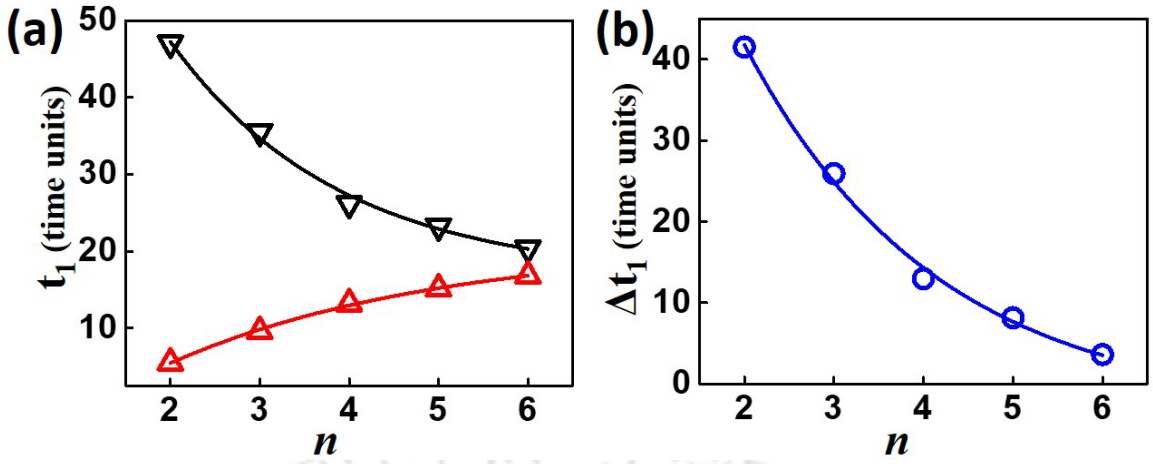

Fig. 4.10: Variation of unpinning time, with number of beads. (a) First unpinning time, t_1, as a function of the number of beads, n. The (black) upturned triangles are for the orientations, where the scroll unpins from two beads simultaneously [eg. Figs. 1(g), 3(a) and 4(e)]. The (red) triangles are for the orientations, where the filament initially detaches from only one bead [eg. Figs. 4.1(a), 4.4(d) and 4.5(a)]. (b) The difference between the first unpinning times, Δt_1, for the two different orientations in (a), as a function of n. The diameter of the obstacles are 3.5 space units in each case, and they are placed 10.5 space units apart. The applied electric field strength is 0.075 units.

tionship is not so simple, as it also depends on the size of the scroll wave, and hence the tension and rigidity of the filament sections between neighboring beads.

One very interesting observation could be made on the unpinning times of the scroll wave filament from different number of beads. Figure 7 illustrates this trend in the results of the numerical simulations. The first unpinning time, t_1, decreases rapidly as the number of beads increase, for those orientations where the scroll detaches from two beads simultaneously [Fig.4.10(a)]. While the nature of change is opposite when it detaches from a single bead at first. The difference in these two unpinning values, Δt_1, is again a decreasing function of the number of beads [Fig. 4.10(b)]. The drop in Δt_1 values with increasing n could be due to the change in the final geometry of the pinned filament. A closed filament stably pinned to n beads could be thought of as consisting of n filament sections. For a regular geometry of beads, the arclength of these n filament sections are equal. As we change the orientation of a pinned filament with respect to the gradient, the time required for the first unpinning changes. When the filament unpins from two beads simultaneously, the time taken is appreciably more than that which is required to unpin from only one bead. However, as the number of pins increases, the gap between these two times decreases. When the number of obstacles is small, the difference is most evident. For example, when $n = 2$, unpinning from two beads simultaneously would mean unpinning of the entire scroll wave filament. On the other hand, while unpinning from one bead, the filament is still pinned at half the initial number of pins. As n becomes large, the filament is anchored at many points even after it has unpinned from one or two beads. For $n = 4$, the filament is pinned at two

beads in the first scenario, as compared to three in the second [Fig. 4.4]. And when $n = 6$, the ratio of pins is 4:5 after the first unpinning [Fig. 4.5]. As the number of beads increases, the change in the shape of the filament after the first unpinning from just one pinning site, differs lesser and lesser from that when unpinning occurs from two sites simultaneously. As a result, the term Δt_1 falls off with increase in the value of n. No such definite tendency could be extracted from the results of the experiments, because the electric field strength had to be increased as we increase the number of beads. Hence, we do not have enough data to get an exact comparison of t_1 with n (for a constant value of E). Nevertheless, the qualitative plot generated from the available experimental results show a similar trend in the values of t_1 and Δt_1 [Fig. 4.11].

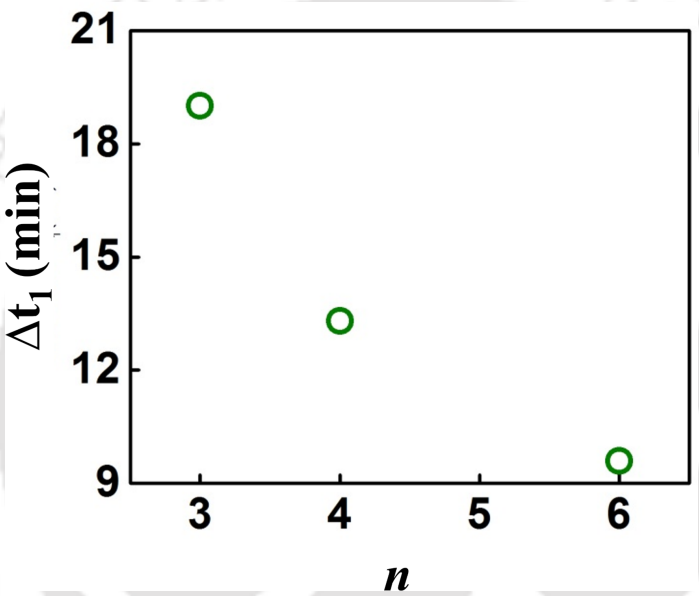

Fig. 4.11: The difference between the first unpinning times, t_1, for the two different orientations of the beads as a function of n in experiments. The diameter of the beads are 0.183 cm, 0.216 cm and 0.216 cm, while the electric field applied is 0.25 V cm^{-1}, 0.50 V cm^{-1}, and 1.0 V cm^{-1} for $n = 3$, 4, and 6, respectively.

Future experiments could be designed to study the unpinning of scroll waves anchored to differently shaped heterogeneities, like rods, disks and rings. Again, short electric pulses could be used for unpinning instead of using a continuous electric field. This may help alienate the expansion of the filament under the influence of strong electric fields. Other interesting variations could be changing the nature of the obstacles. Such modifications will shed more light on the dynamics of filaments occurring in natural systems, like cardiac tissues.

BIBLIOGRAPHY

[1] F. Seigert and C. J.Weijer, Proc. Natl. Acad. Sci. USA **89**, 6433 (1992).

[2] S. J. Schiff, X. Y. Huang, and J. Y. Wu, Phys. Rev. Lett. **98**, 178102 (2007).

[3] N. A. Gorelova and J. Bures, J. Neurobiol. **14**, 353 (1983).

[4] J. M. Davidenko, A. M. Pertsov, R. Salomonsz, W. Baxter, and J. Jalife, Nature (London) **355**, 349 (1992).

[5] P. Wiegmann and A. G. Abanov, Phys. Rev. Lett. **113**, 034501 (2014).

[6] I. Chuang, R. Durrer, N. Turok, and B. Yurke, Science **251**, 1336 (1991).

[7] A. Kamada, M. Kaplinghat, A. B. Pace, and H.-B. Yu, Phys. Rev. Lett. **119**, 111102 (2017).

[8] J. Jalife, M. Delmar, J. Anumonwo, O. Berenfeld, and J. Kalifa, *Basic cardiac electrophysiology for the clinician* (Wiley-Blackwell, Oxford, UK, second edition 2009).

[9] S. Nettesheim, A. von Oertzen, H. H. Rotermund, and G. Ertl, J. Chem. Phys. **98**, 9977 (1993).

[10] A. Pertsov, E. Ermakova, and A. Panfilov, Physica (Amsterdam) **14D**, 117 (1984).

[11] J. P. Keener and J. J. Tyson, SIAM Review, **34**, 1 (1992).

[12] I. R. Epstein and J. A. Pojman, *An introduction to nonlinear chemical dynamics* (Oxford University Press, Oxford 1998).

[13] Z. A. Jiméenez and O. Steinbock, Phys. Rev. Lett. **109**, 098301 (2012).

[14] S. Dutta and O. Steinbock, J. Phys. Chem. Lett. **2**, 945 (2011)

[15] D. Mahanta, S. Dutta, and O. Steinbock, Phys. Rev. E **95**, 032204 (2017).

[16] C. Luengviriya, S. C. Müller, and M. J. B. Hauser, Phys. Rev. E **77**, 015201(R) (2008).

[17] M. Vinson, S. Mironov, S. Mulvey, and A. Pertsov, Nature (London) **386**, 477 (1997).

[18] N. P. Das and S. Dutta, Phys. Rev. E **96**, 022206 (2017).

[19] N. P. Das, D. Mahanta, and S. Dutta, Phys. Rev. E **90**, 022916 (2014).

[20] Z. A. Jiménez, Z. Zhang, and O. Steinbock, Phys. Rev. E **88**, 052918 (2013).

[21] E. Nakouzi, Z. A. Jiménez, V. N. Biktashev, and O. Steinbock, Phys. Rev. E **89**, 042902 (2014).

[22] D. Barkley, Physica D **49**, 61 (1991).

[23] A. T. Winfree, R. Kapral, and K. Showalter, *Chemical Waves and Patterns* (Springer, Netherlands 1995).

[24] S. Dutta and D. S. Ray, Phys. Rev. E **75**, 066206 (2007).

Chapter 5

RECONNECTION OF MULTIPLE SCROLL RINGS

5. RECONNECTION OF MULTIPLE SCROLL RINGS

5.1 Introduction

Chemical waves have been the subjects of extensive theoretical and experimental investigations in the recent decades as they form an integral part of nonlinear phenomena occurring far from thermodynamic equilibrium. Specific chemical reactions coupled with diffusion give rise to waves and patterns, similar to those widely encountered in numerous systems spreading across biology, physics, ecology, sociology, economics, medicine and many other disciplines [1,2]. Two dimensional spirals and their three dimensional analogues, known as scroll waves [3], arise in excitable chemical media as well as in biological systems such as chicken retina [4], mammalian neocortex [5], frog oocytes [6], colonies of *Dictyostelium discoideum* [7], and myocardium of the heart [8]. The propagation of these waves in the heart tissue has been suggested to be linked with abnormal cardiac rhythms, a condition referred to as cardiac arrhythmia . Some of the cardiac arrhythmias are life threatening and may even lead to death of the patient within minutes [9, 10]. The studies of spiral and scroll waves in chemical media are often motivated by their occurrence in the heart and these chemical systems, especially the Belousov Zhabotinsky system, have proved extremely useful as the simplest models of wave propagation in cardiac tissue [11]. Extensive numerical and analytical work on scroll wave dynamics have been reported since 1980s [12, 13]. However, these three dimensional vortices are relatively less explored in experimental systems, perhaps due to the difficulties in visualizing the actual dynamics in the interior of a thick system.

Scroll waves are three dimensional waves that rotate around one dimensional curves called filaments [5]. The dynamics of these vortices are much more complicated than that of their two dimensional counterparts. Even in the same excitable medium, the dynamics of scroll waves may vary depending on the configurations of their respective filaments [15]. This makes the study of scroll wave interaction extremely interesting, which may reveal crucial information regarding the propagation and control of reentrant waves in the myocardial tissue. Although the interaction of spiral waves in 2D systems is a well studied phenomenon [16–19], there have been very few experimental demonstrations involving scroll waves interacting among themselves and this area still remains understudied. The interaction between a pair of parallel scroll waves was investigated in detail using optical tomography technique by Hauser and coworkers in 2013 [20]. In another recent study, Das *et al.* reported how the interaction between a pair of scroll rings having circular filaments may lead to either reconnection or repulsion depending on whether they have the same

or opposite sense of rotation [21]. This was the first ever experimental demonstration of scroll wave reconnection, where they showed that two scrolls placed side by side in the same plane can reconnect when their filaments lie within one core length of each other [21]. However, if the initial waves are too close to one another, they merge to form a single scroll wave. In contrast when the distance between the filaments is more than a core length, two independent scroll rings emerge, whose interfilament distances go on increasing as they shrink with time. Thus the filaments can reconnect only within a very specific range of initial wave distances. Motivated by this work, we have carried out a detailed investigation on the interaction of multiple coplanar scroll rings placed in close vicinity of one another. We show that within the specific range of inter wave distances, the scrolls reconnect to form filaments of complex geometries. The filaments then undergo reshaping over time and shrink under a medium-specific positive filament tension. Early theoretical works on scroll waves suggest that any non-intersecting closed curve of arbitrary shape evolves towards a circle and disappears in finite time [22, 23]. It has been established by these mathematical studies that temporal evolution of a filament occurs according to local speeds that are functions of the local curvatures:

$$\frac{d\mathbf{s}}{dt} = \alpha\kappa\hat{\mathbf{N}} \tag{5.1}$$

where $\mathbf{s}$ is the one-dimensional curve, α describes a system-specific constant line tension, κ is the local curvature, and $\hat{\mathbf{N}}$ denotes the curve's unit normal vector [13]. When α is positive we say the filament has positive tension and it shrinks with time. This is seen in the case of the BZ scroll wave. If α is negative, the scroll would evolve as an expanding circle.

In this chapter, we aim to explore the dynamics of the reconnected filaments in detail. We carried out experiments to study the interaction of three to six scroll waves. By changing the arrangement of the scroll rings, for a particular number of interacting filaments, we investigate the change in the properties of the resulting reconnected filaments of varying geometry. Further numerical studies have been performed using the Barkley model that sheds light on the reconnection and the detailed dynamics of the resulting filaments.

5.2 Experimental Methods

We used the gel immobilized ferroin catalyzed BZ reaction for our experimental work. The reaction was carried out in a Petri dish using two BZ gel layers. Each layer had a thickness of 4 mm. The concentrations of all the chemicals were identical in both the gel layers containing 0.8% (w/v) Agar. The initial concentrations of the reactants were $[NaBrO_3]$ = 0.04 M, $[CH_2(COOH)_2]$ = 0.04 M, $[H_2SO_4]$ = 0.16 M, and $[Fe(o\text{-}phen)_3SO_4]$ = 0.5 mM. In this concentration range the scroll waves have positive filament tension [24] which implies gradual shrinkage of free scroll rings and disappearance in finite time. Every solution and

gel was prepared in ultra-pure water with a resistivity of 18.2 MΩ cm. All experiments were carried out at room temperature (22±1 °C).

For our experiments to study reconnection of n number of scroll waves ($n \geq 3$), the tips of equal number of clean silver wires of diameter 0.5 mm each were simultaneously inserted into the bottom gel layer for a few seconds. It led to the creation of n expanding chemical waves by decreasing the local concentration of the inhibitor bromide ion. When the waves reached the desired dimensions, the second layer was poured over the first. Special care was taken so that the distances between any two neighbouring waves were identical and within the range where reconnection can occur [21]. Subsequently, the rim of the waves curled into the upper gel layer and gave rise to n number of scroll waves. The system was illuminated by a cold white light from below. The reaction was monitored with a charge coupled device (CCD) camera equipped with a blue dichroic filter mounted above the Petri dish. Top view of the reaction chamber (640×480 pixels) was recorded at 2 s intervals. The resulting time lapse images were finally analyzed using in-house MATLAB scripts.

5.3 Experimental Results

Fig. 5.1 shows the result of a typical experiment, where three independent scroll rings placed side by side reconnect. In Fig 5.1(a-d), top view of the experiment are shown during the first four rotations of the scrolls. The corresponding filaments reconstructed with the help of a MATLAB code are shown in the second column (e-h). The intense black curves represent the filament. The scrolls undergo one rotation individually [Fig. 5.1(a)], and reconnect at two points during the next cycle of rotation Fig. 5.1(b). The three independent circular filaments are seen in Fig. 5.1(e), which attract each other and merge to form one large filament in Fig. 5.1(f). After reconnection the bottle necks in the newly formed filament start to expand slowly [Fig. 5.1(c,d,g,h)] and the filament acquires a hot-dog like shape.

Result of another experiment with same number of scroll rings, generated in a different arrangement, is seen in Fig. 5.2. Here two of the circular waves are too close in the beginning of their formation and hence they form a single dumbbell shaped scroll, which then reconnects with the remaining one in two consecutive steps. The pair of disconnected scrolls (large dumbbell shaped one and smaller circular one) seen in Fig. 5.2(a,e) attract each other at two points [as in Fig. 5.2(f)]. Reconnection occurs on one side (left in the picture) during the second rotation [Fig. 5.2(c,g)] while they continue to attract each other at the other point of nearest approach. Finally they merge at that point (right side in picture) forming a club shaped filament.

The initial conditions of the experiments corresponding to Fig. 5.1 and Fig. 5.2 are shown in Fig. 5.3(a) and Fig. 5.3(b) respectively. The initial wave diameters (d_0) are in the range of 9.1-10.2 mm. The values indicate that in both experiments, the initial interfilament

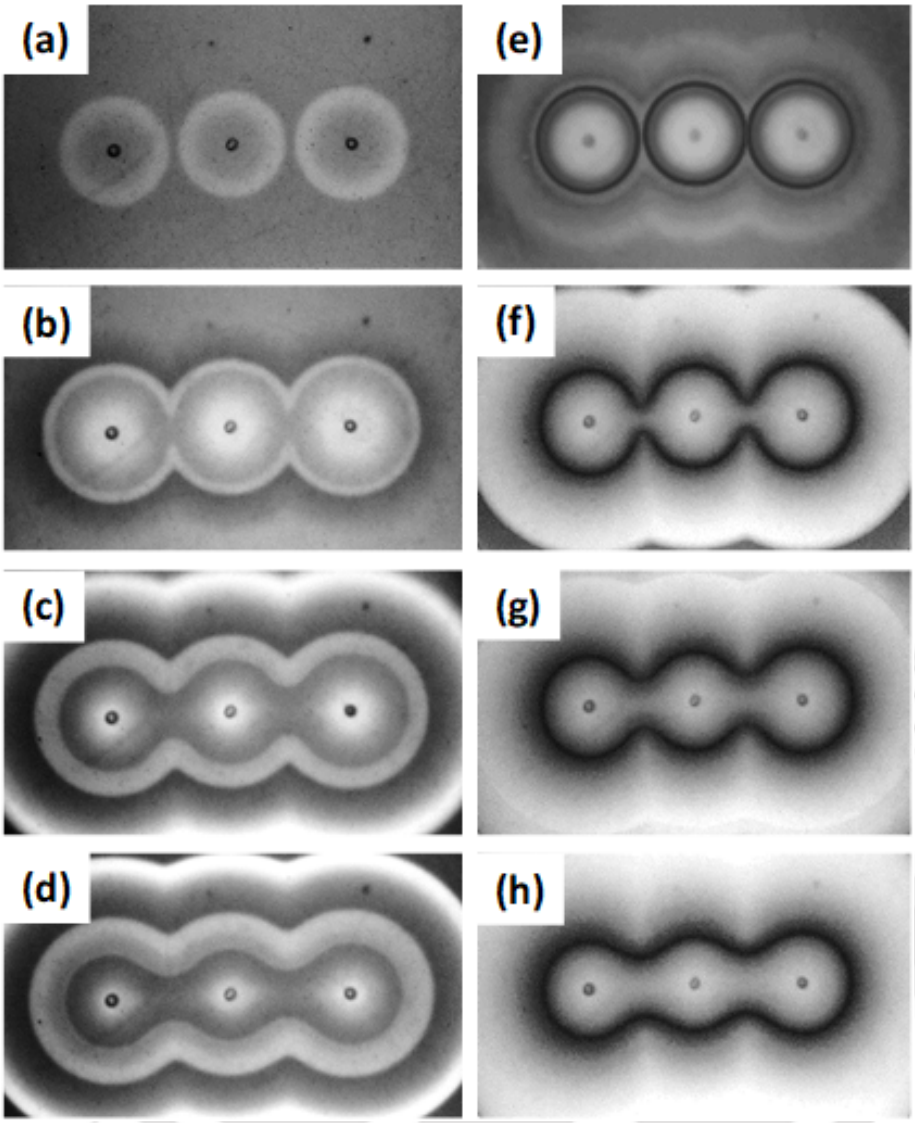

Fig. 5.1: Reconnection of three scroll waves generated in a linear fashion: (a-d) show the top view of the reaction chamber at time intervals of 7 min.(e-h) are the reconstructed filaments corresponding to the snapshots in the left column. Area of each snapshot is 3.4 cm $\times$ 2.3 cm.

separation (Z_0) of the reconnecting scrolls are less than or equal to 1.1 mm. This is in agreement with an earlier study on reconnection of two vortices [21].

In the aforementioned experiments, we monitored the filament dynamics for prolonged durations. It has been observed that after the reconnection takes place, the large reconnected filament undergoes curvature dependent motion, like any other closed filament, and finally acquires a shape conserving geometry [17]. For the experiment shown in Fig. 5.1, the filaments will form a hotdog, which is like two fused hairpins. It has been shown that hairpin shaped vortices show shape-conserving steady motion. Similarly, this hotdog-shaped filament will shrink according to Eq. 5.1, while preserving its shape, until it becomes a circle and finally disappears. Any series of reconnected scroll rings placed side-by-side will show the same nature of shrinkage. The filament in Fig. 5.2 will acquire circular shape much faster and will eventually continue shrinking as a circle.

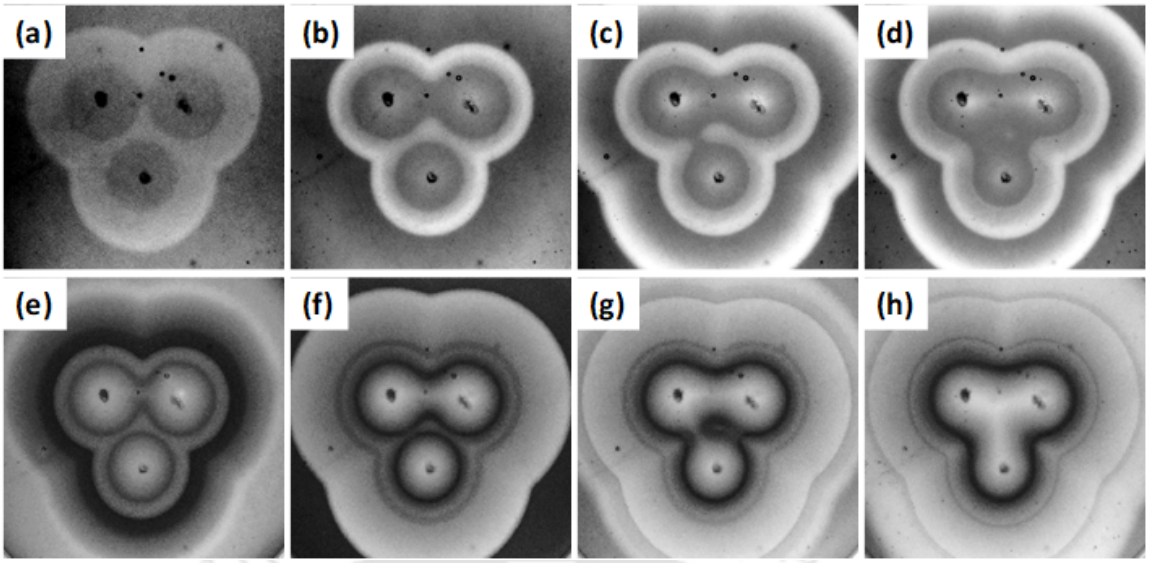

Fig. 5.2: Reconnection of three scroll waves generated in an angular fashion: (a-d) show the top view of the experiment at an interval of 7 min. The black curves in (e-h) are reconstructed filaments corresponding to the snapshots above them. The area of each snapshot is 3.3 cm $\times$ 3.1 cm.

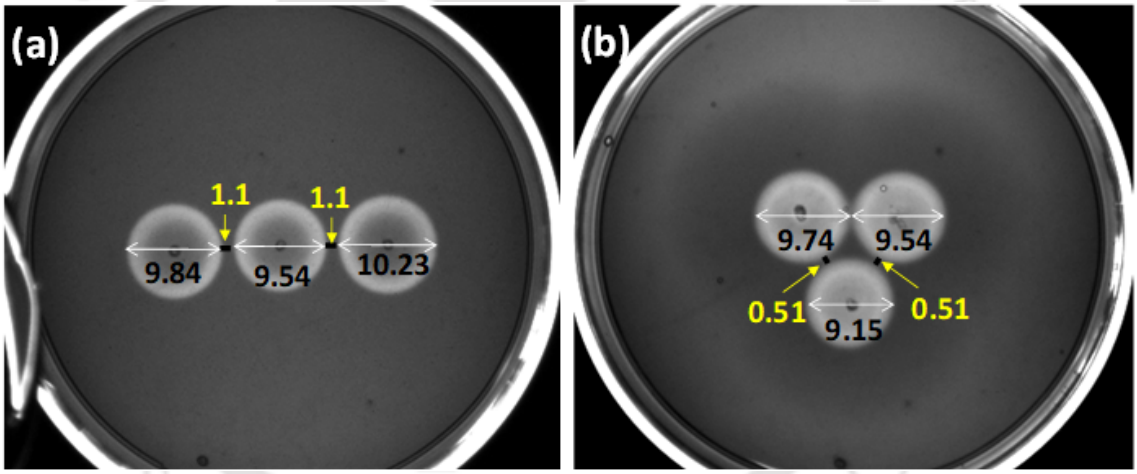

Fig. 5.3: Initial conditions of two experiments involving three scroll waves each. The waves are generated in (a) a linear arrangement and (b) an angular fashion. Both the snapshots show the top view of the entire Petri dish where the reactions were carried out. The snapshots are recorded at the moment when the second gel layer is poured into the reaction chamber. The rim of the beaker used to pour the pre-gel solution is seen on the left side in (a). The initial semi-spherical waves appear as white circles in the snapshots. The initial ring diameters (d_0) are written in black below each circle. The values written in yellow represent the initial interwave separation (Z_0) distances. All the values are in mm. The units have been omitted due to insufficient space available within the central area.

In order to compare the dynamics of the reconnected filaments in these two experiments, we used an in house MATLAB code to monitor the area enclosed by the filament with passing time. We extracted several (50-70) points on the filaments and computed the area enclosed by these closed curves. Fig. 5.4 shows the plots of enclosed area versus time for experiments similar to Fig. 5.1 and Fig. 5.2. In the first case [Fig. 5.4(a)], which involves a linear arrangement of the reconnecting vortices, the enclosed area decreases al-

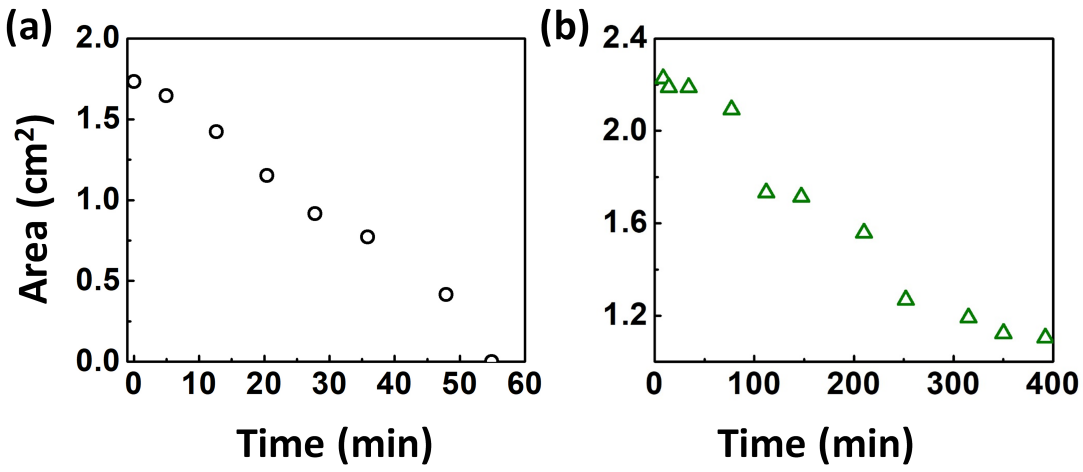

Fig. 5.4: Enclosed Area vs. time plot: the area enclosed by the filament is calculated and plotted after definite intervals for (a) linear arrangement and (b)triangular arrangement of three scrolls (experiments). Initial size of the scroll in (b) is much higher than that in (a). The filament in (a) shrinks and disappears within 55 mins, while in (b) the large reconnected filament pins to CO_2 bubbles after sometime and the area does not decrease further.

most linearly with time until it falls suddenly towards the end. In this case the lifetime of the reconnected scroll was found to be 55 minutes. On the other hand, in case of the triangular configuration [Fig. 5.4(b)], the area decreases in a not-so-linear fashion. The initial area of this filament is much higher as compared to its linear counterpart [Fig. 5.4(a)]. This also creates further complications, as the large filament eventually gets attached to CO_2 bubbles formed in the reaction. After around 5 hours (300 minutes) the decrease in the filament area slows down due to this. The lifetime of a completely pinned scroll can theoretically become infinite and in experiments the pinned scroll retains its size until the end of the reaction, ie. when all the reactants get depleted. This is a hurdle in ascertaining the actual lifetime of the filament.

Next we made an attempt to study the interaction of an increased number of scrolls. We will discuss here an experiment with six scroll rings generated close to one another. The initial distances along with initial wave diameter values are summarized in Fig. 5.5. Fig. 5.6 shows the result of the experiment. It is seen that all of them undergo one rotation individually [Fig. 5.6(a,e)], during the following rotations five of them reconnect, and one continues to rotate independently. It is clearly revealed by Fig. 5.5 that the Z_0 values along all sides are much greater for this scroll, and hence lie beyond the range in which reconnection can occur. The reconnection of the five scroll rings leads to the formation of one large filament having a complex geometry. Additionally, a small circular filament [Fig. 5.6(g)] is also formed inside this large scroll. This circular filament, due to its small size, rapidly shrinks and disappears very quickly [Fig. 5.6(j)]. The large ring diminishes slowly with a smoothening of its geometry.

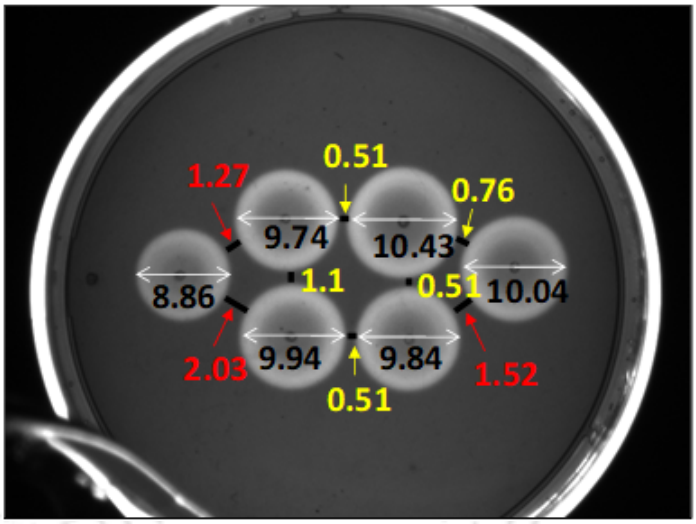

Fig. 5.5: Initial condition of an experiment involving six scroll waves. The snapshot shows the top view of the entire Petri dish at the moment when the second gel layer was poured into the reaction chamber. The initial semi-spherical waves appear as white circles in the snapshot. The d_0 values are written in black inside each circle. The values written in yellow represent the inter wave separation (Z_0), for which reconnection has occured. In contrast, wherever reconnection has not been observed, the Z_0 values are shown in red. indicated by the arrows. All the values are in the unit of mm. The units have been omitted due to insufficient space available within the central area.

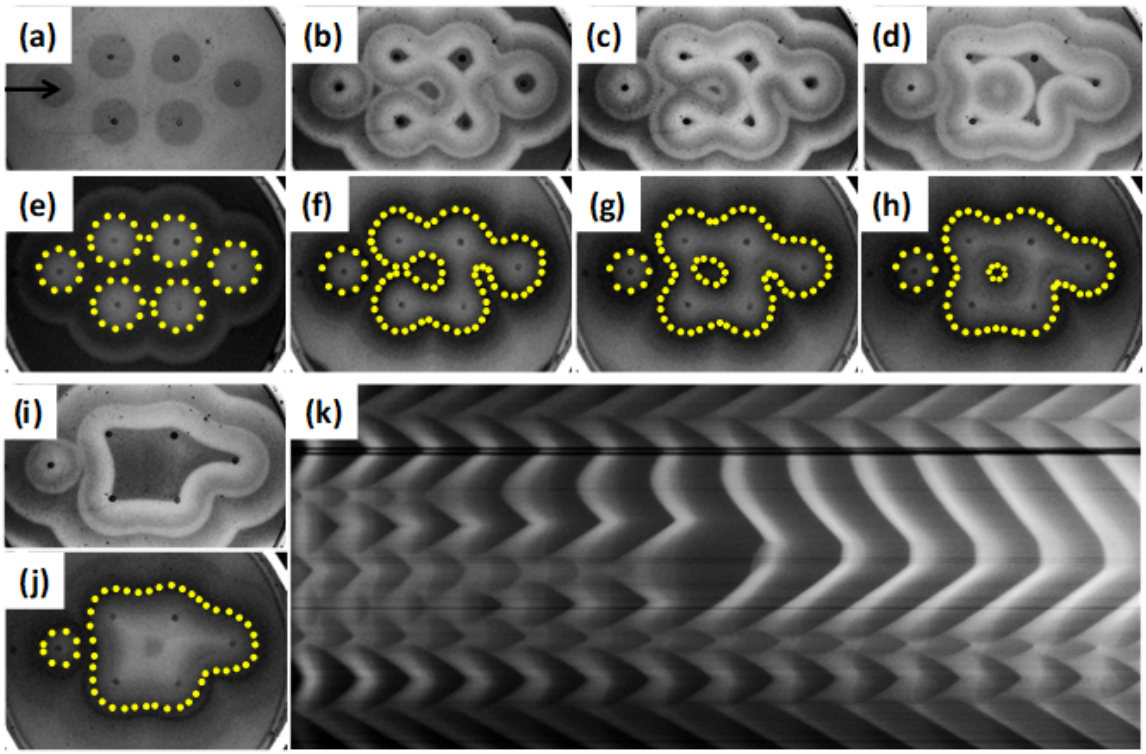

Fig. 5.6: Interaction of six scroll waves. (a, b, c, d, i) Top view of the experiment. (e, f, g, h, j) Show the reconstructed filaments, corresponding to the snapshots above them, as yellow dotted lines. Time interval between two neighboring frames are 14 min, 7 min, 14 min and 14 min. (k) Time space plot constructed along the black arrow in (a). Here, x (space) increase from bottom to top and t (time) increases horizontally from left to right.

5.4 Model and Simulation Methods

Numerical simulations were performed with the two variable Barkley model [17]. This simple model involving an activator u and inhibitor v is given by the reaction-diffusion equations 5.2 and 5.3:

$$\frac{\partial u}{\partial t} = \frac{1}{\varepsilon}\left\{u(1-u)\left(u-\frac{v+b}{a}\right)\right\}+D_u\nabla^2 u, \tag{5.2}$$

$$\frac{\partial v}{\partial t} = u-v+D_v\nabla^2 v. \tag{5.3}$$

The fast variable u and the slow variable v qualitatively describe the concentrations of $HBrO_2$ and ferroin, respectively. The reaction system is modelled as a three dimensional lattice measuring 800$\times$ 800 $\times$ 150 grid points having zero flux boundaries for all diffusing species. The two partial differential equations were numerically integrated using explicit Euler scheme and a nineteen point Laplacian stencil. The integration time step was kept constant at 0.012. The three dimensional lattice had a grid spacing of 0.35. The values of system parameters were a = 0.84, b = 0.07, ε =0.02 and the diffusion coefficients $D_u = D_v$ = 1.0. This set of parameters were chosen because it showed negligible drift of the scroll in binormal direction and positive filament tension. The filament of the scroll wave was identified as regions where $u = 0.5$ and $v = a/2 - b$.

5.5 Simulation Results

Figure 5.7 shows the results obtained from a typical simulation. It illustrates the evolution of a reconnected wave pattern from three independent scroll waves. The initiation process of the scrolls in the numerical simulations with the Barkley model was similar to the initial experimental condition. In the experiments, after pouring the top gel layer a semi-spherical wave already created in the lower gel layer started to curl in to the upper gel layer and it resulted in the formation of the scroll ring. Similarly in simulations, uniformly distributed semi-spherical waves were created by erasing the upper halves of required number of expanding spheres having high concentrations of the activator u. In this simulation, three waves have been generated in such a way that their centres lie along a straight line. At the moment when they started curling in, each wave has a diameter of 35.7 space units and distance between the neighbouring waves are 4.1 space units each. Initially they give rise to three independent scroll rings with circular filaments. This is seen in Fig. 5.7(a). The filaments are sufficiently close to interact with each other and with time they begin to attract. Fig. 5.7(b) shows the attraction taking place between the neighbouring filaments at the points of nearest approach. They eventually reconnect at these two points and give rise to a single large filament [Fig. 5.7(c)]. The newly formed huge filament then undergoes curvature dependent motion [Fig. 5.7(d)].

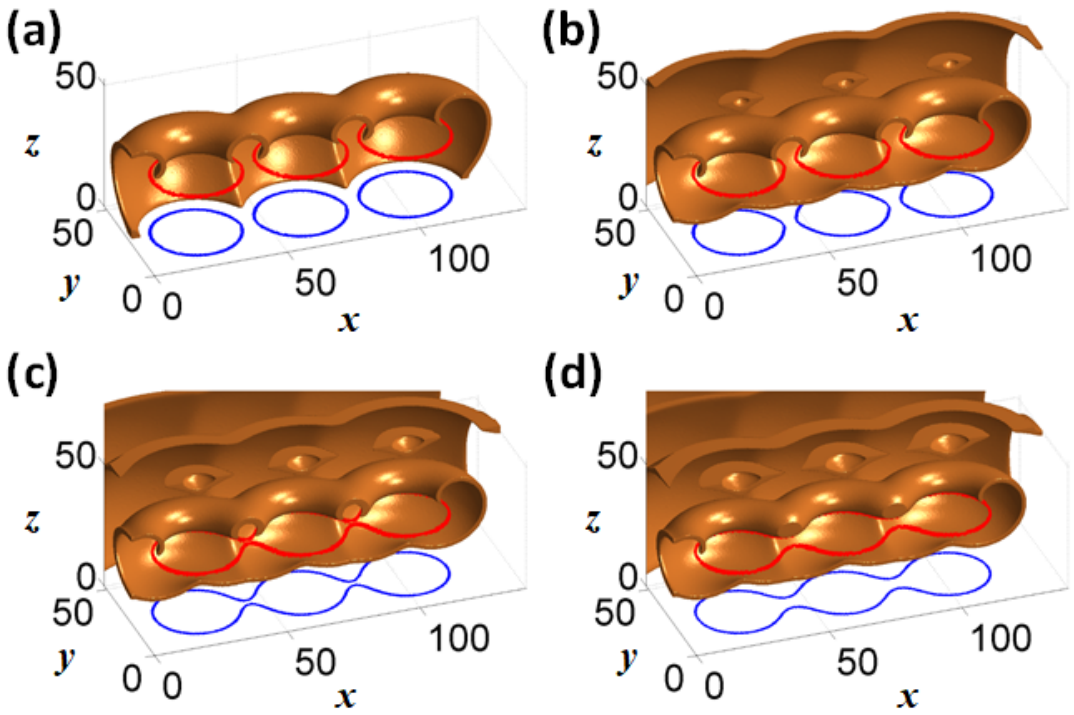

Fig. 5.7: Numerical simulation of the reconnection of three scroll waves arranged in a linear fashion. The wave patterns are seen as solid brown areas. The red curves are the filaments. The two-dimensional projections of the filaments are shown in blue at the bottom of the box ($z = 0$). Time interval between each pair of successive frames is 5.4 time units. The computed volume has been cropped along the boundaries.

We carried out numerical simulations for two other arrangements of three scroll waves. In one of them the scrolls are generated in a triangular fashion, equidistant from one another, like in the Fig. 5.2. Figure 5.8 depicts the filament dynamics during the first eight rotations of the scrolls. Initially the three scroll waves start rotating individually around their own circular filaments. Even though there is considerable attraction among them at three points [Fig. 5.8(a)], they continue to rotate separately [Fig. 5.8(b)]. As seen in figure Fig. 5.8(c), reconnection occurs at two of the three points of contact during the third rotation. In Fig. 5.8(d), the three waves get reconnected at all the three points of nearest approach with the formation of a small closed filament inside the large reconnected filament. As both these filaments undergo curvature dependent motion, the tiny circular filament rapidly shrinks in size [Fig. 5.8(d-g)] and quickly disappears [Fig. 5.8(h)]. This is exactly similar to the experimental results observed in [Fig. 5.2].

Simulation results have revealed that different configurations of same number of scroll rings having same initial size (d_0) and separation distance (Z_0) take considerably different time durations to shrink and disappear. It is evident from the time space plots in Fig. 5.9. Both the time space plots have been constructed for same time duration. However, in the first case [Fig. 5.9(a)], the reconnected scroll collapses in visibly less time.

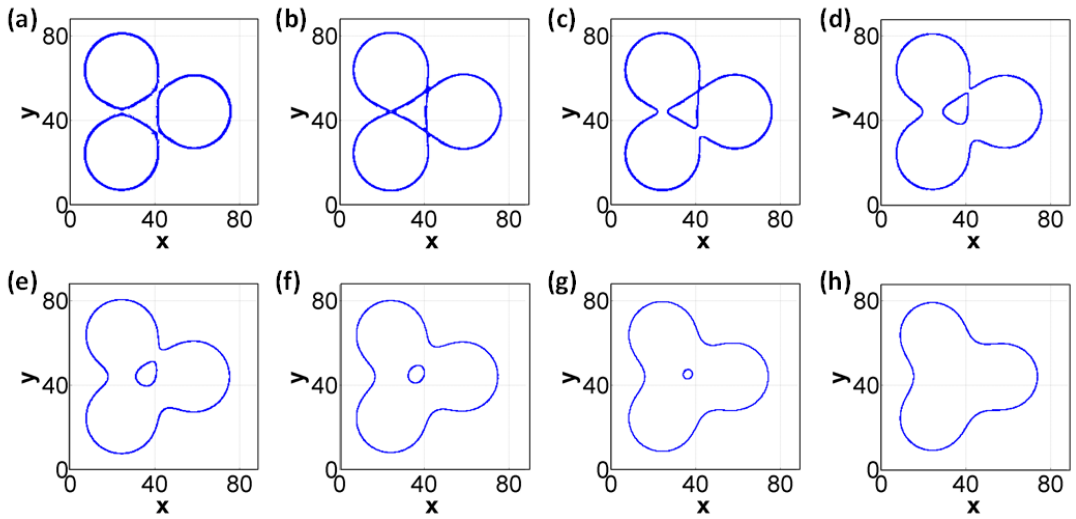

Fig. 5.8: Filament dynamics of the reconnection of three circular filaments placed in a triangular arrangement. The first eight rotation cycles of the filaments are shown in (a-d) respectively. The filaments are viewed from the top. Time interval between each pair of neighbouring frames is 5.4 time units. The diameter of the initial waves are 35.7 space units and they are separated from one another by a distance of 4.1 space units at the points of nearest approach.

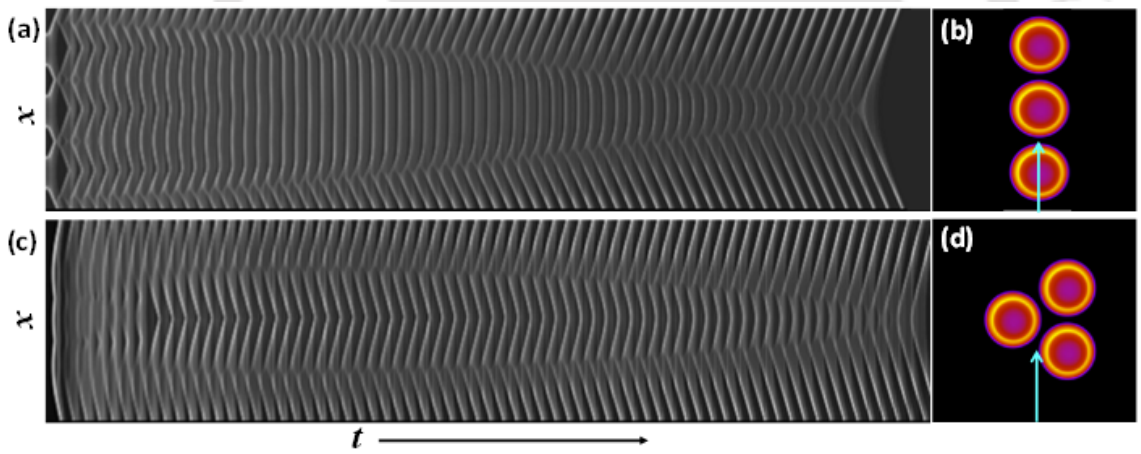

Fig. 5.9: Time space plots for reconnection of three scroll rings having different initial arrangements. (a,c) Time space plots along the cyan lines in (b,d). The two different initial arrangements of the three waves are seen in (b) and (d). Each time space plot spans a duration of 384 time units, where time increases horizontally from left to right. The initial size of the waves and distance of separation from one another are same in both the cases.

Motivated by this observation we calculated the lifetimes of reconnected scroll waves obtained from different initial arrangements of three and four scrolls. The results are graphically shown in Fig. 5.10 (a) and (b). The data suggest that the life time varies depending on the specific geometries of the initial arrangements. We define a width-to-height (height being shorter than width) ratio, r, that can explain the observed trends of life time of the filaments. The vortices formed upon the reconnection of three or four scrolls arranged in a

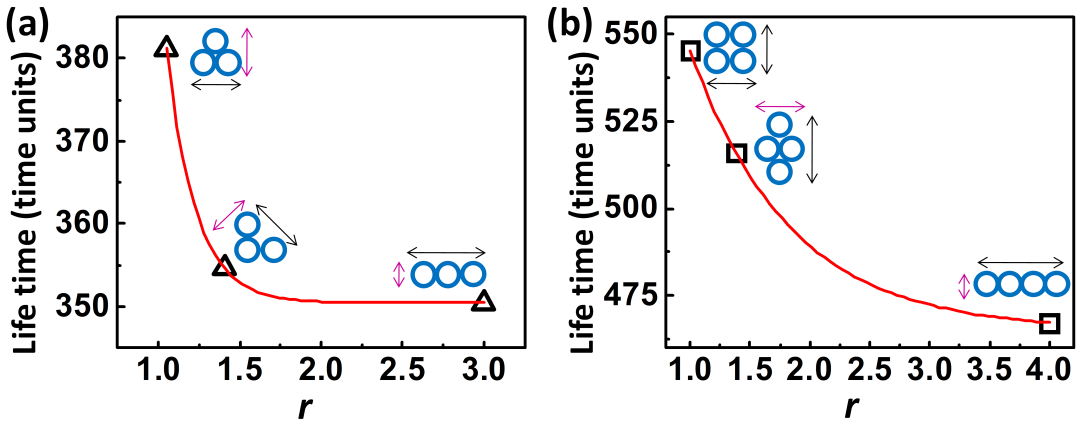

Fig. 5.10: Lifetime vs. aspect ratio plot. The lifetimes of reconnected scrolls are plotted as a function of r for three different initial arrangements of (a) three scrolls and (b) four scrolls, where r is defined as the ratio of width w to height h of the initial filament. On top of each data point the initial arrangement of the filaments along with h and w are shown. A pink arrow represents h while a black one indicates w, with $w \geq h$ in all cases. In both the plots the lifetime decreases almost exponentially with an increasing value of r.

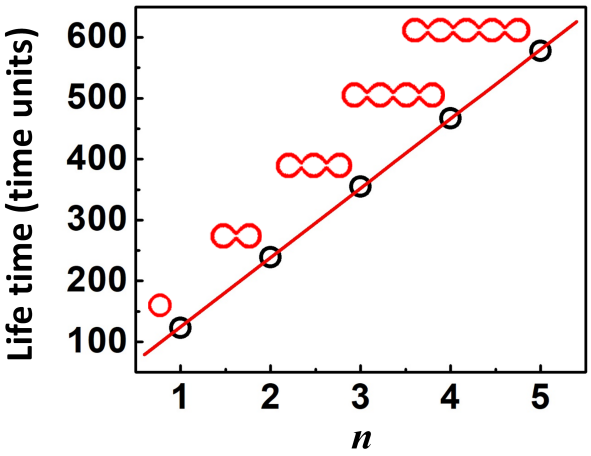

Fig. 5.11: Simulation results showing the variation of lifetime of reconnected scrolls, each arranged in a linear fashion, as a function of initial number of scrolls, n. The initial shape of the corresponding reconnected filament is shown on top of each data point. The lifetime is seen to increase linearly with increasing n. All the scrolls have been generated from initial waves of same size separated by equal distances as before.

linear fashion have the highest values of r and have much smaller lifetimes than the other geometries. Numerical simulations were then performed for various possible arrangements of n number of scrolls with n in the range 2 to 6. Similar results have been obtained for higher numbers of scrolls. Also, it has been observed that the lifetimes of the reconnected filaments for n scrolls, whose centers are placed in a straight line, increase as a linear function of n [Fig. 5.11].

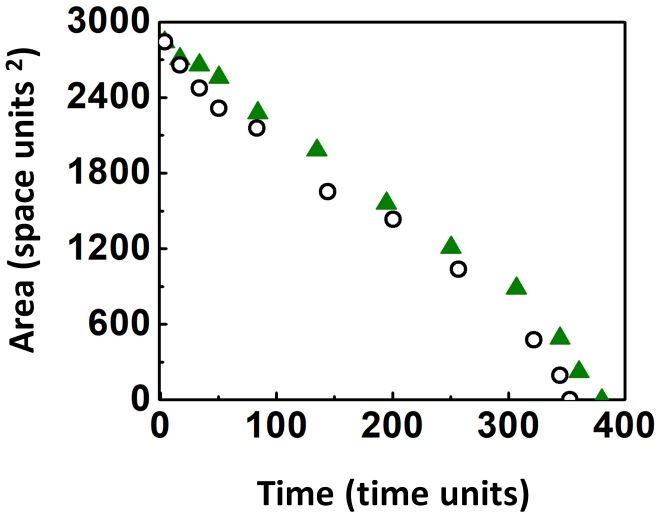

Fig. 5.12: Enclosed area versus time plot for linear and triangular arrangements with $n = 3$. Area enclosed by the filaments are plotted with time along x-axis. The green triangles represent the triangular arrangement and black open circles represent the linear arrangement. The plot shows how the two different geometries of three reconnected scrolls of same initial size take different amounts of time to shrink and collapse.

In order to have further details about the variation of the lifetimes of the reconnected filaments with their respective shapes, for same number of initial scrolls n, we analyzed how their areas change with time. We computed the area enclosed by the reconnected filaments after definite time intervals. For linear and triangular arrangements of three scrolls, these data are plotted as a function of time in Fig. 5.12.

It is seen that though the area for both geometries of reconnected waves fall off with time, as expected by their positive filament tension, the nature of the decrease is not exactly the same. Two interesting observations can be made here. First, the triangular arrangement [Fig. 5.13(f)] of scrolls gives rise to a club-shaped geometry [Fig. 5.13(g)], where convex and concave filament sections try to move inward and outward respectively [Fig. 5.13(h,i)], according to Eq. 5.1. This results in a slowing down of the shrinkage. So the two filaments with initially identical area (at $t = 0$) start deviating. The scrolls arranged along a straight line [Fig. 5.13(a)] also have their own peculiarity. once the dumbbell-shaped filament [Fig. 5.13(b)] becomes smoother to acquire a hotdog-shape [Fig. 5.13(c)], its geometry is now shape conserving [Fig. 5.13(d)]. Hence its shrinkage will not be identical to that of a circular filament [17]. Studies on other filaments could give similar results depending on the speciality of the geometry of the reconnected filament. Qualitatively similar plots have been obtained from experimental data [Fig. 5.4].

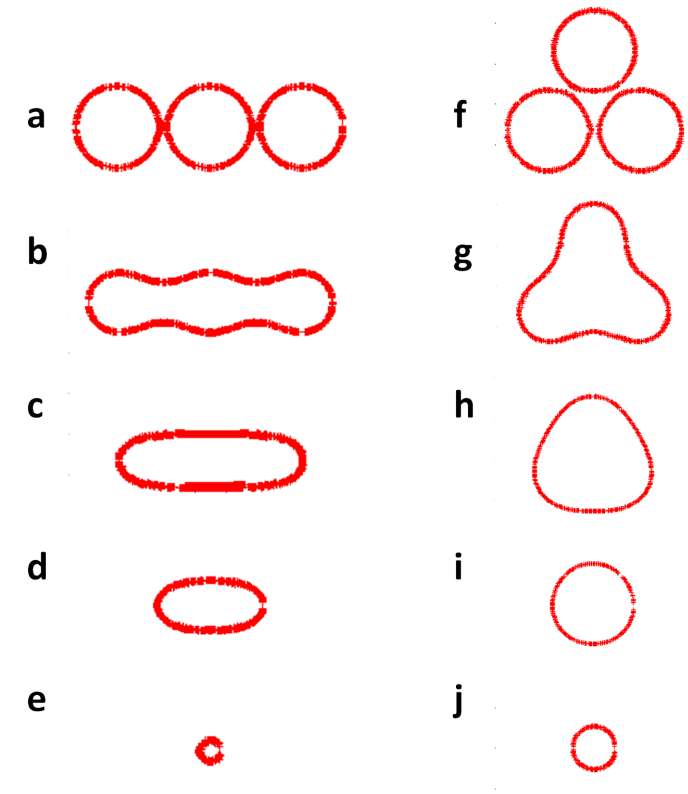

Fig. 5.13: Gradual reshaping of the reconnected filaments for linear and triangular arrangements with $n = 3$. The time of the filaments are, (a) 9 time units, (b) 56.4 time units, (c) 155.4 time units, (d) 250.2 time units, (e) 347.4 time units, (f) 8.4 time units, (g) 57 time units, (h) 153.6 time units, (i) 250.8 time units and (j) 347.4 time units.

5.6 Conclusions

In this chapter we have demonstrated how multiple scroll-wave filaments undergo reconnection to form large filaments of complex geometry. When these scrolls lie sufficiently close to one another, within a specific range of interfilament distance, their filaments undergo crossover collision and merge after one or more cycles of individual rotations of the scrolls. The reconnected waves may have substantially large filaments of different irregular geometries in the initial stage following reconnection. Due to the curvature dependent behaviour, the complex shapes of the huge filaments smoothen and gradually approach a regular geometry. The positive tension of the filaments makes them shrink with time and finally they collapse. It has been observed that the reconnected filaments have elongated life times that could be many times the multiple of same number of independent scroll waves. Moreover, equal number of scroll waves in the same excitable medium may reconnect in several ways to give rise to filaments having noticeably different lifetimes. We have theoretically studied various possible configurations for same values of n in detail and shown that the lifetime depends on the initial arrangement of the reconnecting scrolls. We propose that there exists a relationship between the aspect ratio of the filament geometries

and their lifetimes. Extensive investigation has revealed that for any value of n, a linear arrangement of the reconnecting scroll waves has the lowest lifetime among all the possible geometries, which again is a function of n and increases linearly with n. An analysis of the area enclosed by the filaments after definite intervals of time has helped us gain a better insight into the variation of lifetime with varying initial arrangements of the same number of scrolls.

Further studies can be carried out to deduce an exact mathematical relationship between the elongation of life time to the geometry of the complex reconnected filaments. We hope that these reconnection studies and their results will contribute towards a better understanding of scroll-wave interaction in other excitable media such as the myocardial tissues of heart.

BIBLIOGRAPHY

[1] R. Kapral and K. Showalter, Chemical Waves and Patterns (Springer Netherlands, 1995).

[2] S. C. Müller, P. J. Plath, G. Radons, and A. Fuchs, Complexity and Synergetics (Springer International Publishing, 2018).

[3] V. N. Biktashev, D. Barkley, I. V. Biktasheva, G. V. Bordyugov, H. Dierckx, A. J. Foulkes, S. W. Morgan, G. Plank, N. A. Sarvazyan, O. Selsil, and H. Verschelde, in *Proceedings of the International Conference Instabilities and Control of Excitable Networks: From Macro- to Nano-Systems*, 2012.

[4] Y. Yu, L. M. Santos, L. A. Mattiace, M. L. Costa, L. C. Ferreira, K. Benabou, A. H. Kim, J. Abrahams, M.V. L. Bennett, and R. Rozental, Proc. Natl. Acad. Sci. **109**, 2585 (2012).

[5] X. Huang, W. Troy, Q. Yang, H. Ma, C. Laing, S. Schiff, and J. Y. Wu, J. Neurosci. **24**, 9897 (2004).

[6] J. Lechleiter, S. Girard, E. Peralta, and D. Clapham, Science. **252**, 123 (1991).

[7] O. Steinbock, F. Siegert, S. C. Müller, and C. J. Weijer, Proc. Natl. Acad. Sci. **90**, 7332 (1993).

[8] A. T. Winfree, Science **266**, 1003 (1994).

[9] F. H. Fenton, E. M. Cherry, H. M. Hastings, and S. J. Evans, Chaos **12**, 852 (2002).

[10] R. A. Gray, J. Jalife, A. V. Panfilov, W. T. Baxter, and C. Cabo, Science **270**, 1222 (1995).

[11] J. Jalife, M. Delmar, J. Anumonwo, O. Berenfeld, and J. Kalifa. Basic Cardiac Electrophysiology for the Clinician, 2nd ed. (Wiley-Blackwell, Oxford, UK, 2009).

[12] J. P. Keener, Physica D **34**, 378 (1989).

[13] J. P. Keener and J. J. Tyson, SIAM Rev. **34**, 1 (1992).

[14] A. T. Winfree and S. H. Strogatz, Physica D **8**, 35 (1983).

[15] M. Vinson, S. Mironov, S. Mulvey, and A. Pertsov, Nature (London) **386**, 477 (1997).

[16] J. Schutze, O. Steinbock, and S. C. Müller, Nature (London) **356**, 45 (1992).

[17] S. Dutta and O. Steinbock, Phys. Rev. E **81**, 055202(R) (2010).

[18] V. I. Krinsky and K. I. Agladze, Physica D **8**, 50 (1983).

[19] M. Vinson, Physica D **116**, 313 (1998).

[20] D. Kupitz and M. J. B. Hauser, J Phys. Chem. A **117**, 12711 (2013).

[21] N. P. Das and S. Dutta, Phys. Rev. E **91**, 030901(R) (2015).

[22] A. V. Panfilov, R. R. Aliev, and A. V. Mushinsky, Physica D **36**, 181 (1989).

[23] J. P. Keener and J. J. Tyson, Science **239**, 1284 (1988).

[24] T. Bánsági, Jr. and O. Steinbock, Phys. Rev. Lett. **97**, 198301 (2006).

[25] D. Barkley, Physica D **49**, 61 (1991).

Chapter 6

SPIRALS IN A REACTION-DIFFUSION SYSTEM: DEPENDENCE OF WAVE DYNAMICS ON EXCITABILITY

6. SPIRALS IN A REACTION-DIFFUSION SYSTEM: DEPENDENCE OF WAVE DYNAMICS ON EXCITABILITY

6.1 Introduction

Rotating spiral waves have been observed ubiquitously in thin layers of excitable media like aggregating slime mold [1], cardiac tissue [2, 3], frog oocyte [4], chemical reactions [5–7], etc. Spirals of electrical activity have been suggested to be responsible for cardiac arrhythmias, instabilities of which may further lead to ventricular fibrillation, the leading cause of heart failure in the modern world [2, 8, 9]. The first experimental evidence of spiral waves in a reaction diffusion system was found in the Belousov-Zhabotinsky (BZ) reaction [10]. Since then the BZ system has been a subject of particular interest due to its resemblance to other excitable systems in nature that sustain spiral waves.

A significant feature of spiral waves is the spiral center or core, the small area around which the wave rotates. Intensive investigation has shown that the dynamics of a spiral wave can be described by the motion of its tip. Initially it was believed that spiral tips follow circular paths until Winfree showed that under certain conditions, spirals can also be meandering (cycloidal curves) [11]. Since then, many results on meandering spiral waves have been published [12–15]. Experimental and theoretical analyses have shown that spiral tips can follow epicycloid orbits (flowerlike orbits with inward petals) or hypocycloid orbits (flowerlike orbits with outward petals) [5, 16, 17]. The dependence of the spiral tip on system parameters has been studied earlier in numerical simulations using reaction diffusion models, especially the Oregonator model [11, 18]. Some other studies report the effects of the concentration of the inorganic acid on the geometry of the spiral [19, 20]. It was found that in highly acidic conditions, spirals are Archimedean, whereas there occur deviations from the trend with decreasing acidity.

In this chapter, we investigate the effects of excitability on the wave nature of the spirals. The Oregonator model of the BZ reaction system is chosen for our studies. By changing the value of the parameters, we are able to change the excitability of the system. We show that there is a strong dependence of the nature of the phase portrait, and hence the oscillatory character of the system, on ε, a parameter of the model. Also, the changes in spiral wave characteristics with ε are studied in detail. To confirm our numerical results, we carry out experiments in thin layers of the Ferroin-catalyzed BZ system. Our experimental results are able to verify some earlier mathematical conclusions drawn about the Oregonator model that relates it to the actual concentration of the chemical species in the reaction. We show that such relationships are not restricted to the average wave properties alone, but also to

the dynamics of the spiral tip.

6.2 Model

The Oregonator model, first proposed by Field and Noyes [21], is widely used to study spatio-temporal pattern formation in the BZ reaction. The model in the presence of diffusion can be described as below:

$$\frac{\partial u}{\partial t} = \frac{1}{\varepsilon}\left(u(1-u) - \frac{fv(u-q)}{(q+u)}\right) + D_u\nabla^2 u, \tag{6.1}$$

$$\frac{\partial v}{\partial t} = u - v + D_v\nabla^2 v. \tag{6.2}$$

Here, the time dependent variables u and v are dimensionless forms corresponding to the concentrations of bromous acid and the oxidized form of the metal catalyst respectively, q and f are kinetic parameters, and $D_u = 1.0$, $D_v = 0.6$ are the respective diffusion coefficients of u and v. ε represents the ratio of the time scales of the dynamics of the fast and slow variables.

Winfree in one of his papers [11] suggested a relationship between ε and the concentrations of the different chemical species in the BZ reaction, which is as given below:

$$\varepsilon = \frac{k_5}{k_3}\frac{[organics]}{[H^+][BrO_3^-]}, \tag{6.3}$$

where [organics] = [BrMA] + [MA] (MA stands for malonic acid), $k_5 = 0.4\ \mathrm{M^{-1}s^{-1}}$, $k_3 = 40\ \mathrm{M^{-2}s^{-1}}$.

The value of epsilon for any set of reactant concentrations can be calculated from the above equation. Since this parameter relates directly to the experimental conditions, we focussed our attention to a methodical study of the system for varying values of ε.

For our simulations, equations 6.1 and 6.2 were integrated using an explicit Euler scheme for a two dimensional lattice of 300×300 grid points having zero flux boundaries along all the four walls. A time step of $dt = 0.001$ and a grid spacing of $dx = 0.1$ were employed. The above set of conditions can sustain spirals depending upon the values of ε, f, and q. Spirals were generated using the same initial conditions as in [11]. The tip of the spiral was identified as the isoconcentration points of u and v.

6.3 Numerical Results

Simulations were performed varying ε from 0.002-0.50. In Fig. 6.1(a-c), snapshots of spiral waves for three different values of ε are depicted. The figures show that the frequency of the spiral wave decreases with an increase in ε. Figure 6.1(d) is a representative time-space plot which is created by stacking a cross-section [yellow line in Fig. 6.1 (b)] of

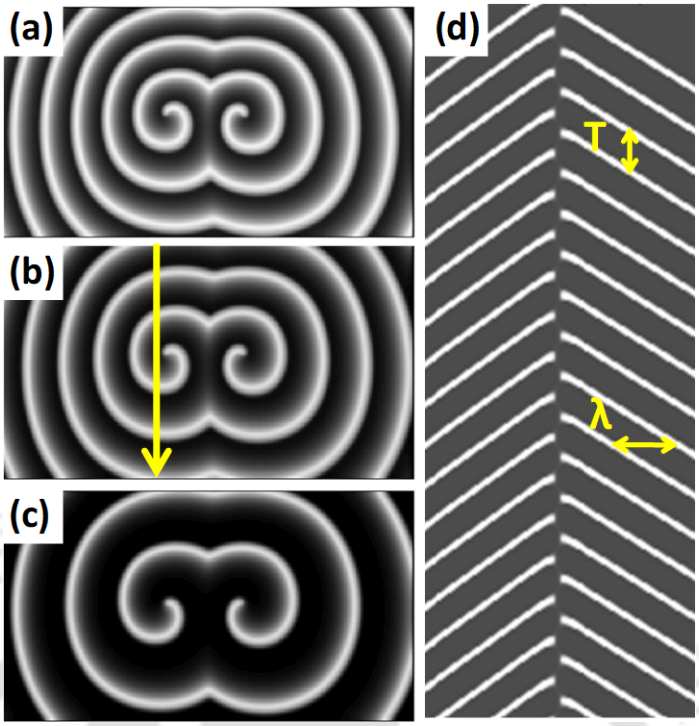

Fig. 6.1: Simulations of spiral waves generated using Oregonator model. (a-c) Snapshots of the stable spiral for three different values of ε: (a) 0.02, (b) 0.03, and (c) 0.04. $f = 2.0$ and $q = 0.002$ across all the simulations. (d) Time-space plot generated along the yellow arrow in (b), showing the time period T, and the wavelength λ. Time increases from top to bottom.

the time-lapse snapshots of the system. The fish-bone shape of the time-space plot, with the phase difference between the lines going on either side from the center, confirms the presence of the spiral.

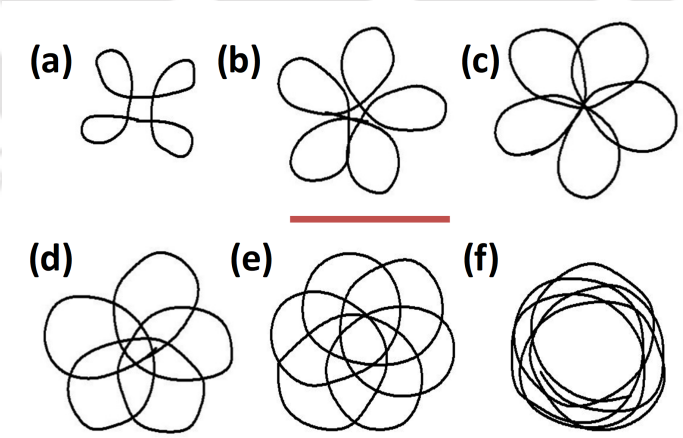

Fig. 6.2: Tip trajectories of spiral waves obtained from numerical simulation for ε values (a) 0.006, (b) 0.02, (c) 0.03, (d) 0.04 (e) 0.05, and, (f) 0.06, respectively. Length of the bar shown below (b) is 3.6 space units.

In order to study the detailed dynamics of the spiral waves we analyzed the tip trajectories for different values of ε. It was found that depending on the value of the kinetic terms and ε, the tip either follows a circular path or meanders, giving rise to a flower like pattern with petals of varying size. For parameter values $f = 2.0$ and $q = 0.002$ and ε varying in

the range of 0.002 to 0.06, the spiral meanders with outward petals. The trajectories of the spiral tip for some of the ε values are shown in Fig. 6.2. There is a marked increase in the core size of the trajectories with increasing value of ε. For higher values of ε, the petals become very large and merge to give almost circular trajectories.

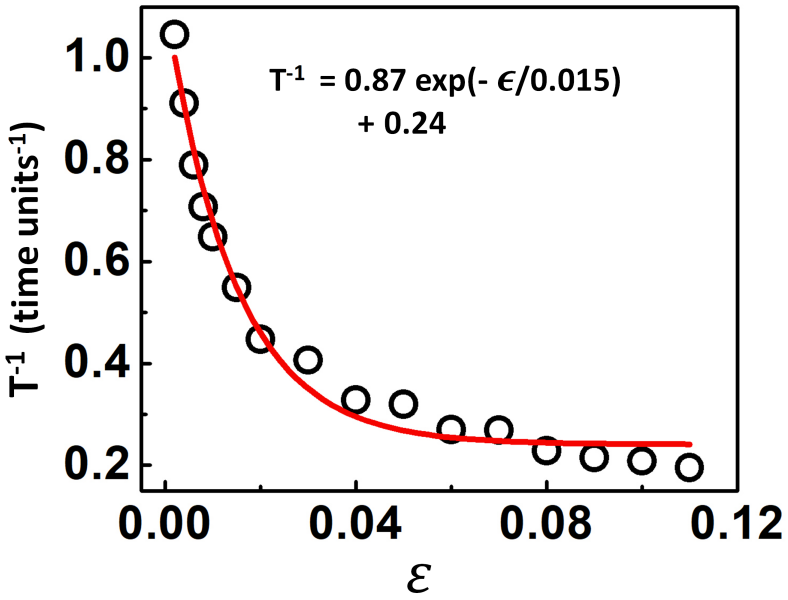

Fig. 6.3: Frequency vs. ε plot for the region where spirals are obtained. The data has been obtained from numerical simulations of the Oregonator model. The curve represents a fitting of the data as an exponential decay.

The time periods for different ε values are calculated from the corresponding time-space plots as depicted in Fig. 6.1(d). Figure 6.3 and Fig. 6.4 show the plot of the inverse of the time-period, which is closely related to the frequency, as a function of ε. It is observed in Fig. 6.3 that the frequency decays almost exponentially with the increase in ε values from 0.002 to 0.11. For $\varepsilon > 0.11$, there is no formation of spirals, but only bulk oscillations and phase waves are obtained. In Fig. 6.4, the values beyond $\varepsilon = 0.11$ are the frequencies of these phase waves. We have included them in this graph for a discussion of the oscillatory nature of the system with further increase of ε values. For ε just above 0.11 ($\sim$ 0.12) we see the system undergoing random oscillations that finally reaches a stable nature after a long time. Similar nature is found for ε values around 0.15. In the intermediate range, however, only random oscillations are seen, and the system does not reach a state of regular oscillations even at t = 5000 time units. It is possible that they reach such a state after much longer times. The values plotted in the figure for such states are averages over 30 oscillations. Just beyond ε = 0.12, we observe a sudden jump in the frequency values. This jump marks the change in the spatial behavior of the system. For higher ε values, the frequency of the oscillations are almost constant, or vary very slightly.

We analyze the dynamics of the model on the phase plane for varying values of ε. Stable limit cycles are obtained for $\varepsilon \leq 0.12$, followed by a regime of random oscillations,

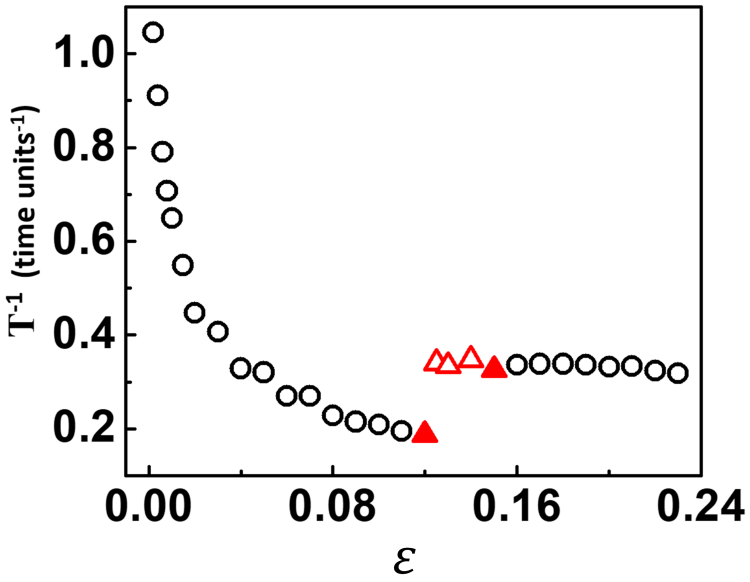

Fig. 6.4: Frequency of excitation waves in the Oregonator model as a function of ε. The black open circles are frequencies of stable oscillations, while the red triangles denote the average amplitude for a system displaying transience. In the beginning and end of this range, simulations for long times shows that the system eventually reaches a state of stable oscillations. However, we have not been able to see any such phenomenon in the case of the data points given by open triangles. Here, the average value of its oscillating frequency has been reported.

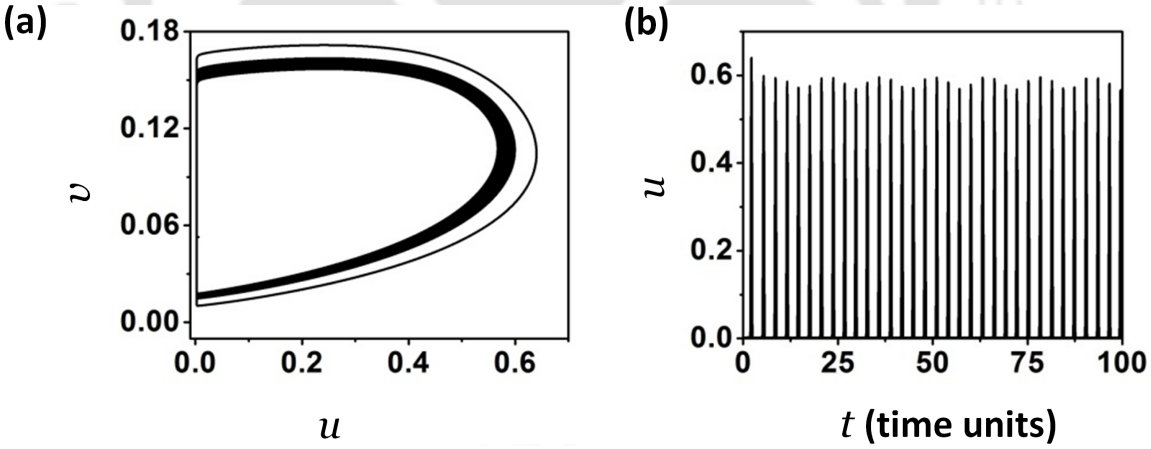

Fig. 6.5: (a) Dimensionless phase space diagram and (b) nature of oscillations observed in the spiral forming range ($0.002 \leq \varepsilon \leq 0.11$). These results have been obtained for $\varepsilon = 0.04$.

stable limit cycles and finally fixed points. The frequency and amplitude of the oscillations also reflect the phase-space behavior. There are high amplitude, regular oscillations for $0.002 \leq \varepsilon \leq 0.11$ [Fig. 6.5(b)]. This is the region where well-behaved spirals are formed [Fig. 6.1]. The corresponding limit cycle is shown in Fig. 6.5(a). In this parameter space, there is an exponential relationship between frequency and ε [Fig. 6.3].

Beyond $\varepsilon = 0.11$, for a small parameter region, there are no existence of rotors, but the system initially oscillates with erratic amplitude as well as frequency [Fig. 6.6]. However,

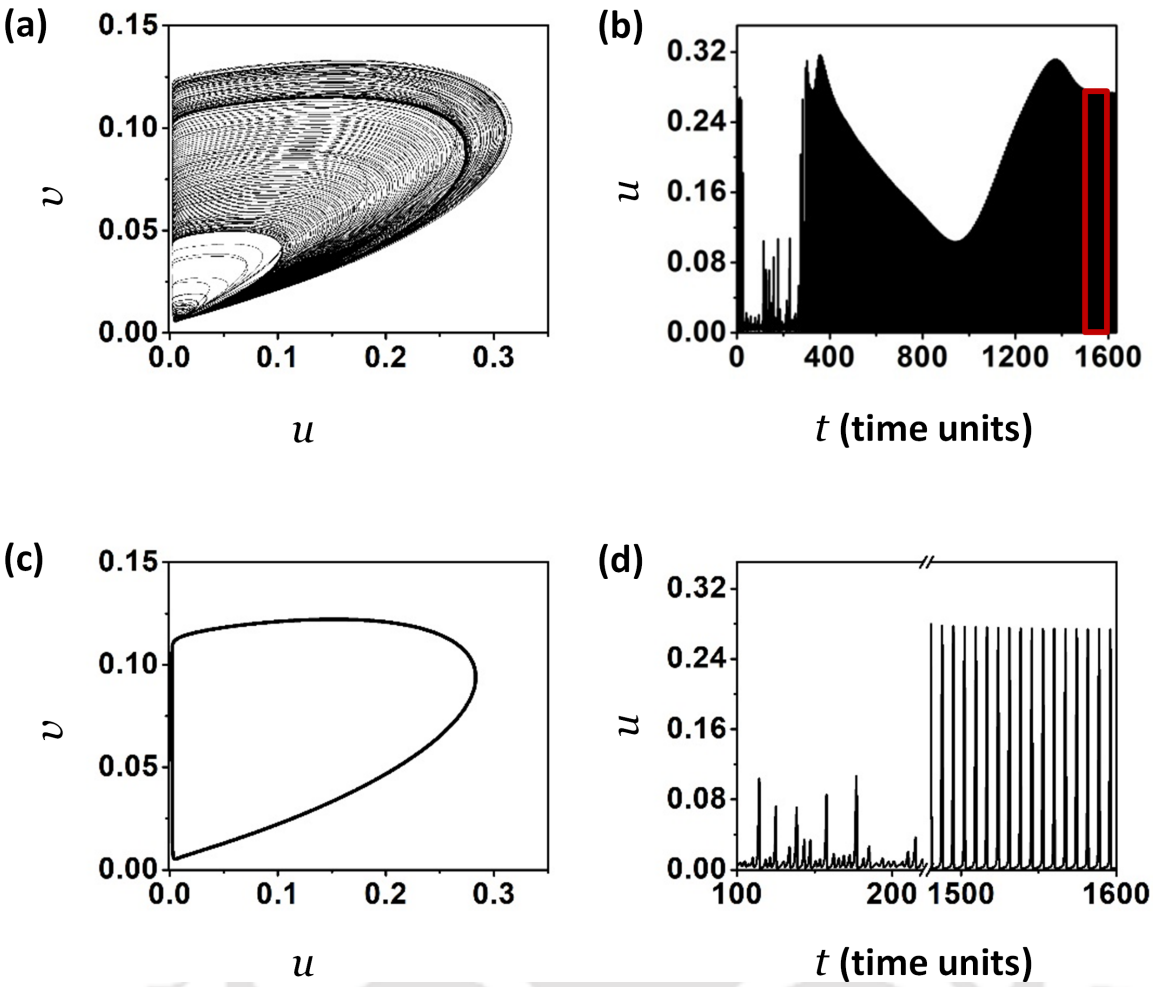

Fig. 6.6: Behaviour of excitation waves for $\varepsilon = 0.12$. (a) Phase space diagram. (b) Oscillations that are initially random but stabilizes after a long time. (c) shows the limit cycle where the system finally settles down (the region marked by the red rectangle in (b), t = 1500-1600 time units). (d) The two types of oscillations observed at initial (t = 100-200 time units) and later (t = 1500-1600 time units) stages.

stable oscillations are observed after a period of transience, as seen in Fig. 6.6(d). The phase space [Fig. 6.6(c)] shows that the system finally settles down to a limit cycle.

As we further increase the value of the excitability parameter, through a short range of values ($0.12 < \varepsilon < 0.15$), even though simulations were carried out for very long times ($t > 5000$ time units), we failed to observe any tendency of the system to reach stable oscillations. We carried out detailed analysis of the data to check for the existence of a limit cycle, but could not find any. The possibilities of a chaotic system in this parameter range cannot be ruled out but since we are dealing with a two-dimensional system, no such signatures could be detected. More detailed analysis of the three-dimensional Oregonator model will be required for this purpose. Figure 6.7 shows representative snapshots of the system for $\varepsilon = 0.13$, which exhibited only random oscillations. At the end of this range, around $\varepsilon \sim 0.15$, the transient system is again seen to reach a state of stable oscillations. Over a parameter range $0.16 \leq \varepsilon < 0.24$, low-amplitude sustained oscillations are obtained [Fig. 6.8(b)]. This corresponds to the limit cycle behavior in Fig. 6.8(a). Finally beyond

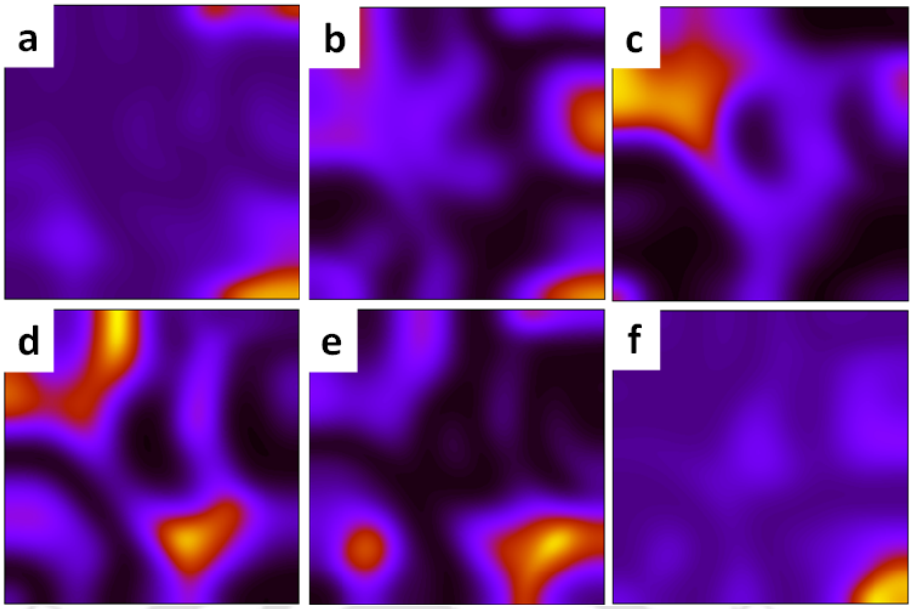

Fig. 6.7: Snapshots of the system in simulations of the Oregonator model for epsilon =0.13. The system is viewed from top at (a) 45.00, (b) 46.05, (c) 47.10 (d) 48.15 (e) 49.20 (f) 50.25 time units. Simulation was carried out with a lattice of size 300×300 grid points. Area of each image is 30 space units×30 space units.

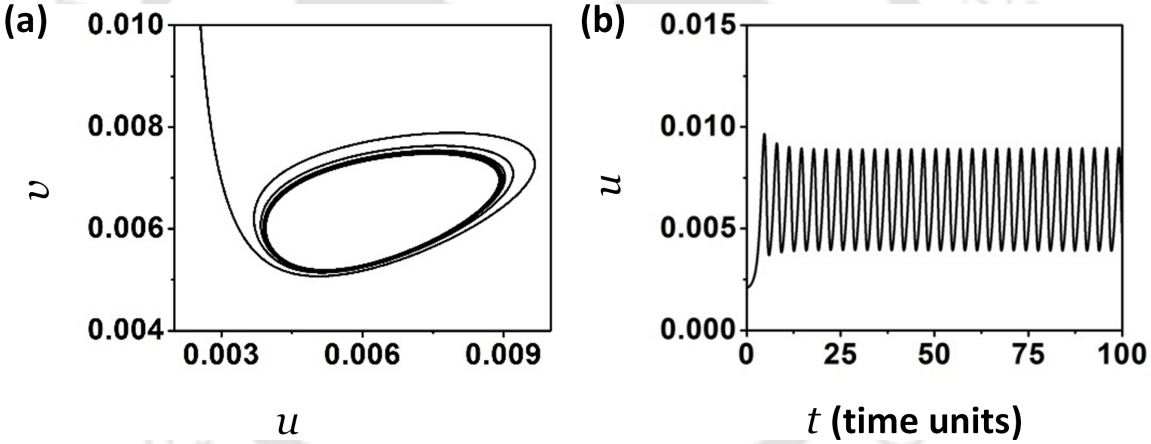

Fig. 6.8: (a) Phase space diagram and (b) sustained oscillations observed for $\varepsilon = 0.20$.

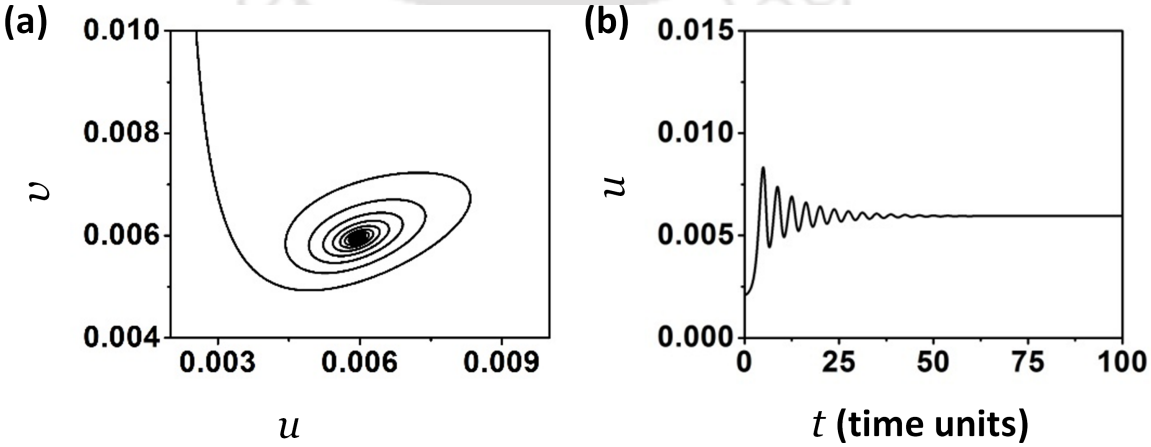

Fig. 6.9: (a) Phase space diagram and (b) damped oscillations observed for $\varepsilon = 0.24$.

$\varepsilon = 0.23$, the system demonstrates damped oscillations. This can be seen in Figs. 6.9(b). The low amplitude oscillations quickly die down to reach a steady state. This is reflected in the presence of a fixed point in the phase diagram [Fig. 6.9(a)]. The simulations were repeated for a single spiral, and identical results were obtained. Since the excitability of the medium depends so vividly on the parameter ε, we henceforth call it the excitability parameter.

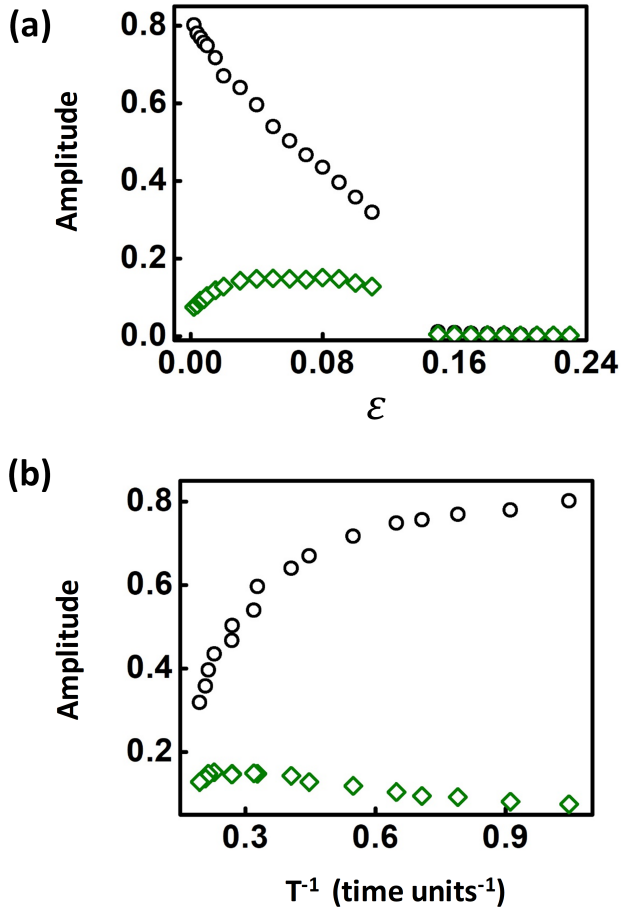

Fig. 6.10: Variation of amplitude of the oscillations with change in (a) ε value and (b) frequency. The values for the range ($0.11 < \varepsilon < 0.15$) where random oscillations are observed, have been omitted. The black open circles denote values for u and olive diamonds are amplitudes in the variation of v.

It was observed that the amplitude of the oscillations in u, reduce with the increase in the value of the excitability parameter, ε. We plot the variation of amplitude as a function of ε and the frequency of the waves [Fig. 6.10]. A linear decrease in the amplitude of u is seen for those values of epsilon where spirals are formed ($\varepsilon \leq 0.11$), however, beyond this range of values, there is a sudden drop in the amplitude. For higher values of epsilon ($\varepsilon > 0.15$), the amplitude decreases very slowly, and eventually becomes zero for ($\varepsilon > 0.23$). Beyond this parameter range, sustained oscillations are absent. With increase in the frequency, the amplitude in the oscillations of u show a logarithmic growth. Interestingly, amplitudes of variable v show a decreasing rate, after an initial increase, in both the cases (ε and T^{-1}).

This change is however much less as compared to u. This may be due to the fact that v is the inhibitor, which is the slower variable, and in the BZ, it denotes concentration of the metal catalyst, ferroin.

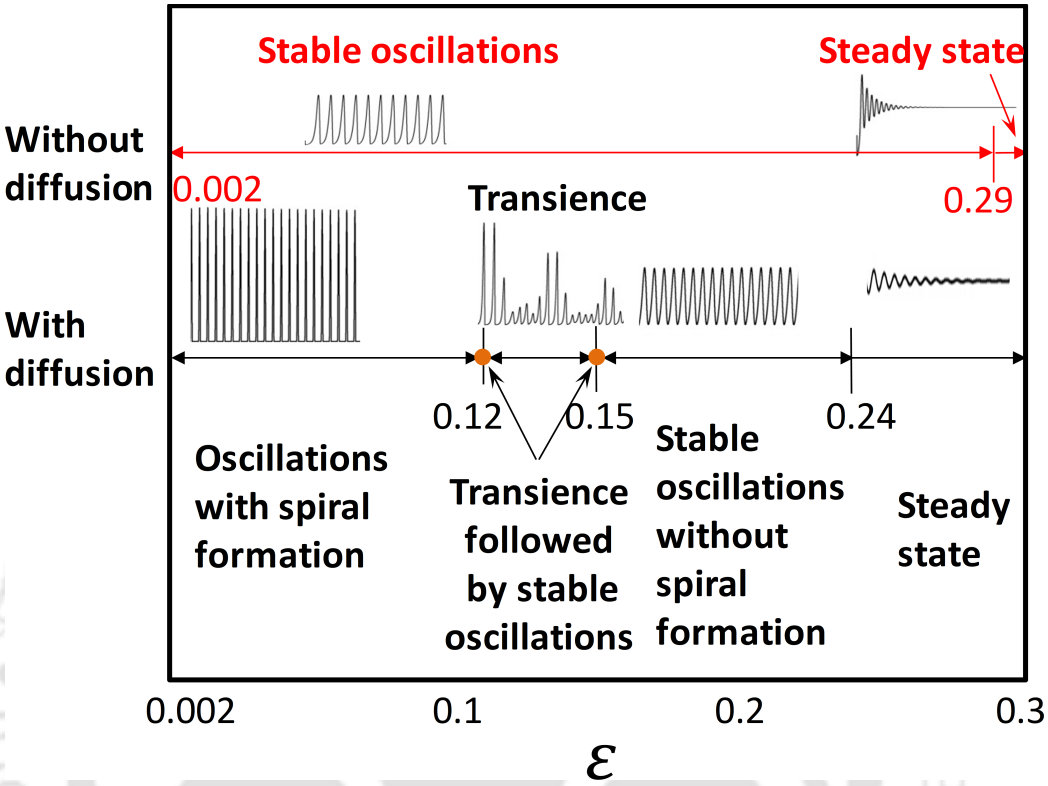

Fig. 6.11: Bifurcation diagram with (bottom, black) and without (top, red) diffusion. The change in the oscillatory nature of the system and corresponding wave nature with the variation in ε value has been depicted here.

We summarize our numerical results in the form of a bifurcation diagram, generated as a function of the excitability parameter [Fig. 6.11]. A system without diffusion shows two regions: one region ($0.002 \leq \varepsilon \leq 0.29$) demonstrates stable oscillations. In this region, there is an unstable fixed point surrounded by a stable limit cycle [Fig. 6.12]. The size of the limit cycle keeps on decreasing with the increase in ε value, till it engulfs the fixed point at around $\varepsilon \sim 0.29$, and a stable fixed point is created. Beyond this value of the excitability parameter, there are no limit cycles, and all oscillations damp down to a final steady state. This is a case of Supercritical Hopf Bifurcation. In the presence of diffusion, the system displays similar dynamics, but the Hopf Bifurcation now sets in around $\varepsilon \sim 0.24$. Also, there are some interesting variations in the nature of the excitation waves in the region where limit cycles are found. Spiral waves are obtained for low values of ε. They are followed by a short range of random oscillations, beyond which, low-amplitude stable oscillations are observed. The limit cycle shrinks with the increase in the value of the excitability parameter, until a stable fixed point is created at the bifurcation point.

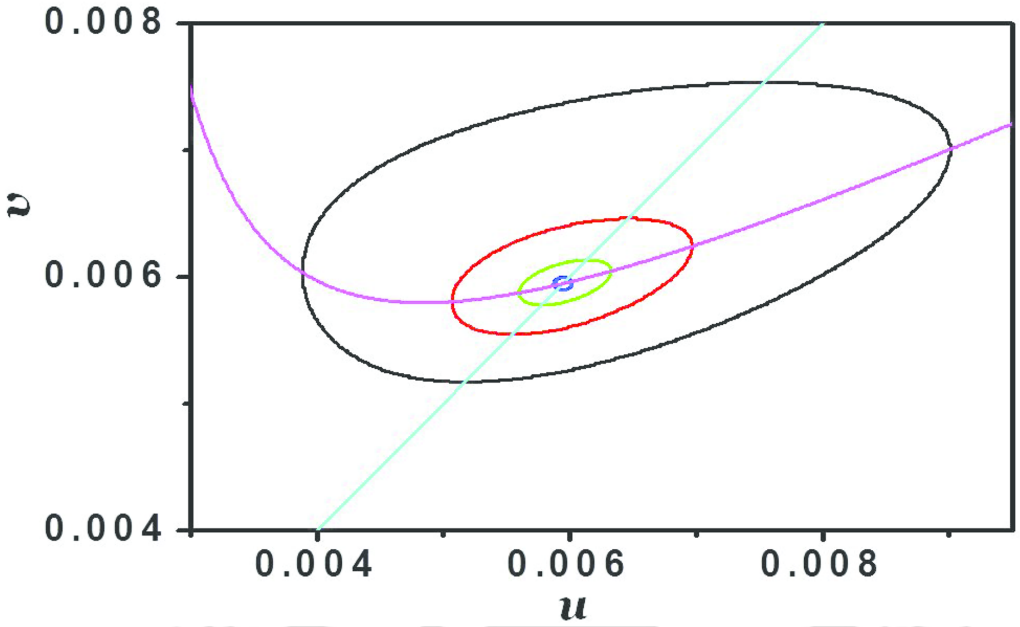

Fig. 6.12: Limit cycles and fixed points in the Oregonator model without diffusion. An analysis demonstrating the Supercritical Hopf Bifurcation in the system. The black, red, green ellipses are the limit cycles for ε values of 0.20, 0.23, and 0.235, respectively. The blue circle shows the position of the fixed point for $\varepsilon = 0.30$. Intermediate ε values yield limit cycles that are too small to see in this figure. The trajectories for $\frac{du}{dt} = 0$ and $\frac{dv}{dt} = 0$ are plotted as magenta and cyan lines respectively.

6.4 Experimental Section

In this and later sections of this chapter, we show that the influence of the excitability parameter on the dynamics of excitation waves can also be observed in real experimental systems. Our experiments were performed using thin layers of ferroin-catalyzed BZ reaction with malonic acid as the organic substrate. A series of experiments were carried out with concentrations of different reactants in the following range: $[H_2SO_4] = 0.16 - 0.32$ M, $[NaBrO_3] = 0.04 - 0.12$ M and $[MA] = 0.04 - 0.12$ M. [Ferroin] = 0.001 M was kept constant for each reaction. Across these ranges of substrate concentrations spiral waves can be successfully initiated. Reaction mixtures outside the above range are either of high or low excitability. Therefore, only traveling waves or turbulent waves can be observed in the latter. The prepared BZ solution was transferred to a petri dish of 8 cm diameter. The thickness of the solution layer was about 2 mm. The mixture was swirled as the first oscillation completes and then kept undisturbed to attain a homogeneous state. A circular wave was generated by dipping for a few seconds, the tip of a silver wire in the middle of the petri dish to prevent boundary effects. The main reason behind using the silver wire is the removal of the inhibitor Br^- from the vicinity as AgBr. The expanding circular wave front when cleaved resulted in the formation of a pair of spiral waves with two tips of opposite chirality. We then placed a flat glass plate over the reaction mixture to eliminate the chances of aerial oxidation. The petri dish was covered to prevent any undesired hydro-

dynamics. In the above solution, oscillations continue for four hours or more. To capture images of our experiment, a charge coupled device (CCD) camera (mvBlueFOX 22a) was mounted above the system which was illuminated from below by a cold white light source. Snapshots were recorded onto a computer every two seconds and the data analyzed using inhouse MATLAB codes.

6.5 Results and Discussion

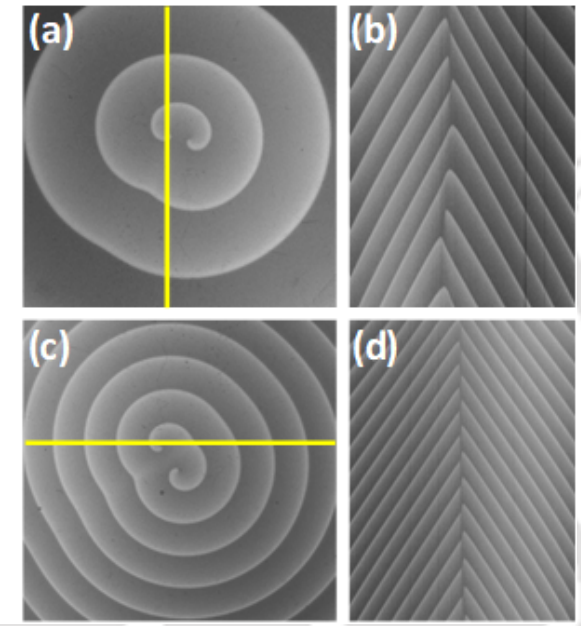

Fig. 6.13: Spirals in experiments with the BZ reaction. (a,c) Snapshots of spiral waves with [$NaBrO_3$]= 0.04 M, [$CH_2(COOH)_2$]= 0.04 and [Ferroin] = 1 mM. H_2SO_4 concentration in (a) is 0.2 M and in (c) is 0.28 M. Each snapshot has an area of 6.4 cm $\times$ 4.8 cm. (b,d) Time space plot of the spirals along the yellow lines in (a) and (c) respectively.

Figure 6.13 shows snapshots of two spirals along with their time space plots. The concentration of H_2SO_4 is varied in these two sets of experiments keeping the concentrations of $NaBrO_3$, Malonic Acid and ferroin constant at 0.04 M, 0.04 M and 1 mM respectively. In Fig. 6.13 (a) and (b) the concentration of H_2SO_4 is 0.2 M while in (c) and (d) it is 0.28 M. It is clearly revealed by the snapshots and time space plots that the properties of the spiral waves are dependent on the initial concentration of H_2SO_4. An increase in the concentration of H_2SO_4 results in a visible decrease in the time period and wavelength of the spirals. A similar trend is observed with an increasing concentration of $NaBrO_3$ as shown in Fig. 6.14.

In order to have a close comparison of our experiments with the numerical results, ε value for each experiment was calculated from equation 6.3 and plotted against frequency. Figure 6.15 shows that frequency decays exponentially with increasing value of epsilon. Thus, it follows the same trend as shown in our simulations [Fig. 6.4].

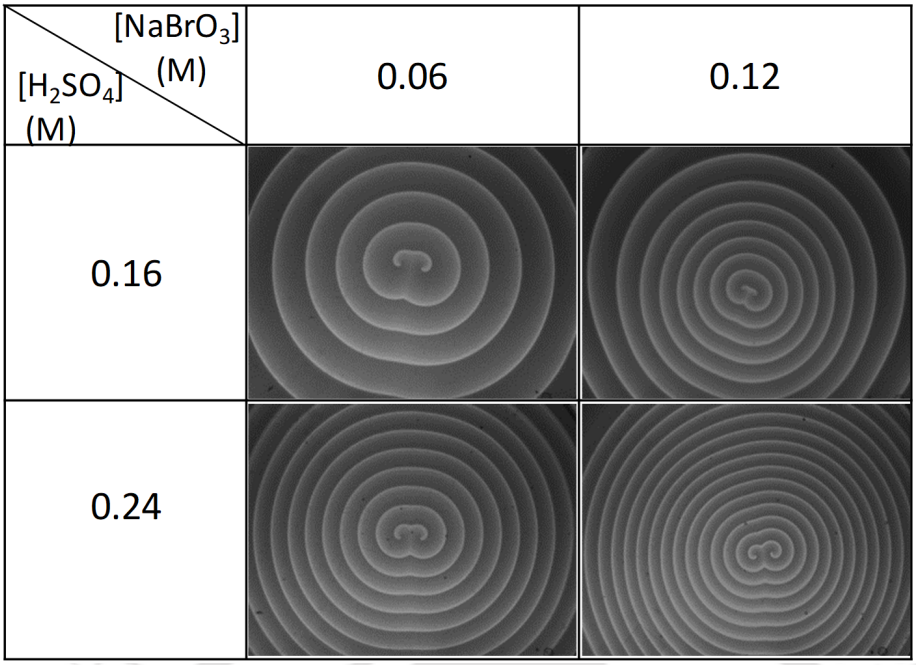

Fig. 6.14: Dependence of spiral behaviour on the concentration of H_2SO_4 and $NaBrO_3$. Each snapshot has an area of 6.4 cm × 4.8 cm. In all the experiments, [MA] = 0.04 M, and [Ferroin] = 0.001 M.

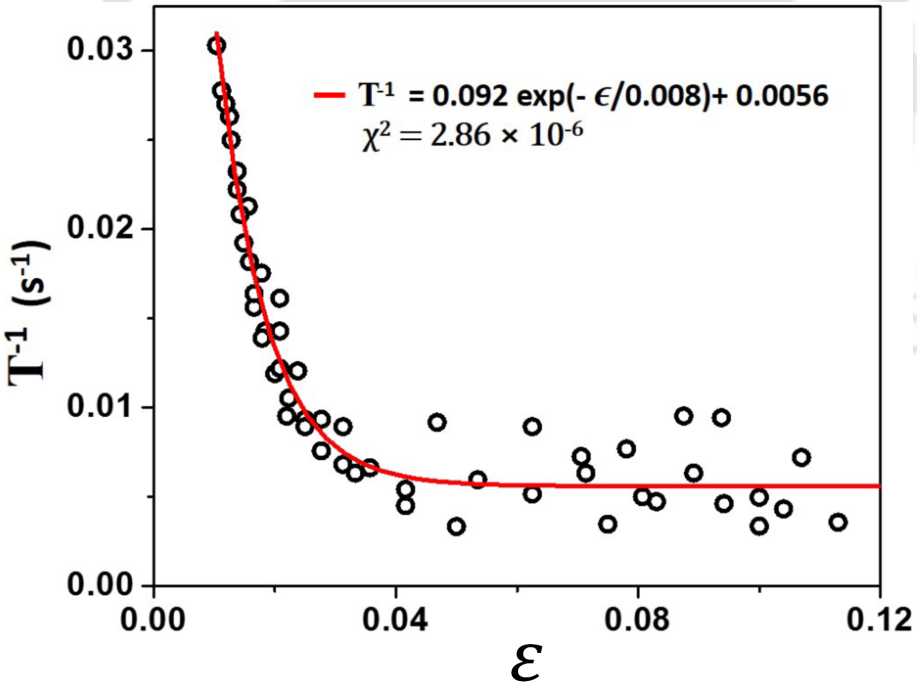

Fig. 6.15: Frequency of spirals in the BZ reaction as a function of the excitability parameter, ϵ.

The time-period and wavelength of every experiment was measured from its corresponding time-space plot. The other important parameters of wave dynamics, viz. frequency and velocity were also calculated from these values. For an increase in the concentration of sulphuric acid, the frequency increases almost linearly, while the wavelength

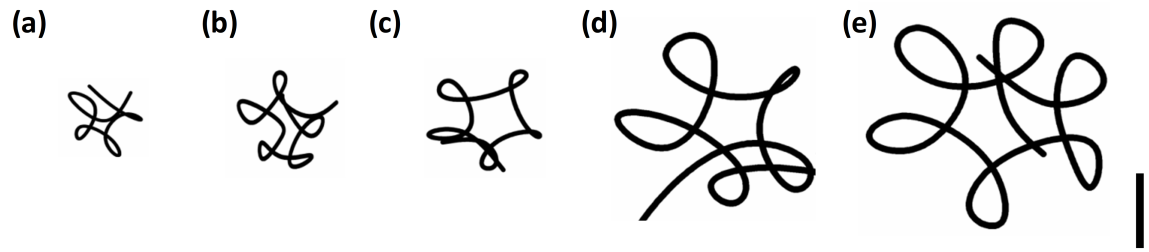

Fig. 6.16: Tip trajectories of spiral waves for different values of ε. Length of the bar shown at the bottom right corner is 1 mm. The values of ε are 0.0227, 0.025, 0.027, 0.0313 and 0.0416 in (a-e) respectively.

seems to decay exponentially [23]. With the increase in the concentrations of $NaBrO_3$, time period increases with a linear trend, and the wavelengths of the spirals decrease. The velocities of the waves increase with the increase in the concentrations of the inorganic acid and the bromate. However, there is no such appreciable change in any of the parameters with change in the malonic acid concentration. Thus, it can be said that the dynamical properties mostly depend on the concentrations of H_2SO_4 and $NaBrO_3$.

From simulations with the Oregonator model, it is seen that the spiral core can trace different types of floral trajectories whose nature and size depend on the kinetic parameters [Fig. 6.2]. For our experiments with the BZ reaction, we analyze the time-lapse snapshots of each experiment with some in-house MATLAB scripts to trace the trajectories of the spiral tips. In all our experiments, we get hypocycloid curves, i.e. floral patterns with the petals facing outward. It is also observed that the core size, outer diameter of the trajectories and number of petals decreases for increased concentrations of $NaBrO_3$ and H_2SO_4 [22, 23]. On the other hand, if we increase the concentrations of MA while keeping $[H_2SO_4]$ and $[NaBrO_3]$ constant, it is seen that the number of petals as well as the trajectory size increase [22, 23]. For each of these experiment ε value was calculated from equation 6.3. From the Fig. 6.16 it is seen that the core size decreases with decrease in the value of ε. A similar trend was found in the results of our numerical simulations [Fig. 6.2]. Thus, changing the excitability can induce changes in the dynamics of a spiral wave that also leaves its mark on the nature of the tip trajectories.

6.6 Conclusions

In this study of spiral waves in the two dimensional BZ system, we have shown that the initial concentrations of the substrates have a marked effect on the wave nature of the medium. Through experiments with thin layers of BZ solution as well as numerical simulations involving the Oregonator model, we have made a detailed quantitative analysis of the wave properties of the spirals from their time space plots.

An important aspect of this study revolves around the Oregonator model parameter, ε, and the influence it has on the excitation dynamics of the BZ system. Our experiments and corresponding numerical simulations are a simple demonstration that the suggested

relationship of ϵ with the concentrations of the reactants in the BZ system, as reported by earlier researchers, is valid not only in a "loose" qualitative sense, but in a very quantitative way. In our present study we show how the increase in this parameter brings about Hopf Bifurcation in the system, as it passes from a regime of spiral waves, to phase waves and finally collapses to a steady state. We also discover a short range of parameter values where random oscillations are observed. Further studies of the three-variable Oregonator model may shed more light on the dynamics of the system in this regime of parameter values. From our numerical simulations and experiments we have shown that there is an exponential decay in the frequency of the waves with increase in ϵ value, in the region where spirals are formed. The effect it has on the excitability of the medium and also in the spiral tip dynamics, inspires us to call ϵ the excitability parameter.

The changes in the dynamics of the three dimensional scroll waves as a function of substrate concentrations will also be of much interest. Scroll wave turbulence and drift in the BZ reaction are still elusive phenomena. Further studies with the 3D BZ system may enable us to achieve these by tweaking the excitability of the medium with a wise choice of reactant concentrations.

BIBLIOGRAPHY

[1] F. Siegert and C. J. Weijer, Physica D **49**, 224 (1991).

[2] R. A. Gray, A. M. Pertsov, and J. Jalife, Nature **392**, 75 (1998).

[3] G. Bub, A. Shrier, and L. Glass, Phy. Rev. Lett. **88**, 058101 (2002).

[4] J. Lechleiter, S. Girard, E. Peralta, and D. Clapham, Science **252**, 123 (1991).

[5] A. T. Winfree, Science **175**, 634 (1972).

[6] S. Nettesheim, A. von Oertzen, H. H. Rotermund, and G. Ertl, J. Chem. Phys. **98**, 9977 (1993).

[7] F. Haudin, J. H. E. Cartwright, F. Brau, and A. De Wit, Proc. Nat. Acad. Sci. **111**, 17363 (2014).

[8] J. Jalife, R. A. Gray, G. E. Morley, and J. M. Davidenko, Chaos **8**, 79 (1998).

[9] L. Gaztañaga, F. E. Marchlinski, and B. P. Betenskya, Rev. Esp. Cardiol. **65**, 174 (2012).

[10] A. N. Zaikin and A. M. Zhabotinsky, Nature **225**, 535 (1970).

[11] W. Jahnke, W. E. Skaggs, and A. T. Winfree, J. Phys. Chem. **93**, 740 (1989).

[12] G. Li, Q. Ouyang, V. Petrov, and H. L. Swinney, Phy. Rev. Lett. **77**, 2105 (1996).

[13] G. S. Skinner and H. L. Swinney, Physica D **48**, 1 (1991).

[14] M. Braune and H. Engel, Chem. Phys. Lett. **211**, 534 (1993).

[15] C. K. Tung and C. K. Chan, Phys. Rev. Lett. **89**, 248302 (2002).

[16] D. Barkley, Phy. Rev. Lett. **72**, 164 (1994).

[17] D. Barkley and I. G. Kevrekidis, Chaos **4**, 453 (1994).

[18] W. Jahnke and A. T. Winfree, Int. J. Bifurcat. Chaos **1**, 445 (1991).

[19] T. Plesser, S. C. Müller, and B. Hess, J. Phys. Chem. **94**, 7501 (1990).

[20] A. L. Belmonte, Q. Ouyang, and J. M. Flesselles, J. Phys. II France **7**, 1425 (1997).

[21] R. J. Field and R. M. Noyes, J. Chem. Phys. **60**, 1877 (1974).

[22] N. P. Das, PhD dissertation, Indian Institute of Technology Guwahati, 2016.

[23] D. Mahanta, N. P. Das, and S. Dutta, Phys. Rev. E **97**, 022206 (2018).

Chapter 7

CONCLUSIONS AND FUTURE PROSPECTS

7. CONCLUSION AND FUTURE PROSPECTS

The results presented in this thesis mostly revolves around the dynamics of two dimensional spiral waves and three dimensional scroll waves in presence of inhomogeneities. Using the Belousov Zhabotisky reaction and numerical simulations of simple reaction diffusion models, we have investigated some of the important aspects of excitation wave dynamics, that had remained unexplored.

In the first two studies, we have carried out detailed and systematic investigations on pinning and unpinning phenomena. The pinning of scroll waves to a large, flat and branched obstacle has been found to produce a huge number of possible filaments of complex geometries. It has been observed that pinning prevents the collapse of the filaments. The stabilization of the pinned scrolls is accompanied with the reshaping of their filaments. Factors such as the initial size of the waveform and its proximity to the nearest heterogeneities decide the final stable form of the filament. Furthermore, depending on the filament geometries, the pinned waves stabilize with different rotation periods.

In our work on unpinning, we have successfully detached the pinned vortices from three to six anchoring points. The unpinning times have been found to depend on the geometry of the pinned filaments, orientation of the obstacles with respect to the gradient, strength of the applied field and bead diameter.

Reconnection of multiple scroll rings have been achieved both in experiments and numerical simulations. The reconnected filaments of much larger size and complex geometry show substantially elongated lifetimes. The lifetimes are found to vary depending on the arrangements of the reconnecting scrolls. An analysis of the temporal change in enclosed area of the reconnected filaments help better understand the curvature dependent shrinkage of the filaments.

Finally in Chapter 6, we have shown the dependence of the properties of two dimensional waves on system excitability. Extensive numerical studies with the Oregonator model have revealed different regimes of wave behaviour for different ranges of the excitability parameter ε. We have also observed a supercritical Hopf bifurcation with changing excitability of the medium.

Through our studies, we have tried to focus on various aspects of the excitation waves, their interactions and control. It would be interesting to extend the work to more complex scenarios. For example, further studies on scroll wave pinning can be carried out in presence of heterogeneities of random shape, size and chemical nature, which will better mimic real biological systems. Branched obstacles can be designed with non-uniform

distribution of holes or unequal hole sizes. Besides, the reconnection of scroll waves is a phenomenon that is still very less investigated in chemical systems. In order to understand the phenomenon better, more work requires to be done. We have started looking at interactions of scroll waves having straight filaments, and our initial simulations have yielded some interesting results.

We hope the results presented in this thesis will lead the way for a future that better understands spiral and scroll waves in complex biological systems.

RIGHTS AND PERMISSIONS FOR REPRINTED FIGURES

Permission for Fig1.2(a)

ELSEVIER LICENSE
TERMS AND CONDITIONS

Mar 08, 2018

This Agreement between DHRITI MAHANTA ("You") and Elsevier ("Elsevier") consists of your license details and the terms and conditions provided by Elsevier and Copyright Clearance Center.

License Number	4304011025082
License date	Mar 08, 2018
Licensed Content Publisher	Elsevier
Licensed Content Publication	Cell
Licensed Content Title	Molecular mechanisms of intracellular calcium excitability in X. laevis oocytes
Licensed Content Author	James D. Lechleiter,David E. Clapham
Licensed Content Date	Apr 17, 1992
Licensed Content Volume	69
Licensed Content Issue	2
Licensed Content Pages	12
Start Page	283
End Page	294
Type of Use	reuse in a thesis/dissertation
Portion	figures/tables/illustrations
Number of figures/tables/illustrations	1
Format	print
Are you the author of this Elsevier article?	No
Will you be translating?	No
Original figure numbers	figure 5(A)
Title of your thesis/dissertation	Dynamics of spiral and scroll waves around other filaments and heterogeneities
Expected completion date	Jul 2018
Estimated size (number of pages)	150
Requestor Location	DHRITI MAHANTA Department of Chemistry Indian Institute of Technology Guwahati Guwahati, Assam 781039 India Attn: DHRITI MAHANTA
Publisher Tax ID	GB 494 6272 12
Total	0.00 USD
Terms and Conditions	

Permission for Fig1.2(b)

American Physical Society
Reuse and Permissions License

31-May-2018

This license agreement between the American Physical Society ("APS") and Dhriti Mahanta ("You") consists of your license details and the terms and conditions provided by the American Physical Society and SciPris.

Licensed Content Information

License Number:	**RNP/18/MAY/004718**
License date:	31-May-2018
DOI:	10.1103/PhysRevLett.76.1174
Title:	Competing Patterns of Signaling Activity in Dictyostelium Discoideum
Author:	Kyoung J. Lee, Edward C. Cox, and Raymond E. Goldstein
Publication:	Physical Review Letters
Publisher:	American Physical Society
Cost:	USD $ 0.00

Request Details

Does your reuse require significant modifications: No

Specify intended distribution locations:	India
Reuse Category:	Reuse in a thesis/dissertation
Requestor Type:	Student
Items for Reuse:	Figures/Tables
Number of Figure/Tables:	1
Figure/Tables Details:	figure 1
Format for Reuse:	Print and Electronic
Total number of print copies:	Up to 1000

Information about New Publication:

University/Publisher:	
Title of dissertation/thesis:	SPIRAL AND SCROLL WAVE DYNAMICS IN AN EXCITABLE MEDIUM AND THEIR BEHAVIOUR AROUND EXCITATION PATTERNS AND HETEROGENEITIES
Author(s):	Dhriti Mahanta
Expected completion date:	Jul. 2018

License Requestor Information

Name:	Dhriti Mahanta
Affiliation:	Individual
Email Id:	mdhriti@gmail.com
Country:	India

Permission for Fig1.4

American Physical Society
Reuse and Permissions License

19-Aug-2018

This license agreement between the American Physical Society ("APS") and Dhriti Mahanta ("You") consists of your license details and the terms and conditions provided by the American Physical Society and SciPris.

Licensed Content Information

License Number:	**RNP/18/AUG/006963**
License date:	19-Aug-2018
DOI:	10.1103/PhysRevLett.65.3013
Title:	Spatiotemporal concentration patterns in a surface reaction: Propagating and standing waves, rotating spirals, and turbulence
Author:	S. Jakubith et al.
Publication:	Physical Review Letters
Publisher:	American Physical Society
Cost:	USD $ 0.00

Request Details

Does your reuse require significant modifications: No

Specify intended distribution locations:	India
Reuse Category:	Reuse in a thesis/dissertation
Requestor Type:	Student
Items for Reuse:	Figures/Tables
Number of Figure/Tables:	3
Figure/Tables Details:	Fig 1,2,3
Format for Reuse:	Print and Electronic
Total number of print copies:	Up to 1000

Information about New Publication:

University/Publisher:	IITG
Title of dissertation/thesis:	SPIRAL AND SCROLL WAVE DYNAMICS IN AN EXCITABLE MEDIUM AND THEIR BEHAVIOUR AROUND EXCITATION PATTERNS AND HETEROGENEITIES
Author(s):	Dhriti Mahanta
Expected completion date:	Aug. 2018

License Requestor Information

Name:	Dhriti Mahanta
Affiliation:	Individual
Email Id:	mdhriti@gmail.com
Country:	India

Permission for Fig1.5

THE AMERICAN ASSOCIATION FOR THE ADVANCEMENT OF SCIENCE LICENSE TERMS AND CONDITIONS

Jun 03, 2018

This Agreement between DHRITI MAHANTA ("You") and The American Association for the Advancement of Science ("The American Association for the Advancement of Science") consists of your license details and the terms and conditions provided by The American Association for the Advancement of Science and Copyright Clearance Center.

License Number	4361301208785
License date	Jun 03, 2018
Licensed Content Publisher	The American Association for the Advancement of Science
Licensed Content Publication	Science
Licensed Content Title	An Experimental Design Method Leading to Chemical Turing Patterns
Licensed Content Author	Judit Horváth,István Szalai,Patrick De Kepper
Licensed Content Date	May 8, 2009
Licensed Content Volume	324
Licensed Content Issue	5928
Volume number	324
Issue number	5928
Type of Use	Thesis / Dissertation
Requestor type	Scientist/individual at a research institution
Format	Print and electronic
Portion	Figure
Number of figures/tables	1
Order reference number	
Title of your thesis / dissertation	SPIRAL AND SCROLL WAVE DYNAMICS IN AN EXCITABLE MEDIUM AND THEIR BEHAVIOUR AROUND EXCITATION PATTERNS AND HETEROGENEITIES
Expected completion date	Jul 2018
Estimated size(pages)	150
Requestor Location	DHRITI MAHANTA Department of Chemistry Indian Institute of Technology Guwahati Guwahati, Assam 781039 India Attn: DHRITI MAHANTA
Billing Type	Invoice
Billing Address	DHRITI MAHANTA Department of Chemistry Indian Institute of Technology Guwahati Guwahati, India 781039 Attn: DHRITI MAHANTA
Total	0.00 USD

Permission for Fig1.6

ELSEVIER LICENSE
TERMS AND CONDITIONS

Jun 05, 2018

This Agreement between DHRITI MAHANTA ("You") and Elsevier ("Elsevier") consists of your license details and the terms and conditions provided by Elsevier and Copyright Clearance Center.

License Number	4362540999061
License date	Jun 05, 2018
Licensed Content Publisher	Elsevier
Licensed Content Publication	Medicine
Licensed Content Title	Physiology of the normal heart
Licensed Content Author	David E.L. Wilcken
Licensed Content Date	Jul 1, 2010
Licensed Content Volume	38
Licensed Content Issue	7
Licensed Content Pages	4
Start Page	336
End Page	339
Type of Use	reuse in a thesis/dissertation
Intended publisher of new work	other
Portion	figures/tables/illustrations
Number of figures/tables/illustrations	1
Format	both print and electronic
Are you the author of this Elsevier article?	No
Will you be translating?	No
Original figure numbers	Fig. 1
Title of your thesis/dissertation	SPIRAL AND SCROLL WAVE DYNAMICS IN AN EXCITABLE MEDIUM AND THEIR BEHAVIOUR AROUND EXCITATION PATTERNS AND HETEROGENEITIES
Expected completion date	Jul 2018
Estimated size (number of pages)	150
Requestor Location	DHRITI MAHANTA Department of Chemistry Indian Institute of Technology Guwahati Guwahati, Assam 781039 India Attn: DHRITI MAHANTA
Publisher Tax ID	GB 494 6272 12
Total	0.00 USD

Permission for Fig1.8

Copyright Clearance Center

BOOK

ISBN:	9780126569759	**Pagination:**	1261
Publication year(s):	2000	**Language:**	English
Author/Editor:	Sperelakis, Nick	**Country of publication:**	United States of America
Publisher:	ELSEVIER SCIENCE & TECHNOLOGY BOOKS		
Rightsholder:	ELSEVIER SCIENCE & TECHNOLOGY BOOKS		

Academic

Photocopy or share content electronically

LICENSE COVERAGE

Annual Copyright License for Academic Institutions

This permission type is covered. The Annual Copyright License authorizes the licensee's faculty, staff, students, and other authorized users to distribute print and electronic copies of copyrighted content within your institution through:

- Print or electronic coursepacks
- Classroom handouts
- Electronic reserves
- Institution Intranets
- Course/Learning Management systems (CMS/LMS)
- CD-ROM/DVD
- Other internal academic uses

The description above is provided for summary purposes only. Please refer to your institution's Annual Copyright License for the complete terms and conditions and scope of coverage of the license.

Covered by CCC Annual License - Academic

Permission for Fig1.10

WOLTERS KLUWER HEALTH, INC. LICENSE TERMS AND CONDITIONS

Jun 04, 2018

This Agreement between DHRITI MAHANTA ("You") and Wolters Kluwer Health, Inc. ("Wolters Kluwer Health, Inc.") consists of your license details and the terms and conditions provided by Wolters Kluwer Health, Inc. and Copyright Clearance Center.

License Number	4361960383365
License date	Jun 04, 2018
Licensed Content Publisher	Wolters Kluwer Health, Inc.
Licensed Content Publication	Circulation Research
Licensed Content Title	Spiral waves of excitation underlie reentrant activity in isolated cardiac muscle.
Licensed Content Author	A M Pertsov,J M Davidenko,R Salomonsz,W T Baxter,J Jalife
Licensed Content Date	Mar 1, 1993
Licensed Content Volume	72
Licensed Content Issue	3
Type of Use	Dissertation/Thesis
Requestor type	Individual
STM publisher name	
Portion	Figures/table/illustration
Number of figures/tables/illustrations	1
Figures/tables/illustrations used	16
Author of this Wolters Kluwer article	No
Title of your thesis / dissertation	SPIRAL AND SCROLL WAVE DYNAMICS IN AN EXCITABLE MEDIUM AND THEIR BEHAVIOUR AROUND EXCITATION PATTERNS AND HETEROGENEITIES
Expected completion date	Jul 2018
Estimated size(pages)	150
Requestor Location	DHRITI MAHANTA Department of Chemistry Indian Institute of Technology Guwahati Guwahati, Assam 781039 India Attn: DHRITI MAHANTA
Billing Type	Invoice
Billing Address	DHRITI MAHANTA Department of Chemistry Indian Institute of Technology Guwahati Guwahati, India 781039 Attn: DHRITI MAHANTA
Total	0.00 USD

Permission for Fig1.15(c)

American Physical Society
Reuse and Permissions License

19-Aug-2018

This license agreement between the American Physical Society ("APS") and Dhriti Mahanta ("You") consists of your license details and the terms and conditions provided by the American Physical Society and SciPris.

Licensed Content Information

License Number:	**RNP/18/AUG/006964**
License date:	19-Aug-2018
DOI:	10.1103/PhysRevE.86.036205
Title:	Scroll wave filaments self-wrap around unexcitable heterogeneities
Author:	Zulma A. Jiménez and Oliver Steinbock
Publication:	Physical Review E
Publisher:	American Physical Society
Cost:	USD $ 0.00

Request Details

Does your reuse require significant modifications: No

Specify intended distribution locations:	India
Reuse Category:	Reuse in a thesis/dissertation
Requestor Type:	Student
Items for Reuse:	Figures/Tables
Number of Figure/Tables:	1
Figure/Tables Details:	Fig3
Format for Reuse:	Print and Electronic
Total number of print copies:	Up to 1000

Information about New Publication:

University/Publisher:	IITG
Title of dissertation/thesis:	SPIRALANDSCROLL WAVE DYNAMICS IN AN EXCITABLE MEDIUM AND THEIR BEHAVIOUR AROUND EX- CITATION PATTERNS AND HETEROGENEITIES
Author(s):	Dhriti Mahanta
Expected completion date:	Aug. 2018

License Requestor Information

Name:	Dhriti Mahanta
Affiliation:	Individual
Email Id:	mdhriti@gmail.com
Country:	India

Permission for Fig1.15(d)

Title: Topologically Mismatched Pinning of Scroll Waves
Author: Sumana Dutta, Oliver Steinbock
Publication: Journal of Physical Chemistry Letters
Publisher: American Chemical Society
Date: May 1, 2011

Logged in as:
DHRITI MAHANTA
Account #:
3001258438
LOGOUT

PERMISSION/LICENSE IS GRANTED FOR YOUR ORDER AT NO CHARGE

This type of permission/license, instead of the standard Terms & Conditions, is sent to you because no fee is being charged for your order. Please note the following:

- Permission is granted for your request in both print and electronic formats, and translations.
- If figures and/or tables were requested, they may be adapted or used in part.
- Please print this page for your records and send a copy of it to your publisher/graduate school.
- Appropriate credit for the requested material should be given as follows: "Reprinted (adapted) with permission from (COMPLETE REFERENCE CITATION). Copyright (YEAR) American Chemical Society." Insert appropriate information in place of the capitalized words.
- One-time permission is granted only for the use specified in your request. No additional uses are granted (such as derivative works or other editions). For any other uses, please submit a new request.

If credit is given to another source for the material you requested, permission must be obtained from that source.

BACK CLOSE WINDOW

Permission for reprint of text and figures of Chapter 3

American Physical Society
Reuse and Permissions License

09-Aug-2018

This license agreement between the American Physical Society ("APS") and Dhriti Mahanta ("You") consists of your license details and the terms and conditions provided by the American Physical Society and SciPris.

Licensed Content Information

License Number:	**RNP/18/AUG/006745**
License date:	09-Aug-2018
DOI:	10.1103/PhysRevE.95.032204
Title:	Pinning of scroll waves to flat and highly branched unexcitable heterogeneities
Author:	Dhriti Mahanta, Sumana Dutta, and Oliver Steinbock
Publication:	Physical Review E
Publisher:	American Physical Society
Cost:	USD $ 0.00

Request Details

Does your reuse require significant modifications: No

Specify intended distribution locations:	india
Reuse Category:	Reuse in a thesis/dissertation
Requestor Type:	Author of requested content
Items for Reuse:	Whole Article
Format for Reuse:	Print and Electronic
Total number of print copies:	Up to 1000

Information about New Publication:

University/Publisher:	IIT Guwahati
Title of dissertation/thesis:	SPIRAL AND SCROLL WAVE DYNAMICS IN AN EXCITABLE MEDIUM AND THEIR BEHAVIOUR AROUND EXCITATION PATTERNS AND HETEROGENEITIES
Author(s):	Dhriti Mahanta
Expected completion date:	Aug. 2018

License Requestor Information

Name:	Dhriti Mahanta
Affiliation:	Individual
Email Id:	mdhriti@gmail.com
Country:	India

Permission for reprint of text and figures of Chapter 6

American Physical Society
Reuse and Permissions License

09-Aug-2018

This license agreement between the American Physical Society ("APS") and Dhriti Mahanta ("You") consists of your license details and the terms and conditions provided by the American Physical Society and SciPris.

Licensed Content Information

License Number:	**RNP/18/AUG/006744**
License date:	09-Aug-2018
DOI:	10.1103/PhysRevE.97.022206
Title:	Spirals in a reaction-diffusion system: Dependence of wave dynamics on excitability
Author:	Dhriti Mahanta, Nirmali Prabha Das, and Sumana Dutta
Publication:	Physical Review E
Publisher:	American Physical Society
Cost:	USD $ 0.00

Request Details

Does your reuse require significant modifications: No

Specify intended distribution locations:	india
Reuse Category:	Reuse in a thesis/dissertation
Requestor Type:	Author of requested content
Items for Reuse:	Whole Article
Format for Reuse:	Print and Electronic
Total number of print copies:	Up to 1000

Information about New Publication:

University/Publisher:	IIT Guwahati
Title of dissertation/thesis:	SPIRAL AND SCROLL WAVE DYNAMICS IN AN EXCITABLE MEDIUM AND THEIR BEHAVIOUR AROUND EXCITATION PATTERNS AND HETEROGENEITIES
Author(s):	Dhriti Mahanta
Expected completion date:	Aug. 2018

License Requestor Information

Name:	Dhriti Mahanta
Affiliation:	Individual
Email Id:	mdhriti@gmail.com
Country:	India